Modeling and Simulation of Nanoparticle Formation in Microemulsion Droplets

MODELING AND SIMULATION OF NANOPARTICLE FORMATION IN MICROEMULSIONS

A Dissertation Presented

by

SREEKUMAR R. KURIYEDATH

Submitted to the Graduate School of the
University of Massachusetts Amherst in partial fulfillment
of the requirements for the degree of

DOCTOR OF PHILOSOPHY

September 2011

Department of Chemical Engineering

MODELING AND SIMULATION OF NANOPARTICLE FORMATION IN MICROEMULSIONS

A Dissertation Presented

by

SREEKUMAR R. KURIYEDATH

Approved as to style and content by:

T.J. Mountziaris, Chair

Dimitrios Maroudas, Member

Michael Henson, Member

Nikolay Prokofiev, Member

T.J. Mountziaris, Department Head
Department of Chemical Engineering

Dedicated to my Parents

ACKNOWLEDGMENTS

I would like to acknowledge Professor Henson, Professor Maroudas, and Professor Prokofiev for their time and effort in serving in my dissertation committee. I thank Prof. Maroudas for the opportunity to attend his group meetings which have always been a valuable learning experience. I would like to thank Prof. Prokofiev for his thoughtful criticism that provoked improvements in this work.

I would also like to thank group members JoungMo Cho, Tracy Heckler, Jun Wang, Bing Mei and the recent members of the group for their company and help. I am thankful for having met some wonderful colleagues and friends in the department and outside. I am thankful for the company and help during my stay to Tejinder Singh, Mayur Valipa, Anurag Verma, Kedarnath Kolluri, Vivek Tomar, and George Sfyris.

I would like to thank Prof. Yannis Kevrekidis who helped refine these ideas and gave useful suggestions and criticism which were invaluable to this work.

I would like to acknowledge my thesis advisor Prof. Mountziaris, for being with me in this long journey. His company, always pleasant, also ensured that I kept on in this long journey and his patient attitude always kept me in good spirit. Thank you very much.

My parents' love and many sacrifices afforded me this opportunity. I do not think I would ever be able to thank them, but I do hope to give them joy in the future. Thank you very much Amma and Accha.

ABSTRACT

MODELING AND SIMULATION OF NANOPARTICLE FORMATION IN MICROEMULSION DROPLETS

SEPTEMBER 2011

SREEKUMAR R KURIYEDATH

B.Tech AND M.Tech, INDIAN INSTITUTE OF TECHNOLOGY DELHI

Ph.D. UNIVERSITY OF MASSACHUSETTS AMHERST

Directed by: Professor T.J. Mountziaris

Semiconductor nanocrystals, also known as quantum dots (QDs), are an important class of materials that are being extensively studied for a wide variety of potential applications, such as medical diagnostics, photovoltaics, and solid-state lighting. The optical and electronic properties of these nanocrystals are different from their bulk properties and depend on the size of the QDs. Therefore an important requirement in their synthesis is a proper control on the final nanoparticle size. Recently, a technique has been developed for synthesizing zinc selenide (ZnSe) QDs using microemulsion droplets as templates. In these systems, a fixed amount of a reactant is dissolved in each droplet and a second reactant is supplied by diffusion through the interface. Spontaneous reaction between the two reactants at the droplet interface forms ZnSe nuclei, whose subsequent diffusion and coalescence into clusters ultimately leads to the formation of a single particle in each droplet. The size of the final particle can be adjusted by changing the initial concentration of the reactant that is dissolved in the dispersed phase of the microemulsion.

In this thesis we use a modeling and simulation approach to study the phenomena underlying the formation of QDs in the droplets of a microemulsion. A Lattice Monte-Carlo model was developed to describe Brownian diffusion of a Zn-containing precursor (reactant) inside a droplet, formation of ZnSe nuclei via an irreversible reaction with a Se-containing precursor at the droplet interface, Brownian diffusion and coalescence of nuclei into clusters ultimately leading to the formation of a single nanoparticle inside the droplet. The time required for forming a single particle was found to initially increase as the final particle size was increased by increasing the initial concentration of the reactant in the droplet, but it quickly passed through a maximum, and subsequently decreased. The simulations revealed that this seemingly anomalous result can be explained by studying the intermediate cluster populations that show the formation of a large intermediate "sweeper" cluster. This sweeper cluster is a more effective collision partner to smaller ones and accelerates the coalescence process that eventually leads to the formation of a single particle. A generalized dimensionless equation was obtained that relates the formation time of the final particle to its size for various droplet sizes and diffusivities of the reactant and clusters in the droplet. A parametric study revealed that the final particle formation time is more sensitive to changes in the cluster coalescence probability than in the probability of nucleation.

We subsequently compared these results with those obtained by simulating the coalescence of nuclei that are assumed to be formed spontaneously inside a droplet and to be initially uniformly dispersed in it. Comparison of the time required for forming a single final particle for the two cases revealed that for ZnSe particles with diameter smaller than 3.5 nm the predicted formation times were approximately the same.

Surprisingly, for particles larger than 3.5 nm, the scenario that required diffusion of a reactant to the interface and formation of nuclei via a reaction at the interface led to the formation of a single particle faster than the scenario that started with nuclei uniformly dispersed in the droplet. Analysis of intermediate cluster populations indicates that the "sweeper" clusters are more effective in accelerating cluster coalescence when the nuclei are supplied gradually, as in the first scenario, compared to spontaneous nucleation throughout the domain. Generalized equations were obtained that describe the evolution of the number of different cluster sizes during coalescence starting from an initially monodispersed population of nuclei thus extending the classical theory of coalescence of monodisperse aerosols in an infinite domain to include coalescence in finite spherical domains with reflective boundaries.

Finally, a generalized phenomenological model describing an energy balance during coalescence of two nanoparticles was developed. The reduction in the surface area of the coalescing system was modeled to be the source of thermal energy released due to the formation of additional bonds in the bulk of the coalesced particles. The temperature rise of the coalescing system was predicted for adiabatic coalescence and for coalescence with energy dissipation to a surrounding medium. Generalized equations were developed by scaling the temperature rise with its maximum value that corresponds to adiabatic conditions and the time with a characteristic time for coalescence obtained from the literature that depends on the mechanism (e.g., viscous flow, bulk diffusion, or surface diffusion). As a case study, the effects of the size of coalescing ZnSe nanoparticles on the temperature evolution of the coalescing system were studied by assuming that surface diffusion is the predominant mechanism for coalescence in this system.

This modeling and simulation study of nanoparticle nucleation and coalescence presented in this thesis has revealed new phenomena and led to generalized models that can be used for studying such systems. Our work extended the classical theory for coalescence in an infinite domain to include finite spherical domains with reflective boundaries and provided a generalized approach for the analysis of transient thermal effects occurring during coalescence of two nanoparticles.

TABLE OF CONTENTS

Page

ACKNOWLEDGMENTS……...v

ABSTRACT……...vi

LIST OF TABLES……xii

LIST OF FIGURES……..xiii

CHAPTER

1. INTRODUCTION……..1

1.1 Semiconductor Nanocrystals……..1
1.2 Zinc Selenide Quantum Dots……...…...2
1.3 Synthesis Methods…….…….3
1.4 Simulation of Nanoparticle Synthesis…….8
1.5 Thesis Objective and Summary……...9

2. MODELING AND SIMULATION OF NANOCRYSTAL SYNTHESIS…....13

2.1 Introduction……13
2.2 Model Description…….16
2.3 Model Validation……...23
2.4 Simulation of Quantum Dot Synthesis……..26
2.4.1 Coalescence of large Quantum Dots……..27
2.4.2 Formation of "Sweeper" Cluster…….....31
2.5 Parametric Studies…….34
2.6 Summary and Conclusions……40

3. CLUSTER COALESCENCE KINETICS…….43

3.1 Introduction……43
3.2 Modeling Methodology…….45
3.3 Simulation of Nanoparticle Formation……..50
3.4 Evolution of Cluster Population in Pure Coalescence……..60
3.5 Summary and Conclusions……...64

4. THERMAL ANALYSIS OF NANOPARTICLE COALESCENCE……66

4.1 Introduction……66
4.2 Modeling of Nanoparticle Coalescence…….69

4.3 Effect of Size on Melting Point of Nanoparticles……..74
4.4 Coalescence of Two Nanoparticles under Adiabatic Conditions……..74
4.5 Coalescence of Two Nanoparticles with Heat Heat Transfer to Surrounding Medium…….81
4.6 Summary and Conclusions…….....91

5. SUMMARY, CONCLUSIONS AND FUTURE DIRECTIONS……..94

5.1 Summary and Conclusions……94
5.2 Future Directions……...97

APPENDICES

A. PHYSICAL AND CHEMICAL PROPERTIES OF ZNSE …...……...99

B. EFFECT OF LATTICE SPACINGS ON LATTICE MONTE-CARLO SIMULATION RESULTS ……...……...…...100

BIBLIOGRAPHY…….....……102

LIST OF TABLES

Table Page

Table 3.1. Values of parameter α for ZnSe QDots obtained from Equation (3.7)……50

Table 4.1. Adiabatic temperature rise and mass fraction of the final nanoparticle that melts for coalescence of two ZnSe nanoparticles with different sizes under adiabatic conditions(T_0 = 300 K)……...76

Table 4.2. Values of ($\Delta a_0/a_f$) and B_{max} for coalescence of ZnSe nanoparticles in n-heptane and hydrogen at 300 K under maximum heat transfer conditions (Nu = 2 and no Kapitza resistance)……..……....85

Table 4.3. Values of maximum temperature, T_{max}, and time for complete coalescence, t_c, of two ZnSe nanoparticles in n-heptane for different values of ($\Delta a_0/a_f$) and B. In the calculations the size of one of the particles (the larger of the two) was fixed at 5nm and the size of the second particle was calculated from the value of $\Delta a_0/a_f$……90

Table A1.1 Physical and chemical properties of ZnSe (Madelung et al., 1999):……..99

Table A2.1. Behavior of Root Mean Square (RMS) difference of total formation time with the value for coarsest mesh (lattice spacing =4nm)……100

LIST OF FIGURES

Figure Page

Figure 1.1. Batch reactor system for the hot injection colloidal synthesis method (Wang, 2006)……...……..4

Figure 1.2. Phase diagram showing the structural polymorphism in the PEO-PPO-PEO microemulsion system used as templates for making semiconductor nanostructure (Alexandridis et al., 1998)……..……6

Figure 1.3. Schematic of microemulsion-gas contacting method for quantum dot synthesis (Karanikolos, 2005b)……...7

Figure 2.1. Schematic of the formation of a single semiconductor nanocrystal in a microemulsion droplet. Reactant A is dispersed in the droplet and reactant B diffuses from the continuous phase to the droplet interface. An irreversible reaction at the interface produces $(AB)_1$ nuclei, that coalesce into $(AB)_k$ clusters, and eventually form a single particle (QDot)……..…….15

Figure 2.2. A unit cell surrounding a lattice point containing precursor molecules. Multiple occupancy by the precursor molecules is allowed as long as the fraction occupancy does not exceed the random packing limit of equal sized spheres…….……17

Figure 2.3. Model Validation: Comparison between LMC simulations and Equation (2.8) predictions for diffusion of a solute (diethylzinc) out of a droplet (heptane). The LMC data were collected for concentrations of diethylzinc equal to 0.025, 0.071, and 0.19 M in a droplet with a diameter of 40nm…….……25

Figure 2.4. Dependence of dimensionless formation time on dimensionless final particle size from LMC simulations. By varying the initial Zn precursor concentration in the droplet, the final particle size was varied from $(ZnSe)_2$ to a ZnSe nanoparticle with diameter of 7nm. Domain diameter: 40nm……...…27

Figure 2.5. Particle number evolution predicted by LMC simulation of ZnSe QDot synthesis in a microemulsion droplet: (1) $(ZnSe)_1$ nuclei, (2) $(ZnSe)_2$ clusters, (3) all clusters (m), (4) Zn precursor molecules. Final ZnSe particle diameter: 7nm. Domain diameter: 40nm……28

Figure 2.6. Average snapshots of normalized cluster size distributions at times corresponding to total cluster number (m) equal to: (a) 400, (b) 200, (c) 100, (d) 50, (e) 10, and (f) 5. The number of clusters of a certain size has been normalized by dividing it with m. Final ZnSe particle diameter: 7nm. Domain diameter: 40nm……30

Figure 2.7. Normalized diameter difference between the two biggest clusters, before the last collision that yields a single final particle, as function of dimensionless final particle size. By varying the initial Zn precursor concentration in the droplet, the final particle size was varied from $(ZnSe)_2$ to a ZnSe nanoparticle with diameter of 7nm. Domain diameter: 40nm……..32

Figure 2.8. Dimensionless final particle formation time vs. dimensionless particle size for the following cases: (1) cluster volume and diffusivity are size-dependent (base case), (2) cluster volume is equal to that of a $(ZnSe)_1$ nucleus, but the cluster diffusivity is size-dependent, (3) cluster diffusivity and volume do not change and are equal to those of a $(ZnSe)_1$ nucleus. Same final particle sizes as Figure 2.4. Domain diameter: 40nm……..34

Figure 2.9. Fitting of LMC data to obtain a generalized equation for the Dimensionless formation time as function of dimensionless final particle size for particles bigger than $(Zn\text{-}Se)_5$. Same final particle sizes as Figure 2.4. The LMC simulations correspond to droplet diameters (d_D) of (1) 10 nm, (2) 20 nm, (3) 30 nm, and (4) 40 nm……36

Figure 2.10. Dimensionless final particle formation time vs. dimensionless final particle size for three different droplet diameters: 20, 30 and 40 nm, and three different precursor diffusivities equal to 0.1, 1, and 10 times the base case value. Final ZnSe particle diameters: 1.5nm to 7nm…….37

Figure 2.11. Dimensionless final particle formation time vs. dimensionless final particle size for various probabilities of the nucleation reaction: (1) 1.0, 0.1, and 0.01 (change indistinguishable); (2) 0.001. Same final particle sizes as Figure 2.4.Domain diameter: 40nm……..38

Figure 2.12. Dimensionless final particle formation time vs. dimensionless final particle size for various probabilities of cluster-cluster coalescence: (1) 1.0, (2) 0.5, and (3) 0.1. Same final particle sizes as Figure 2.4. Domain diameter: 40nm……40

Figure 3.1. Predicted dimensionless final particle formation time as function of the dimensionless final particle size for (1) pure coalescence and (2) synthesis runs. Droplet diameter d_D = 40 nm; the particle diameter d_p ranges from 0.56 nm to 7 nm……..52

Figure 3.2. Evolution of normalized total cluster number (m_c) for an average run corresponding to: (1) pure coalescence and (2) synthesis scenario. Droplet diameter d_D = 40 nm; final particle diameter d_p= 7 nm……53

Figure 3.3. Cluster size distribution snapshots during pure coalescence runs corresponding to various total cluster numbers and process times. (a) m_c = 400 and $t = 2.30\text{x}10^{-9}$ s; (b) m_c = 300 and $t = 3.02\text{x}10^{-9}$ s; (c) m_c = 200 and $t = 4.45\text{x}10^{-9}$ s; and (d) m_c = 100 and $t = 8.13\text{x}10^{-9}$ s. The final particle formation time is $9.74\ \text{x}10^{-7}$ s. Droplet diameter d_D = 40 nm; final particle diameter d_p= 7 nm.....54

Figure 3.4. Cluster size distribution snapshots during synthesis runs corresponding to various total cluster numbers and process times. (a) m = 400 and $t = 6.30\text{x}10^{-9}$; (b) m = 300 and $t = 1.06\text{x}10^{-8}$; (c) m = 200 and $t = 1.73\text{x}10^{-8}$ s; and (d) m = 100 and $t = 3.14\text{x}10^{-8}$ s. The final particle formation time is $8.67\text{x}10^{-7}$ s. Droplet diameter d_D = 40 nm; final particle diameter d_p= 7 nm.....55

Figure 3.5. Comparison of cluster size distributions during pure coalescence and synthesis runs corresponding to an approximately equal process time. (1) Pure coalescence: m_c = 100 and $t = 8.13\text{x}10^{-9}$ s. (2) Synthesis: m_c = 300 and $t = 1.06\text{x}10^{-8}$ s. Droplet diameter d_D = 40 nm; final particle diameter d_p= 7 nm.....56.

Figure 3.6. Predicted radial distribution of scaled cluster concentration of $(ZnSe)_1$ nuclei (plots a and b) and all clusters (plots c and d) for pure coalescence (1) and synthesis scenario (2) at two process times: $t = 1\text{x}10^{-10}$ s (plots a and c); $t = 1\text{x}10^{-9}$ s (plots b and d). Droplet diameter d_D = 40 nm; final particle diameter d_p= 7 nm…….58

Figure 3.7. Normalized diameter difference between the two biggest clusters, before the last collision that yields a single final particle, as a function of dimensionless final particle size for (1) pure coalescence and (2) synthesis scenario. Each point is the average of 100 LMC runs. Droplet diameter d_D = 40nm; final particle diameter d_p= 0.56nm to 7nm……60

Figure 3.8. Normalized total cluster number during coalescence of hard spheres in a spherical domain as function of dimensionless process time obtained from LMC simulations for d_D= 20-40 nm and d_p=5-7 nm. The prediction of Equation (3.11) is also plotted for comparison……62

Figure 3.9. Normalized $(ZnSe)_1$ and $(ZnSe)_2$ cluster numbers during coalescence of hard spheres in a spherical domain as function of dimensionless process time obtained from LMC simulations for d_D= 20-40 nm and d_p=5-7 nm. The predictions of Equation (3.12) for k=1 and 2 are also plotted for comparison……63

Figure 4.1. The evolution of dimensionless temperature rise during coalescence of two nanoparticles under adiabatic conditions with particles sizes (2,2), (3,3), and (5,5)nm. ……..….78

Figure 4.2. Temperature rise during coalescence of two 5 nm ZnSe nanoparicles in n-heptane. (1) full model solved numerically, and (2) approximate model based on equation (4.19)……81

Figure 4.3. Dimensionless temperature rise evolution during coalescence of two nanoparicles for different values of B at a constant value of $(\Delta a_0/a_f)$ of (a) 0.05 and (b) 0.1……87

Figure 4.4. Dimensionless temperature rise evolution during coalescence of two nanoparicles for different values of B at a constant value of $(\Delta a_0/a_f)$ of (a) 0.2 and (b) 0.26……88

Figure 4.5. The time for complete coalescence of two ZnSe nanoparticles in n-heptane vs. dimensionless parameter B for $\Delta a_0/a_f$ values between 0.05 and 0.26. In the calculations the size of one of the particles (the larger of the two) was fixed at 5nm and the size of the second particle was calculated from the value of the specific value of $\Delta a_0/a_f$……..89

Figure A2.1. Normalized root mean square difference between the predicted final particle formation time for finer lattice spacing minus the ones obtained from the initial LMC simulation that employed a lattice spacing of 4nm. The RMS difference saturates as finer lattice is used……...…….101

CHAPTER 1

INTRODUCTION

1.1 Semiconductor Nanocrystals

Semiconductor nanocrystals, also known as quantum dots (QDots), are an interesting class of materials exhibiting size-dependent optical and electronic properties (Alivisatos, 1996; Trindade et al., 2001). The optical and electronic properties of QDots are different from bulk and they are also dependent on the size of the nanocrystal. They exhibit size-dependent fluorescence and absorption when their size is smaller than the quantum confinement threshold for that material, broad excitation by any wavelength smaller than the emission wavelength, high quantum yields, high extinction coefficients, and excellent photochemical stability (Murray et al., 2000; Yoffe, 2001). These properties have lead to a tremendous interest in synthesis of these materials due to the wide range of their potential applications.

These materials are candidates for applications in solar energy conversion, solid-state lighting, high-density information storage, and in biological imaging and detection. Semiconductor nanocrystals are being used in conjunction with other materials such as metal oxides or polymers to augment energy conversion efficiency in solar cells (Nozik, 2002; Gratzel, 2005; Kamat, 2008). CdSe QDots have been assembled onto layer of TiO_2 film using linker molecules and shown to increase the light harvesting efficiency of the solar cell (Kongkanand et al., 2008). QDots are replacing traditional organic dyes in biological imaging and clinical diagnostics (Parak, 2005; Michalet et al., 2005; Medintz et al., 2005). Quantum dots are much brighter and do not photo-bleach which makes them

more attractive over the organic dyes. Conjugating DNA molecules onto QDots have been found to enhance the emission significantly leading to better imaging and detection (Wang, 2006). Another energy saving application is in the area of solid state lighting devices (Dai, 2010) where inorganic QDots have shown to generate current efficiencies of 3.5 Ampere cm^{-2} (Caruge et al., 2008).

Quantum confinement occurs when the size of the nanocrystal is smaller than the average separation of an electron-hole pair created by absorption of a photon with energy higher than the band-gap of the material. For typical II-VI semiconductors, such as CdSe and ZnSe, the quantum confinement threshold is a few nanometers (e.g., 9nm for ZnSe). Quantum dots have properties which are in between bulk state and an individual atom. The electron motion is quantized in all three dimensions which produces a discrete energy level spectrum like a single atom. However, they consist of between hundreds and a few thousands of atoms (Shields, 2007).

The most widely studied material for making quantum dots have been typically II-VI and III-V compound semiconductors like CdSe, CdS, InP, AlP, ZnS etc.

1.2 Zinc Selenide Quantum Dots

Zinc Selenide is a II-VI compound semiconductor whose bandgap places the emission from bulk ZnSe in the blue range of the visible spectrum. ZnSe has a crystal structure of Zinc Blende at room temperature with wurtzite being favored at higher temperature. In the Zinc Blende structure, each unit cell has four Zn and Se atoms with both having an interpenetrating FCC lattice which is displaced by 1/4 of the body diagonal. ZnSe is being widely studied for applications where the toxicity of the Cd ions

may be an issue such as in biological applications. Further, doping of ZnSe with transition metal ions such as Mn has enabled the extension of the range of the visible spectrum over which ZnSe QDots can be used.

1.3 Synthesis Methods

Ekimov and Onuschenko (Ekimov and Onuschenko, 1982) and Efros (Efros, 1982) pioneered the controlled synthesis and systematic studies of compound semiconductor nanocrystals by studying inclusions embedded in a glass matrix which had a blue shift in the absorption spectrum. Brus et al. (Brus, 1984; Rossetti et al., 1985) synthesized CdS and ZnS nanoparticles using an arrested precipitation technique at room temperature involving the slow injection of the metal salt into a solution of ammonium or sodium sulfide in a suitable solvent to synthesize CdS and ZnS nanoparticles.

The most common procedure for synthesizing compound semiconductor QDots, such as CdSe or ZnSe and core-shell structures such as CdSe/ZnS and ZnSe/ZnS, involves injection of precursors into a hot coordinating solvent and growth of QDots by nucleation and coalescence of clusters as function of time (Murray et al., 1993; Hines and Guyot-Sionnest, 1998). The precursors are injected into a hot solvent containing surfactant where they react to form clusters which gradually grow thus forming a colloid consisting of solvent or surfactant terminated QDots. The binding by the surfactant prevents the aggregation of the QDots.

This method, the Hot Injection Colloidal Synthesis, aims to achieve temporal separation between the nucleation of ZnSe by reaction between precursors and the subsequent growth by coalescence of the nuclei and clusters to form a population of

nearly monodisperse nanocrystals. Typically diethylzinc and Se powder (the two precursors) are dissolved in Trioctylphosphine (TOP) and this mixture is injected into a solvent of hexadecylamine(HDA) at around 300C. The reactor is supplied with heat to keep the reaction temperature around 270C. TOP acts as a solubilizing agent while the combination of TOP and HDA efficiently passivates the surface of the nanocrystal.

Figure 1.1 shows the batch reactor system used for synthesis by this method. This is an operator-intensive process which is difficult to scale up because of non-uniformities in nucleation and mixing that result in polydisperse particle populations. The use of templates for the growth of nanostructured materials can enable precise control of particle size and shape, while allowing easier scale up for industrial production.

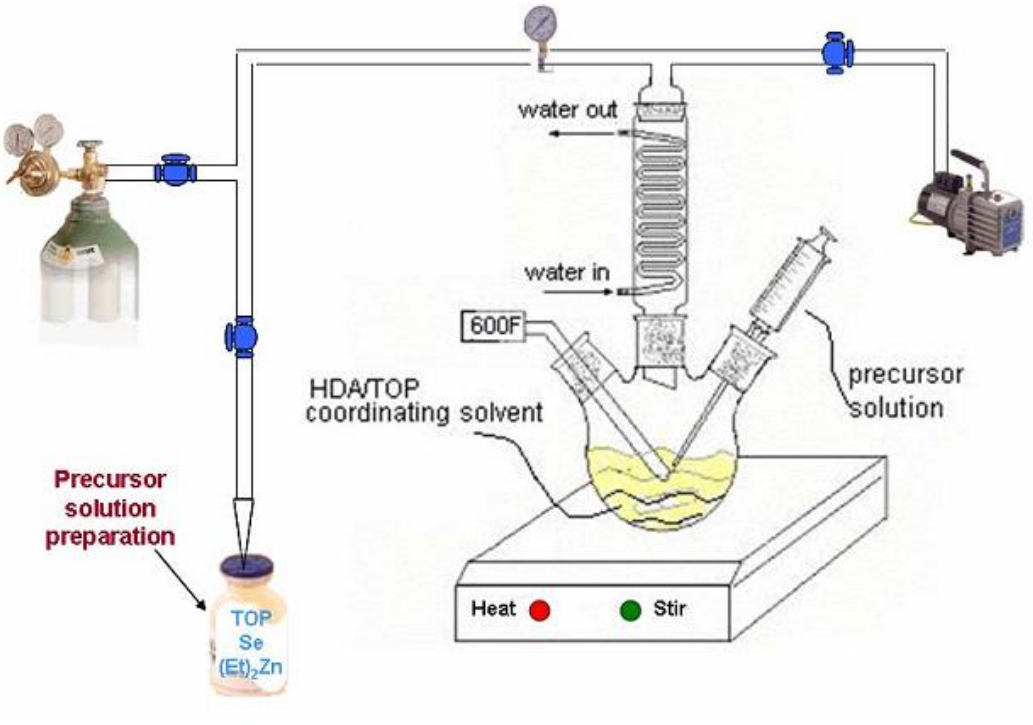

Figure 1.1. Batch reactor system for the hot injection colloidal synthesis method (Wang, 2006).

Various self-assembled templates, such as reverse micelles, microemulsions, and liquid crystals have also been used for precisely controlling the size, size distribution, and shape of nanocrystals, and for allowing easy scale up of the process. Reverse micelles have been used to synthesize a variety of compound semiconductor nanocrystals (Lianos and Thomas, 1987; Li and Park, 1999). ZnSe nanoparticles have been synthesized in AOT reverse micelles by a reaction between zinc perchlorate hexahydrate and sodium selenide (Quinlan et al., 2000).

Microemulsions are a thermodynamically stable mixture consisting of a dispersed phase of droplets stabilized by surfactants in an immiscible continuous phase. Microemulsions have been used as templates for nanocrystal synthesis (Pillai et al., 1995; Pileni, 1997; Holmes et al., 1999; Lopez-Quintela et al., 2004). Two microemulsions, whose droplets contain one dissolved precursor each, are mixed together. This leads to collision of the droplets and exchange of precursors between the droplets. The two precursors react inside each droplet forming the nanoparticle.

Karanikolos et al. (Karanikolos et al., 2004, 2005a, 2006) developed a technique for microemulsion templated synthesis which involves a ternary mixture consisting of an amphiphillic block copolymer, poly(ethyleneoxide)-poly(propyleneoxide)-poly(ethyleneoxide) (PEO-PPO-PEO), a non-polar (n-heptane) and a polar solvent (formamide). The mixture exhibits rich structural polymorphism to self-assemble under equilibrium conditions into a variety of lyotropic liquid crystalline structures with spherical, cylindrical, planar domains or having an interconnected (bicontinous) topology (Alexandridis et al., 1998). The phase diagram showing the equilibrium composition and shape for this mixture is shown in Figure 1.2. The nanodomains formed in the dispersed

phase serve as template for the formation of nanocrystals and other nanostructures such as nanowires and nanowells.

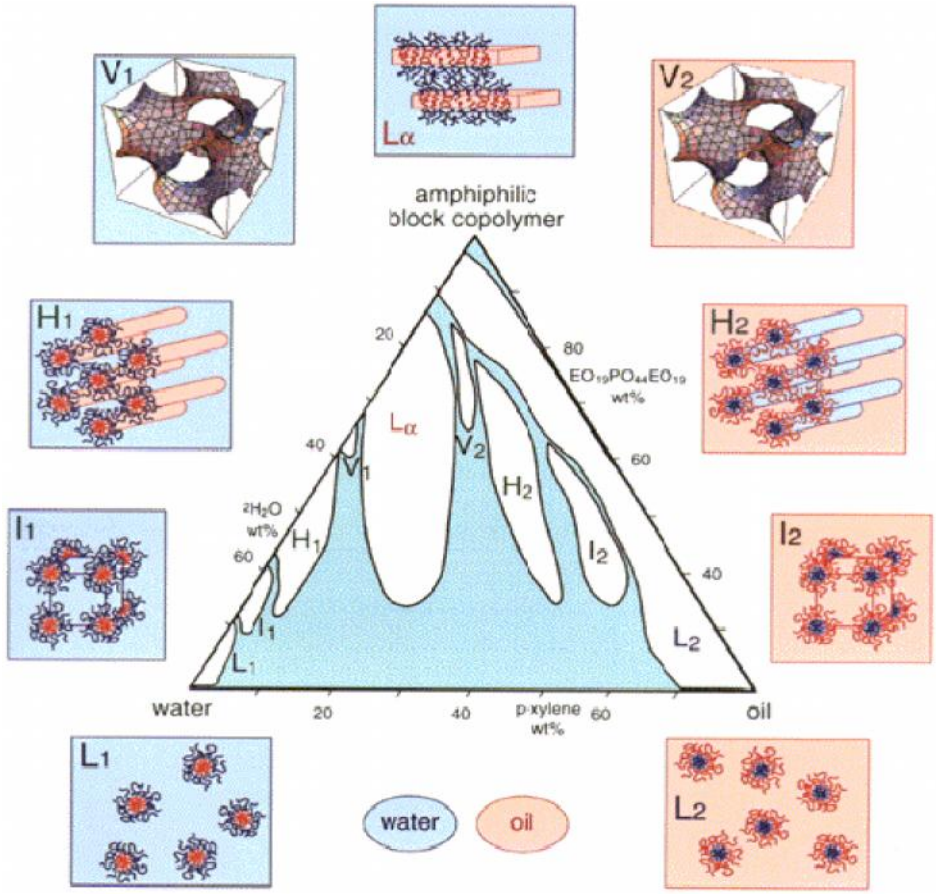

Figure 1.2. Phase diagram showing the structural polymorphism in the PEO-PPO-PEO microemulsion system used as templates for making semiconductor nanostructure (Alexandridis et al., 1998).

An example of this method to form ZnSe Qdots is the microemulsion gas contacting method. A schematic of the mechanism is shown in Figure 1.3. In this method, a microemulsion formed by self-assembly of n-heptane (with dissolved diethyl zinc) as the non-polar dispersed phase, formamide as the polar continuous phase and PEO-PPO-PEO as the surfactant is used. PEO is the polar soluble part and PPO the non-polar soluble part of the surfactant. Hydrogen Selenide gas, diluted in Hydrogen gas, is bubbled through the microemulsion at room temperature and atmospheric pressure. The Selenide

gas diffuses through the continuous phase to the interface of the dispersed phase droplets and reacted with the diethyl zinc to form ZnSe nuclei which coalesce and grow to form a single nanocrystal inside each droplet.

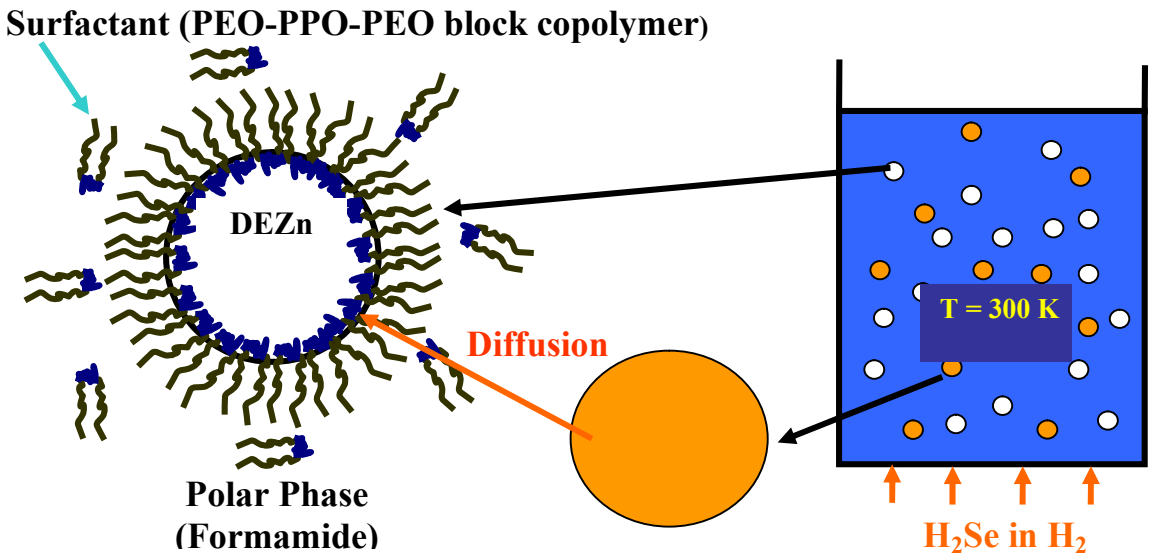

Figure 1.3. Schematic of microemulsion-gas contacting method for quantum dot synthesis (Karanikolos, 2005b)

Another broad category of synthesis methods for making semiconductor nanocrystals are the vapor phase methods. These include Molecular Beam Epitaxy (MBE), Metal-Organic Vapor Phase Epitaxy (MOVPE) and synthesis in a counter flow jet reactor.

In the MBE method, pure elements such as gallium, arsenic etc are heated in an effusion cell and the vapors condense and react on a wafer surface to form a thin film of semiconductor layer. The reactor is kept under ultra high vacuum to prevent impurity incorporation into the film. Quantum dots can be formed by spontaneous breakup of a very thin film (Ledenstov et al., 1998). In the MOVPE method, vapors of organometallic liquids and other precursor gases are brought into contact with a heated substrate leading

to the reaction on the surface and deposition of a thin film which break up to form quantum dots (Ozasa et al., 1997). This process provides lesser control than the MBE, but produces faster epitaxial growth and has lower capital and operating costs.

Nanocrystals have also been produced in a counter flow jet reactor. Here, vapors of organometallic and other precursor gasses diluted with carrier gasses, introduced from opposite streams of the reactor, form a stagnation flow pattern where they meet. Nucleation of the compound semiconductor material starts near the stagnation point. The particles grow by coagulation and surface reactions as they flow in the radial direction away from the stagnation point and form aggregates which are collected on substrates (Gupta et al., 1996).

1.4 Simulation of Nanoparticle Synthesis

The synthesis of nanoparticle formation inside the droplets of microemulsion is simulated in this work using a lattice Monte Carlo model developed. The Monte Carlo Method is amongst the ten algorithms that have had the greatest influence on the development and practice of science and engineering in the 20^{th} century (Beichl and Sullivan, 2000). The most commonly used flavor of the Monte Carlo Algorithm is the Markov Chain Metropolis Algorithm (Metropolis et al., 1953, Hastings, 1970).

The Monte Carlo method was initially developed to numerically solve problems in statistical physics, nuclear and particle physics. It was particularly well-suited to take advantage of the recent tremendous increase in the computational power so as to provide a numerical method of solving complex problems involving large number of dimensions (Allend and Tildesley, 1987). These methods attempts to sample experiments statistically

to solve complex mathematical problems. The most common application of these methods in materials science is to obtain thermodynamic properties of materials by performing experiments which attain equilibrium structures.

MC methods have been developed to study kinetic or non-equilibrium phenomena. The most important aspect here is to obtain a complete list of possible events and accurate kinetic rates for them (Fichthorn and Weinberg, 1991). The time scale of movements of atoms or molecules are typically very small leading to a low sampling of all the possible configurations. In most physical systems the time scales of the vibrations of molecules and macroscopic process are widely separated. Molecular Dynamics (MD) and full MC simulations become too computationally costly in such situations (Chatterjee and Vlachos, 2007). Hence, lattice Monte-Carlo methods (LMC) have been developed to obtain the solution in computationally efficient way. In LMC, the motion of particles is discretized in space by restricting it to be only possible on lattice points.

We have developed a LMC model to understand the formation of ZnSe QDots inside the droplets in the microemulsion-gas contact process. The details of the LMC model are described in Chapter 2.

1.5 Thesis Objective and Summary

This thesis aims at providing an understanding of the formation of nanoparticles by diffusion and coalescence inside a microemulsion droplet in a templated synthesis process (Karanikolos et al., 2004). A LMC model is developed to describe the diffusion of precursors, their reaction at the interface and the subsequent diffusion and coalescence of clusters to form a single particle inside a microemulsion droplet. The probability of

formation of $(ZnSe)_1$ nuclei by reaction between the two precursors and the probability of coalescence during collisions between $(ZnSe)_k$ (k = 1,2,...) clusters were the two parameters used in the model. The LMC model was used to simulate the synthesis of ZnSe QDots of size upto 7nm and the mechanism of formation was obtained. The dependence of the final particle formation time on the initial precursor concentration was explained by obtaining cluster size distribution and relative sizes of various clusters. Finally, a thermal analysis of coalescence between these clusters was studied to understand the energy release occurring in the process which enables the final nanoparticle synthesis.

In Chapter 2, a lattice Monte-Carlo simulation technique of zinc selenide (ZnSe) nanocrystal synthesis by a microemulsion-gas contacting technique (Karanikolos et al., 2004, 2005, 2006) is discussed. Particle synthesis takes place inside droplets of a microemulsion formed by self assembly of a ternary system consisting of heptane as the dispersed phase, formamide as the continuous phase, and an amphiphilic tri-block copolymer (polyethylene oxide, polypropylene oxide, polyethylene oxide) as surfactant. Such microemulsions consist of highly monodisperse droplets that exhibit very slow droplet-droplet coalescence kinetics.

They are ideal templates for nanocrystal synthesis, because they can isolate a particle formed inside a single droplet, from those in neighboring droplets, thus preventing particle aggregation. This template enables the growth of a single QDot in each droplet whose size is controlled by the concentration of a precursor that is dissolved in the solvent forming the dispersed phase of the microemulsion. Nucleation occurs by an irreversible reaction between the precursor dissolved in the droplet and a second

precursor supplied through the droplet interface. The nuclei subsequently diffuse and coalesce to form clusters and ultimately a single particle.

The LMC model is simulated on a droplet whose typical size is of the order of 40nm. The diffusion of precursor molecules and clusters are modeled as Brownian motion on the lattice. A hard sphere interaction potential is used with allowance for coalescence between clusters. The diffusivity of the particles is calculated based on Stokes Einstein Equation and the size of the clusters is calculated assuming all clusters achieve a spherical shape with the volume based on a Zinc Blende structure. The predictions of the LMC model for a test problem agreed well with a deterministic solution. The formation time of QDots ranging in size from the smallest possible (a cluster containing two Zn and two Se atoms) to a 7nm diameter nanoparticle is calculated. The formation of a relatively large intermediate cluster during synthesis of larger QDots in comparison to smaller ones is shown to lead to acceleration in the formation of larger size QDots. The results varying the parameters of the model as well as physical parameters such as diffusivity of the medium were investigated and a generalized dimensionless correlation obtained.

In Chapter 3, we used the LMC model to investigate the coalescence kinetics of clusters during nanoparticle synthesis. The motivation was to understand the role of the interfacial nucleation in the final nanoaparticle formation. Two cases of nucleation were investigated (1) the simulation starting with randomly distributed population of nuclei and (2) the case where the precursors diffuse to the interface and the subsequent nuclei diffuse and coalesce to form the nanoparticle. The intermediate cluster size distribution and radial distribution is investigated to understand the difference in the kinetics of the

two cases. Expression for the evolution of the total and intermediate cluster numbers were obtained based on Brownian coalescence of particles in infinite domain using corrections to the terms to account for the finite domain size and polydispersity of cluster sizes.

In Chapter 4, we present a thermal analysis of coalescence of clusters during the formation of ZnSe QDots. The energy released due to reduction in surface area during coalescence leads to an increase in the nanoparticle temperature which is dissipated to the surrounding. The temperature evolution of the coalescing nanoparticle is obtained. The effect of the size of the coalescing nanoparticles on the temperature of the particle was studied. The time for complete coalescence indicates that atleast for coalescence of bigger nanoparticles, the coalescence of clusters may take about the same time as the time for nanoparticle synthesis by collision.

The results are summarized in Chapter 5 and some future directions of extension of this work is discussed. In Appendices, the property values of ZnSe used in the study and the results for the lattice independence of the Monte-Carlo model are presented.

CHAPTER 2

MODELING AND SIMULATION OF NANOCRYSTAL SYNTHESIS

2.1 Introduction

There has been a tremendous interest in synthesis of semiconductor nanocrystals due to their unique size-dependent optical and electronic properties. The efforts have focused on developing synthesis methods to control the final structure and size of the nanocrystals (Murray et al., 1993) and to develop novel nanostructures such as quantum wires and wells (Gudiksen and Lieber, 2000; and complex assemblies (Alivisatos, 1996). The conventional synthesis method involves the hot injection of precursors and their reaction in the colloids in the presence of surfactants which control the nanocrystal size (Murray et al., 1993). Microemulsions (Lianos and Thomas, 1986) and reverse micelles (Petit et al., 1993) have been used as templates for various metal, oxides and semiconductor nanoparticles.

Modeling of nanoparticle formation in templates has focused on the mixing of two microemulsions or micellar solutions, each containing a reactant in the dispersed phase, and enabling particle formation through collision and coalescence of droplets or micelles. Tojo et al. (Tojo et al., 1997a, b) and de Dios et al. (de Dios et al., 2009) developed a Monte Carlo method to study the kinetics of particle formation after mixing two microemulsions, each containing a separate reactant, and conducted parametric studies of the effect of process variables on the particle size distribution. Monte Carlo schemes for simulating precipitation reactions by mixing two reverse micellar solutions were proposed by Li and Park (Li and Park, 1999) and, in a more general form, by

Bandyopadhyaya, et al. (Bandyopadhyaya, et al., 2000). Population balance models and Monte Carlo simulations of the synthesis of CdS nanoparticles by mixing two water-in-oil microemulsions have been presented and compared with experimental data (Jain and Mehra, 2004; Jain et al., 2005; Ethayaraja and Bandyopadhyaya, 2006).

ZnSe QDots have been synthesized inside the droplets of a microemulsion template formed by self-assembly of a tri-block copolymer surfactant at the interface between a polar solvent (formamide), that forms the continuous phase, and a non-polar solvent (n-heptane), that forms the dispersed phase (Karanikolos et al., 2004). In this system, the concentration of diethylzinc dissolved in the heptane droplets determines the final size of the ZnSe QDot that can be formed in each droplet. The conversion of diethylzinc to ZnSe is carried out by bubbling hydrogen selenide gas through the microemulsion. The hydrogen selenide dissolved in the formamide continuous phase diffuses through the block copolymer layer and undergoes an irreversible reaction with diethylzinc to form ZnSe nuclei at the droplet interface that subsequently diffuse inside each droplet and gradually coalesce to form a single QDot.

A schematic showing the process taking place around the microemulsion droplet is shown in Figure 2.1. In a typical experiment, a microemulsion containing 40nm heptane droplets was used (Karanikolos et al., 2004). The Zn precursor (diethylzinc) was dissolved in heptane and the Se precursor (hydrogen selenide) was bubbled through a microemulsion diluted in hydrogen carrier gas. Particle nucleation was initiated by the spontaneous irreversible reaction at the droplet interface between diethylzinc and hydrogen selenide producing ZnSe nuclei which, in turn, became the ingredients for the formation of clusters and, eventually of a single nanoparticle in each droplet by particle-

particle coalescence. In this system, the concentration of diethylzinc dissolved in the heptane droplets determines the final size of the ZnSe QDot that can be formed in each droplet.

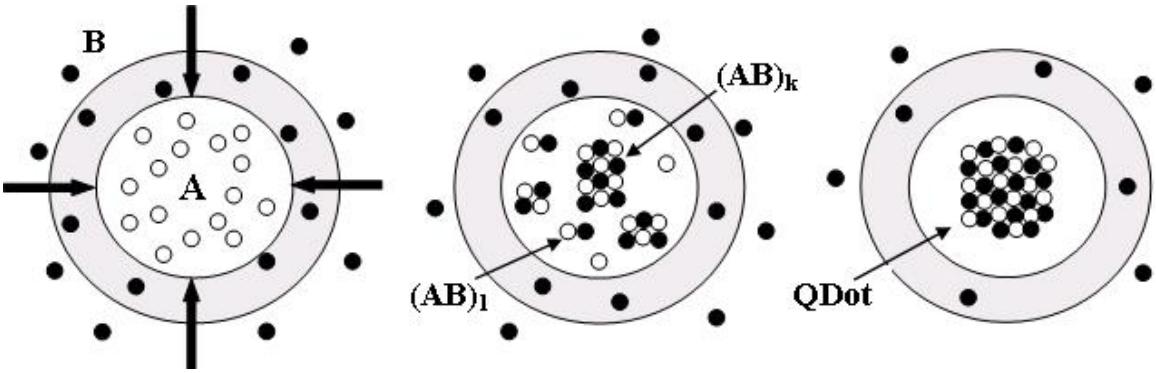

Figure 2.1. Schematic of the formation of a single semiconductor nanocrystal in a microemulsion droplet. Reactant A is dispersed in the droplet and reactant B diffuses from the continuous phase to the droplet interface. An irreversible reaction at the interface produces $(AB)_1$ nuclei, that coalesce into $(AB)_k$ clusters, and eventually form a single particle (QDot).

In this chapter, a lattice Monte-Carlo simulation technique of zinc selenide (ZnSe) nanocrystal synthesis by a microemulsion-gas contacting technique is developed. In Section 2.2, the details of the lattice Monte-Carlo (LMC) model to simulate the nanoparticle synthesis inside the microemulsion droplet is discussed in detail. The model is first used to simulate diffusion of mass out of a sphere with mass sink at the surface and the predictions are compared with the analytical results in Section 2.3. In Section 2.4, the results of simulating the actual synthesis of semiconductor nanocrystals in a microemulsion droplet are presented. For typical ZnSe QDots with sizes ranging from 2-7nm, the predicted final particle formation time decreases as the particle size increases. This behavior can be attributed to the formation of a "sweeper" cluster in the droplet that appears to serve as an efficient collision partner for the smaller ones. The analysis of cluster size distributions during formation of quantum dot of diameter 7nm is used to

elucidate the underlying coalescence mechanism. The results of a parametric study performed to investigate the effect of particle diffusivity, droplet size, cluster-cluster coalescence probability, and probability of nucleation on the final particle formation time is given in Section 2.5. A dimensionless equation is obtained that relates the formation time of the final particle to its size for different operating parameters like droplet diameter and solute viscosity. Finally, the results are summarized in Section 2.6.

2.2 Model Description

A LMC model has been developed to describe the formation of a single semiconductor nanocrystal (QDot) inside a microemulsion droplet during templated synthesis (Kuriyedath et al., 2010a). The LMC model describes the random motion of a number of diethylzinc molecules (A) in a spherical domain, their reaction with hydrogen selenide molecules (B) at the droplet interface to yield $(AB)_1$ nuclei, the growth of nuclei by coalescence into $(AB)_k$ (k=2,3,…) clusters and the formation of a single final particle. The cluster-cluster interactions are modeled by a hard-sphere potential. The domain is discretized using a cubic lattice.

It is assumed that a species containing one Zn and one Se atom is the nucleus for particle formation, based on the fact that the reaction between diethylzinc and hydrogen selenide is spontaneous and irreversible at room temperature. The nuclei subsequently coalesce into clusters whose stability typically increases with size. There is experimental evidence that certain $(AB)_k$ clusters of II-VI compounds, such as CdSe, are ultra-stable at specific values of k ("magic clusters") due to the formation of a core-cage structure that eliminates dangling bonds from the surface of the cluster (Kasuya et al., 2004). In the

LMC simulation discussed here we assign a uniform probability of coalescence to all clusters.

The A molecules, $(AB)_1$ nuclei, and $(AB)_k$ clusters formed after coalescence are considered to occupy lattice points placed at the center of each unit cell. Multiple occupancy by A molecules is allowed as long as their total volume does not exceed that corresponding to random packing of equally sized spheres (that is, 0.64) in that unit cube (Jaeger and Nagel, 1992; Torquato et al., 2000). Larger clusters can occupy volumes that are bigger than a unit cell, and thus render neighboring lattice points inaccessible to other particles, to prevent overlap. A unit cell centered around a lattice point is shown in Figure 2.2.

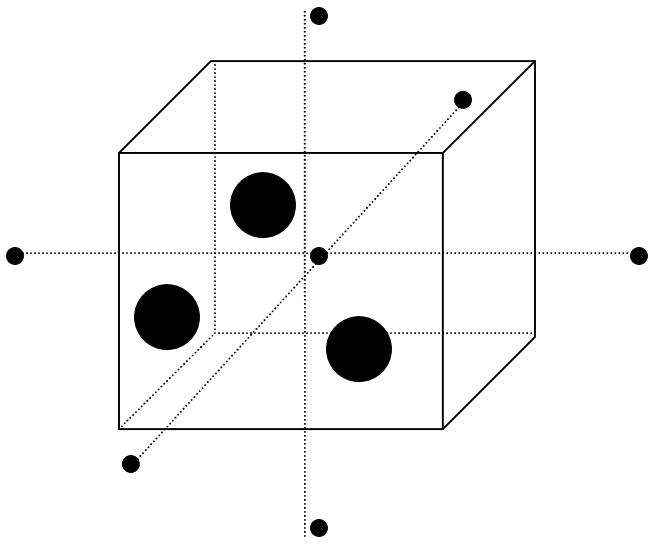

Figure 2.2. A unit cell surrounding a lattice point containing precursor molecules. Multiple occupancy by the precursor molecules is allowed as long as the fraction occupancy does not exceed the random packing limit of equal sized spheres.

A typical LMC simulation is initiated by randomly distributing a certain number of A molecules on the lattice. At each computational step, each molecule is allowed to move randomly to any of the 6 neighboring lattice points if the occupancy limit is not

exceeded due to that move. The A molecules arriving at the droplet interface are allowed to react with B molecules that have arrived by diffusion through the surfactant layer. In this study we assume that B molecules are always in excess at the droplet interface. The flux of B molecules to the droplet interface can be used as a parameter to control the rate of nucleation reaction in an experimental system. When the probability of nucleation is unity, every A molecule that arrives at the droplet interface is converted to an AB nucleus. The AB nuclei move on the lattice following the same rules as the A molecules and undergo coalescence. At each LMC step, a probability is computed for each $(AB)_k$ ($k \geq 1$) cluster to move on the lattice. This probability is computed by using the relative diffusivity of each cluster with respect to the smallest particle present in the lattice (which includes the A molecules):

$$P_i = \sqrt{\frac{D_i}{D_s}} \quad ; \quad i=1,2,\ldots m \tag{2.1}$$

Here P_i is the probability of the i-th particle to move, D_i its diffusivity, m the total number of particles present, and D_s the diffusivity of the smallest particle present in that step. The interface is assumed to be impermeable to clusters. As a result, clusters can only move along the interface or towards the interior of the droplet. We assume that the A and B molecules do not diffuse through the droplet interface, but only react there. This assumption is valid when the solubility of A molecules in the continuous phase and B molecules in the dispersed phase is small.

All precursors and clusters are given the opportunity to move during a certain LMC step. When a move is attempted, the algorithm checks for overlap with particles that may already occupy part of the volume of the neighboring cell. A precursor will not

move if the available free volume in the neighboring cell is not sufficient to accommodate it without exceeding the maximum allowable volume fraction value of 0.64. A cluster will move only if there is sufficient free volume available in the cell to which it is moving. It will be given the opportunity to coalesce with any cluster whose distance from the center of that cell is less than the sum of the radii of the two clusters. A coalescence event will be rejected and the particle will not move from its initial position, if the probability of coalescence is less than unity and a random number generated between 0 and 1 comes out to be larger than the probability of coalescence. A cluster that has been formed by coalescence during an LMC step is given the opportunity to move during the same LMC step and possibly coalesce again, if at least one of its original components was not already given the opportunity to move during the same LMC step. As a result, a cluster can coalesce multiple times during a single LMC step.

The wall-clock time interval, $(dt)_i$, corresponding to a computational step is calculated by using the following expression:

$$(dt)_i = \frac{l^2}{6D_s} \tag{2.2}$$

where l is the LMC lattice spacing, and D_s the diffusivity of the precursor or smallest cluster present in the droplet. The value of the lattice spacing, l, was selected by testing various lattice sizes and studying their effect on the final particle formation time. All LMC simulation results discussed here were obtained using a value of the lattice spacing equal to the diameter of an $(AB)_1$ nucleus. The optimal lattice spacing was selected as follows: We started with a lattice spacing of 4nm and performed several LMC simulations for various particle sizes recording the final particle formation times for each case. We repeated the LMC simulations using progressively smaller lattice spacing and

for each case we computed the root mean square (rms) difference between the new values of predicted final particle formation time minus the ones obtained from the initial LMC simulation that employed a lattice spacing of 4nm. This rms difference initially increases rapidly as the lattice spacing is decreased and starts forming a plateau at a lattice spacing equal to 2nm. Further reduction in the lattice spacing to 1nm and 0.44nm (equal to the estimated diameter of a $(ZnSe)_1$ nucleus) produced rms difference values that are within 5% of each other, and within 10% of the value corresponding to a lattice spacing of 2nm. A smaller lattice spacing of 0.4nm produced vitually identical results to the ones obtained using 0.44nm lattice spacing. The latter value, that corresponds to the estimated diameter of a $(ZnSe)_1$ nucleus, was thus chosen as the optimal lattice spacing for all LMC simulations to ensure lattice-independent predictions. Further details are presented in Appendix A.2

Coalescence of clusters occurs by collision, as determined by volume overlap. The probability for coalescence after a collision is treated as a physical parameter of the simulation ranging from 1 to 0. The effective diameter, d, of a cluster containing N atoms of A and an equal number of B atoms, was calculated from

$$d = \left(\frac{3N}{2\pi} \right)^{\frac{1}{3}} \lambda \qquad (2.3)$$

where λ is the lattice constant of the AB crystal. In the LMC simulations discussed here, all clusters were treated as spheres whose volume is equal to the volume of a ZnSe zinc blende (cubic) lattice consisting of N atoms of Zn and N atoms of Se. This approximation is more accurate for larger clusters, which have a sufficient number of Zn and Se atoms, and can attain a zinc blende crystalline structure. Smaller clusters typically

try to form closed-cage structures to minimize the number of dangling bonds on their surface (Kasuya et al., 2004).

The diameter of the final particle, d_p, was scaled with the droplet diameter, (d_D=2R):

$$\delta = \frac{d_p}{(2R)} \tag{2.4}$$

where δ is the dimensionless particle formation time.

The wall-clock time was scaled using the characteristic time for diffusion of the final particle. The elapsed dimensionless time corresponding to the end of the j-th LMC step, τ_j, was obtained from

$$\tau_j = \frac{\sum_{i=1}^{j} (dt)_i}{\left(\frac{R^2}{D_p}\right)} \quad ; \quad j=1,2,\ldots,n \tag{2.5}$$

where n is the total number of LMC steps corresponding to the formation of a single final particle, D_p is the diffusivity of the final particle, and R is the radius of the droplet. τ_p is the dimensionless time for formation of a single particle when the LMC simulation finishes. The characteristic time was chosen in analogy to the characteristic time for the diffusion of A molecules in a spherical domain. Using the diffusivity of an appropriate "average" particle, instead of the final one, would be more appropriate; yet such estimation cannot be obtained experimentally with currently available instrumentation. Using the diffusivity of the final particle is a reasonable approximation because the final particle formation time is largely determined by the slow coalescence of the last few

clusters, which typically include a large "sweeper" cluster with size and diffusivity not very different from the final particle.

The diffusion of A molecules, AB nuclei, and clusters in the droplet is assumed to be governed by Brownian motion. The diffusivity, D_i, of a particle with an effective diameter, d_i, is calculated using the Stokes-Einstein equation

$$D_i = \frac{k_b T}{3\pi\mu d_i} \tag{2.6}$$

where k_b is Boltzmann's constant, T the absolute temperature, and μ the viscosity of the medium in the droplet.

The LMC model tracks the evolution of individual cluster sizes and their number density during nanoparticle formation. It provides a detailed dynamic picture of the process which is currently impossible to obtain experimentally, and enables studies of the effect of various process parameters on the evolution of clusters and the final particle formation time.

The numerical values of the physical and computational parameters used in the LMC simulations are as follows: Droplet diameter (d_D) =10-40nm, lattice spacing (l) =0.44nm, lattice parameter constant of ZnSe (λ) = 0.5667nm, temperature (T) = 300K, and viscosity of heptane (μ) = 0.38cP at 300K. The diffusivity of diethylzinc in n-heptane was calculated using the Lusis-Ratcliff correlation (Reid et al., 1977) and a Le Bas molal volume for Zn equal to 20.4cm^3/mol. The value obtained at 300K is D = 3.6x10^{-9}m^2/s. For comparison, the diffusivity of a $(ZnSe)_1$ nucleus was estimated using Equation (2.6) to be equal to 4.7x10^{-9}m^2/s.

2.3 Model Validation

The accuracy of the LMC model was tested by simulating a test problem for which analytical solution exists with which the LMC results could be compared. The proposed LMC procedure was used to simulate the depletion of a species from a spherical droplet by reaction with a sink on the domain surface and comparing the results with a well-known, analytical deterministic solution. The LMC model was used to simulate the diffusion of A molecules toward the interface, where they undergo a reaction and are converted to immobile species. The results of the simulations were compared with the predictions of an analytical solution of a deterministic model obtained by writing the diffusion equation in spherical coordinates after invoking spherical symmetry (Crank J., 1956):

$$\frac{\partial \theta_A}{\partial \tau} = \frac{1}{r^2}\frac{\partial}{\partial r}\left(r^2 \frac{\partial \theta_A}{\partial r}\right) \qquad (2.7)$$

It was assumed that the initial concentration of A in the droplet was uniform:

$$\tau = 0 \qquad 0 < r < 1 ; \qquad \theta_A = 1$$

The concentration of A at the droplet interface was set to zero:

$$\tau \geq 0 \qquad r = 1 ; \qquad \theta_A = 0$$

Symmetry was assumed at the center of the spherical droplet:

$$\tau \geq 0 \qquad r = 0 ; \qquad \frac{\partial \theta_A}{\partial r} = 0$$

Here θ_A is the dimensionless concentration of A in the spherical droplet scaled by the initial concentration C_{A_0}, r is the dimensionless radius of the domain scaled by the

actual radius R, D_A is the diffusivity of A in the medium inside the spherical droplet, and τ is the dimensionless time scaled by the characteristic time for diffusion (R^2/D_A).

A series solution of Eq. (2.7) with the above boundary conditions was averaged over the radial coordinate, r, to obtain the dimensionless average concentration of A, $\overline{\theta}_A$, as function of dimensionless time:

$$\overline{\theta}_A = 6\sum_{n=1}^{\infty} \frac{e^{-n^2\pi^2\tau}}{n^2\pi^2} \tag{2.8}$$

The LMC predictions were validated by comparing them with Equation (2.8). This comparison was also used to validate the conversion of LMC steps to wall-clock time. Figure 2.3 shows the predicted dimensionless average concentration of A in the droplet as a function of dimensionless time. The LMC simulations were performed for a spherical droplet of heptane with a diameter of 40nm. The dimensionless average concentration of 30 LMC simulations is plotted using data from three 10-run batches, with each batch corresponding to an initial concentration of A equal to 0.025, 0.071, and 0.19 molar (M), respectively. These concentrations correspond to 505, 1436 and 3941 molecules of A inside the droplet and to a final particle size of 3.53nm, 5nm, and 7nm, respectively.

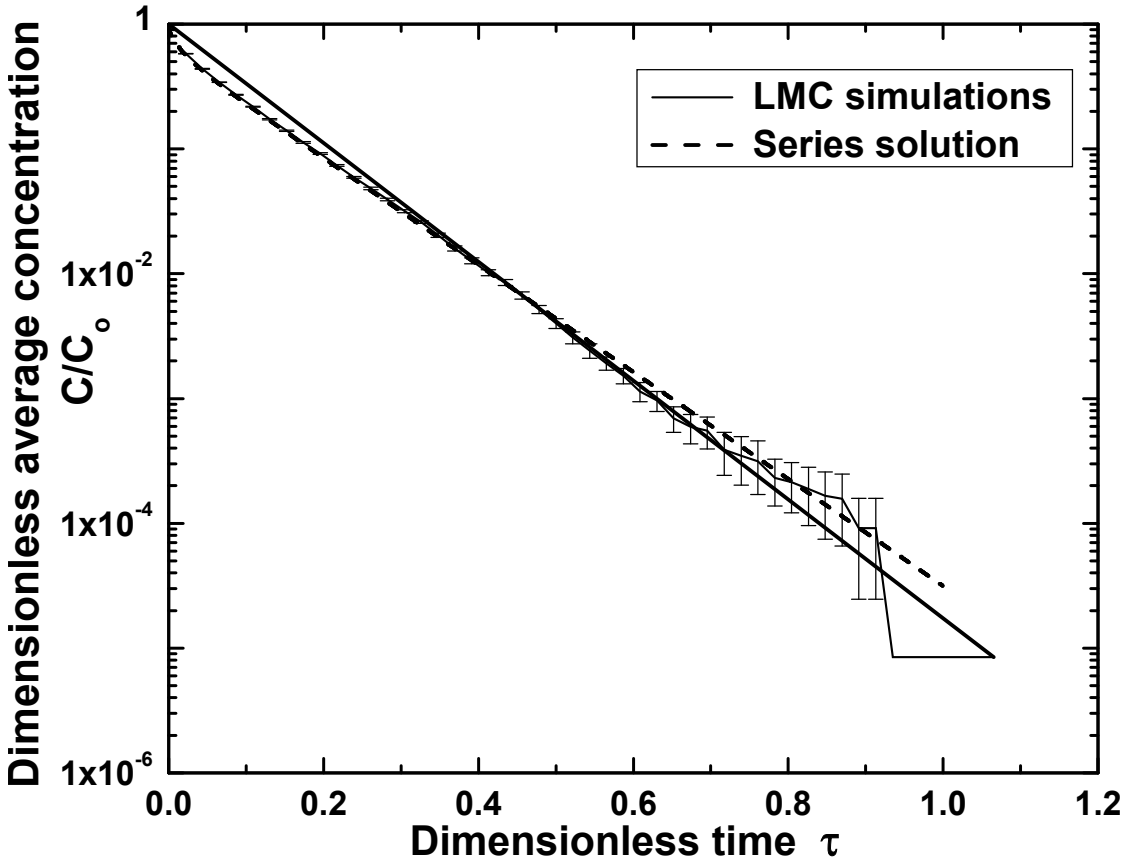

Figure 2.3. Model Validation: Comparison between LMC simulations and Equation (2.8) predictions for diffusion of a solute (diethylzinc) out of a droplet (heptane). The LMC data were collected for concentrations of diethylzinc equal to 0.025, 0.071, and 0.19 M in a droplet with a diameter of 40nm.

Early in the simulation, when the average concentration is high, the agreement between the LMC predictions and the analytical solution is excellent. As the average concentration drops, the statistical variance of the LMC predictions starts becoming larger due to small particle numbers, but the average of the 30 runs remains close to the analytical solution. Overall, there is a good agreement between the LMC simulation results with the analytical solution which validates the assumptions of the LMC model, giving confidence in extending it to the actual problem which involves the diffusion of the species and its coalescence to form bigger particles.

2.4 Simulation of Quantum Dot Synthesis

LMC simulations were performed to predict the dimensionless final particle formation time, τ_p, as a function of the dimensionless final particle diameter, δ, for a base case corresponding to a droplet diameter of 40nm, and probability of coalescence and nucleation reaction equal to unity. A droplet size of 40nm was chosen as the base case because it corresponds to the diameter of the microemulsion droplets used in the experiments (Karanikolos et al., 2004).

Figure 2.4 shows the predictions of the LMC simulations for final particle sizes ranging from that of $(ZnSe)_2$ up to 7nm. The formation time of each final particle size is the average of 10,000 LMC runs and the associated standard error is also shown. The formation time initially increases with final particle size, quickly reaches a maximum corresponding to the formation of a final particle consisting of five Zn and five Se atoms, $(ZnSe)_5$, and subsequently decreases as the final particle size increases. This behavior can be attributed to the formation of large "sweeper" clusters at the intermediate stages of coalescence during the synthesis of large particles. These large clusters, due to their larger surface area, appear to be more efficient collision targets for smaller clusters. For the droplet sizes considered here, the larger volume of the bigger clusters enables them to overcome the adverse effects of their reduced mobility leading to faster coalescence. Therefore, there is acceleration in the formation of a larger nanoparticle compared to a smaller one.

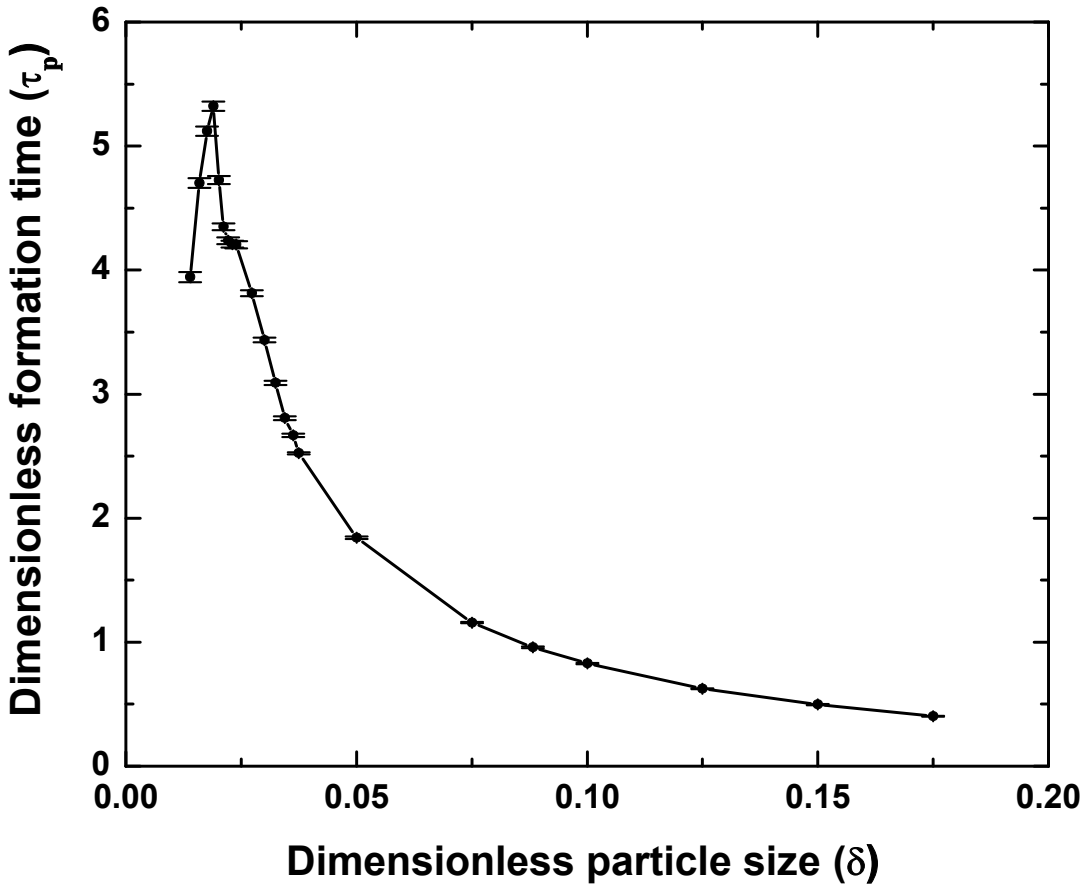

Figure 2.4. Dependence of dimensionless formation time on dimensionless final particle size from LMC simulations. By varying the initial Zn precursor concentration in the droplet, the final particle size was varied from $(ZnSe)_2$ to a ZnSe nanoparticle with diameter of 7nm. Domain diameter: 40nm.

2.4.1. Coalescence of large Quantum Dots

Figure 2.5 shows the evolution of the precursor concentration, the concentration of $(ZnSe)_1$ nuclei, $(ZnSe)_2$ clusters and the total cluster concentration in a typical LMC simulation for a droplet with diameter of 40nm and a final ZnSe particle diameter of 7nm. The nucleation of ZnSe at the interface is completed at least an order of magnitude faster than the total formation time. The consumption of Zn precursor molecules via the nucleation reaction that occurs at the interface takes about 10% of the total formation

time. The total number of clusters initially increases, passes through a maximum and subsequently decreases as the rate of coalescence surpasses the nucleation rate because of depletion of the precursor. The number density of any given cluster follows the same trend, as shown in Figure 2.5 for cluster sizes of 1 and 2. The initial increase is due to the formation of these clusters by coalescence of smaller ones or by the nucleation reaction for the smallest of them, the $(ZnSe)_1$ nuclei. As the number density of clusters increases, the coalescence of a certain size with all available clusters leads to a decrease in the particle number density and eventually in the elimination of that size from the population.

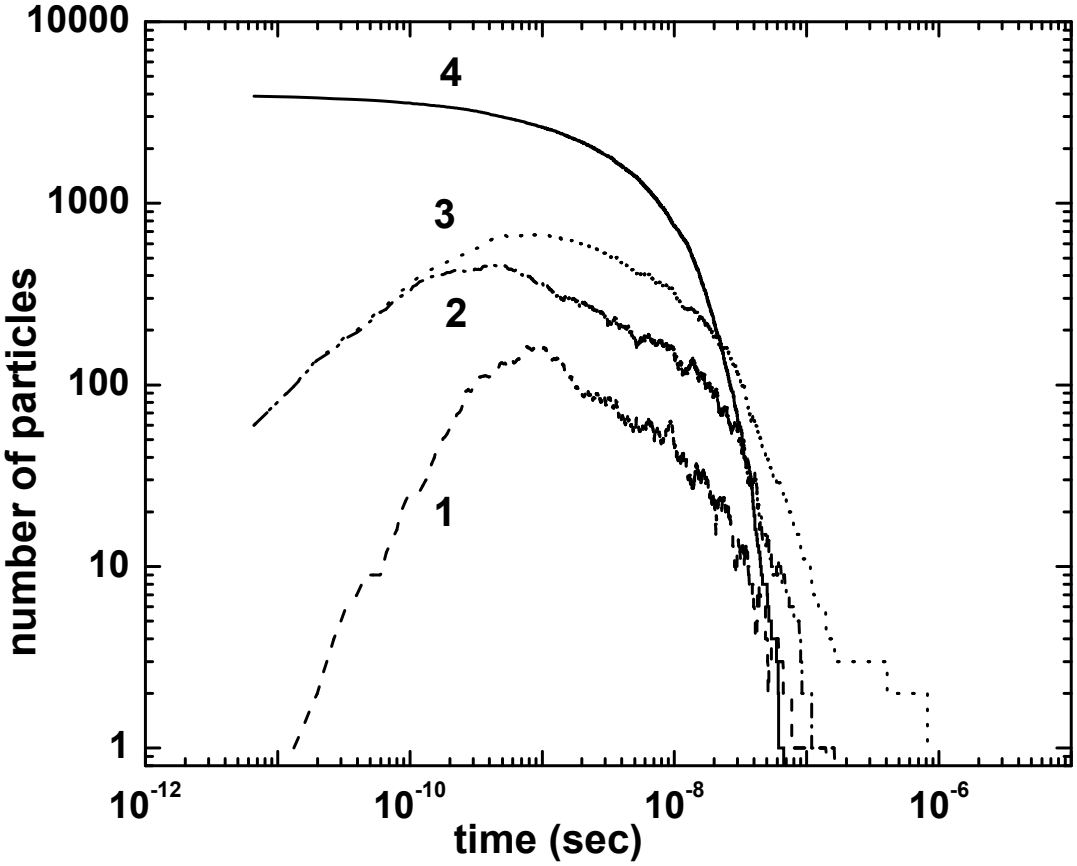

Figure 2.5. Particle number evolution predicted by LMC simulation of ZnSe QDot synthesis in a microemulsion droplet: (1) $(ZnSe)_1$ nuclei, (2) $(ZnSe)_2$ clusters, (3) all clusters (*m*), (4) Zn precursor molecules. Final ZnSe particle diameter: 7nm. Domain diameter: 40nm.

In Figure 2.6, we plot average cluster size distributions for process times that are longer than the time corresponding to the maximum in the total cluster number evolution shown in Figure 2.5. The results were obtained from 10 LMC simulations that were performed under the same conditions as of Figure 2.5. In the plots of Figure 2.6 the total cluster number (m) decreases from 400 to 5. The normalized number of clusters in each plot is obtained by dividing the number of clusters of each size by m. For m between 400 and 50 (Figures 2.6a, b, c and d), the number of smaller clusters (k=1-5) is significant and their numbers monotonically decrease with size. The number of larger clusters is smaller and exhibits significant run to run fluctuations both in size and number density, due to low total particle counts. For m=10 and m=5 (Figures 2.6e and f), the number density of small clusters starts exhibiting fluctuations, the distribution of intermediate clusters becomes sparse, and a single large cluster is present in the droplet, what we call a "sweeper" particle. Since the data plotted is the average of 10 LMC simulations, individual large cluster sizes have an average number density ranging from 0 to at most 2.

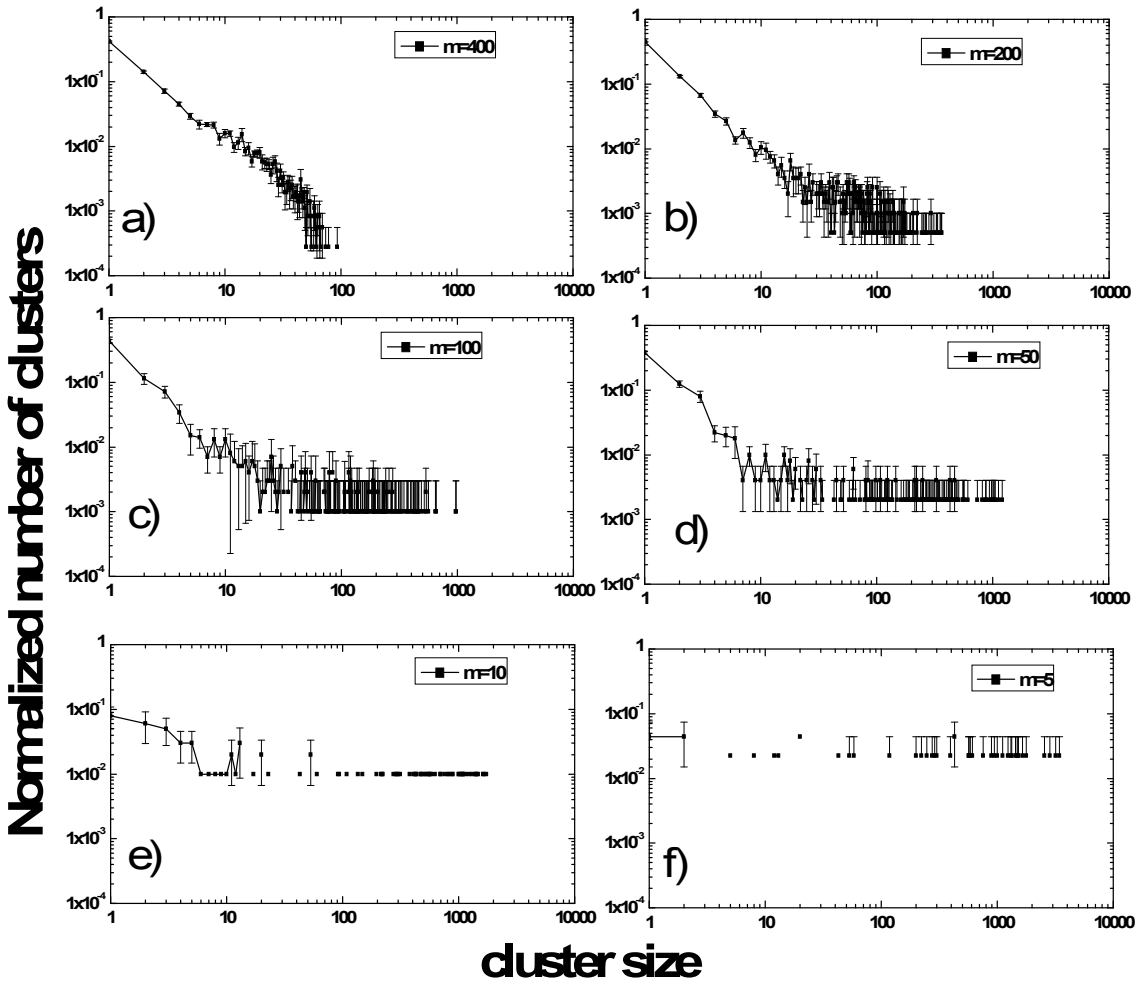

Figure 2.6. Average snapshots of normalized cluster size distributions at times corresponding to total cluster number (m) equal to: (a) 400, (b) 200, (c) 100, (d) 50, (e) 10, and (f) 5. The number of clusters of a certain size has been normalized by dividing it with m. Final ZnSe particle diameter: 7nm. Domain diameter: 40nm.

Towards the end of the process, if the few remaining clusters have relatively similar sizes, then their coalescence into a single particle takes longer to be completed. On the other hand, a less mobile larger cluster acts as an effective collision partner for the remaining ones and their coalescence into a single particle is faster. This indicates that collisions between a large and a small cluster would be more frequent than the collisions between two mid-size clusters of similar mass. This mechanism is also supported by results obtained from Langevin dynamics simulations of Brownian coagulation of

aerosols in an unconfined (infinite) domain. In that case, the calculated collision frequency of two particles of different size was larger than that of two similarly sized particles (Heine and Pratsinis, 2007).

2.4.2. Formation of "Sweeper" Cluster

To investigate the effects of the initial concentration of A molecules (and hence the final particle size), the relative sizes of the two clusters remaining before the last collision, a normalized diameter difference, (Δd), was defined as

$$\Delta d = \frac{(d_1 - d_2)}{d_p} \tag{2.9}$$

where d_1 is the diameter of the bigger cluster, and d_2 the diameter of the smaller cluster present just before the final collision leading to the QDot formation.

In Figure 2.7, the average value of (Δd) from 1,000 LMC base case simulations is plotted as function of dimensionless final particle size. The value of (Δd) increases monotonically with final particle size, indicating that the difference in size between the biggest and second biggest cluster, before the final collision, increases too. This supports the hypothesis of the formation of larger intermediate clusters during synthesis of bigger final particles. Hence, the rate of coalescence of the final few clusters is accelerated in the synthesis of bigger particles due to the formation of a large cluster which becomes a more efficient collision partner for the remaining clusters.

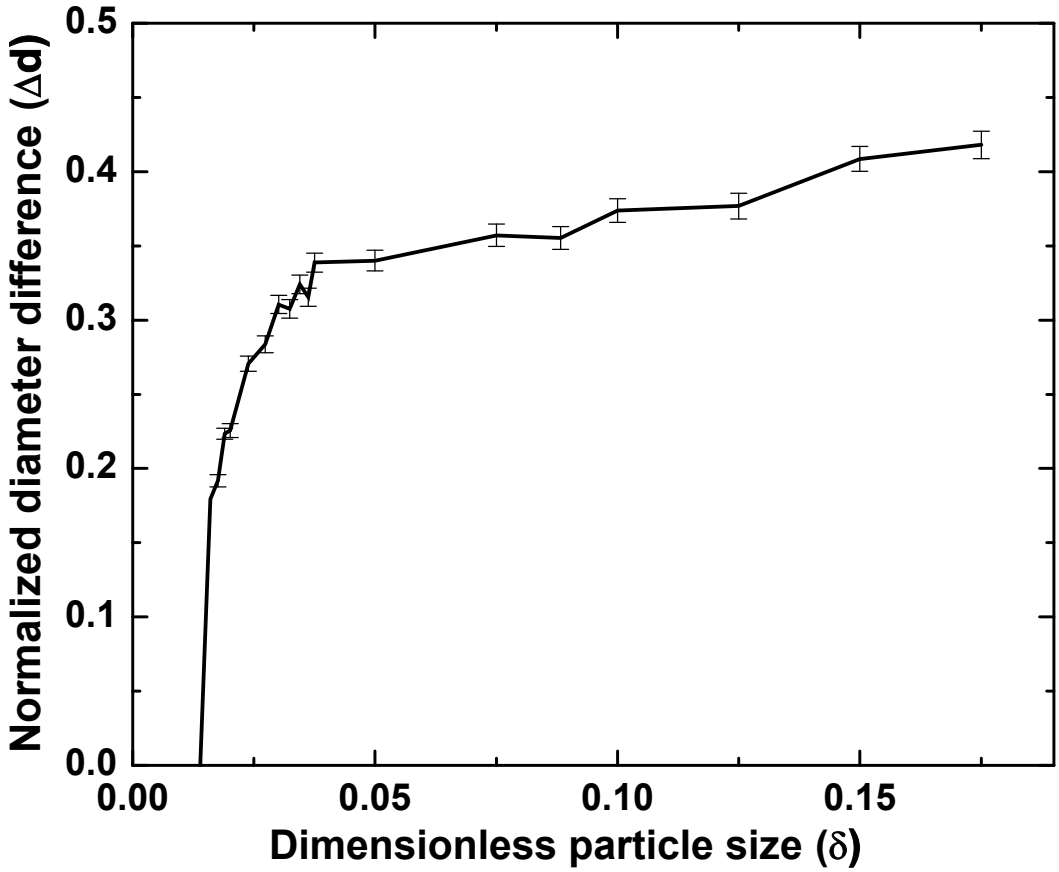

Figure 2.7. Normalized diameter difference between the two biggest clusters, before the last collision that yields a single final particle, as function of dimensionless final particle size. By varying the initial Zn precursor concentration in the droplet, the final particle size was varied from $(ZnSe)_2$ to a ZnSe nanoparticle with diameter of 7nm. Domain diameter: 40nm.

To investigate the effects of size and mobility of intermediately formed clusters on the final particle formation time, LMC simulations were performed for the following cases: (1) The base case. (2) A modified base case in which the cluster volume was artificially kept constant and equal to the value corresponding to a $(ZnSe)_1$ nucleus, whereas the diffusivity was allowed to vary with size. (3) A modified base case in which both the volume and diffusivity of all clusters were artificially kept constant and equal to

the values corresponding to a $(ZnSe)_1$ nucleus. In Figure 2.8, the results of 1,000 LMC runs for each of the above cases are compared.

For small final particle sizes, corresponding to the regime in which the final particle formation time increases with particle size, neither cluster volume nor cluster diffusivity appear to be important in determining the final particle formation time. In those cases, the concentration of precursor is small and, as a result, the variation of particle size and diffusivity of all cluster sizes is small. It is evident that the cluster volume is a more important quantity in determining the final particle formation time for large particles when compared to cluster diffusivity. When cluster volume is artificially kept constant, but the diffusivity is size-dependent (case 2), a significant increase in the final particle formation time is observed for large particles. The shortest formation times (and the maximum acceleration over case 2) are obtained for case 1. In case 3, the artificially high mobility of clusters causes accelerated particle formation thus overcoming the adverse effects of the artificially small cluster volume. The acceleration of particle formation due to the higher mobility in case 3 over case 2 is less than in comparison to case 1. This result indicates that larger clusters, although slow moving, are more effective collision partners for smaller clusters, for the droplet sizes considered here in the actual synthesis process.

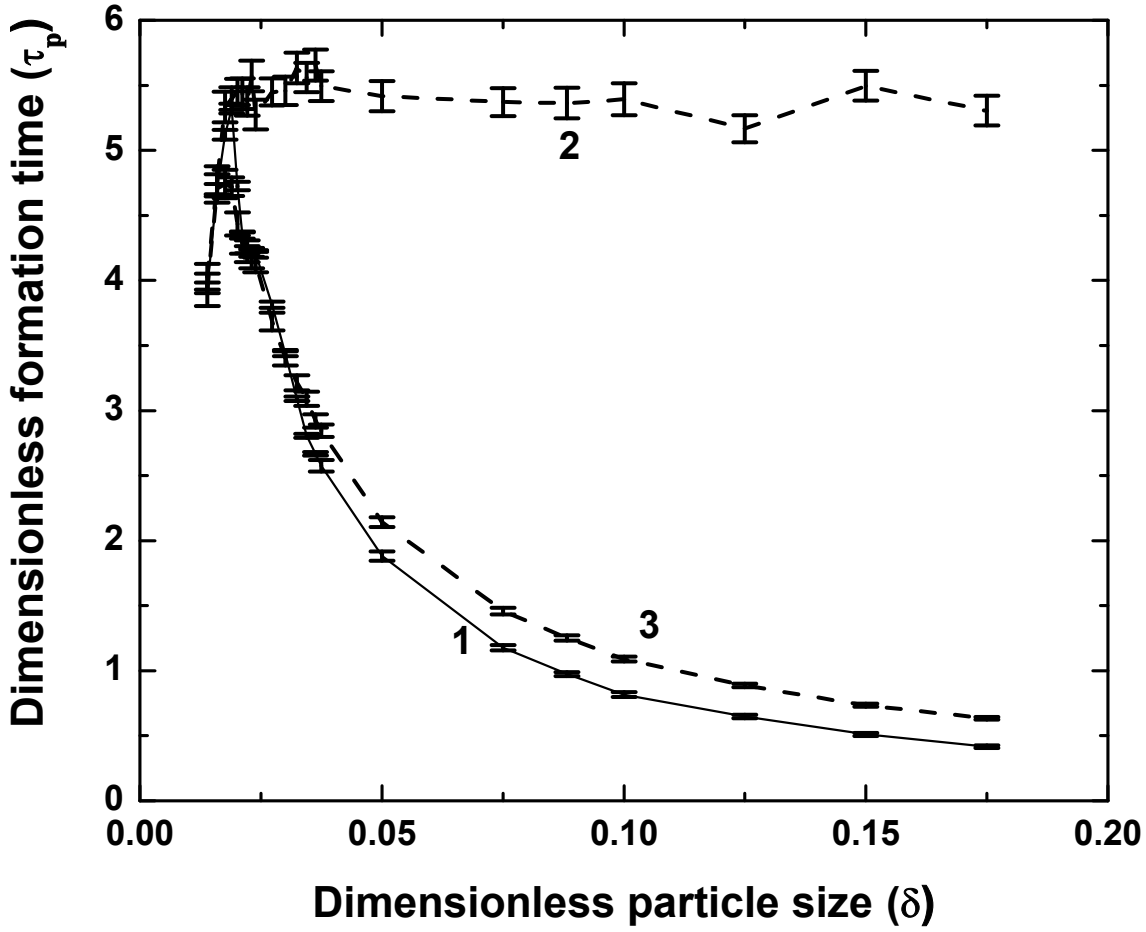

Figure 2.8. Dimensionless final particle formation time vs. dimensionless particle size for the following cases: (1) cluster volume and diffusivity are size-dependent (base case), (2) cluster volume is equal to that of a $(ZnSe)_1$ nucleus, but the cluster diffusivity is size-dependent, (3) cluster diffusivity and volume do not change and are equal to those of a $(ZnSe)_1$ nucleus. Same final particle sizes as Figure 2.4. Domain diameter: 40nm.

2.5 Parametric Studies

The sensitivity of final particle formation time to process parameters such as droplet size, diffusivity of precursor and cluster molecules, and probability of coalescence and nucleation was studied by LMC simulations. Four droplet sizes (10, 20, 30, and 40 nm) were used and simulations of particle formation of final sizes ranging from $(ZnSe)_2$ to 7nm were performed. The average scaled final particle formation time

from 10,000 LMC runs was plotted as a function of scaled final particle size in Figure 2.9. In each case, the behavior is similar to the one plotted in Figure 2.4. In all four cases, the maximum formation time corresponds to a $(ZnSe)_5$ particle and the dashed lines are used to connect data corresponding to smaller sizes. The data for particles larger than that size can be fitted reasonably well by the equation

$$\tau_p = 0.064\delta^{-1.13} \qquad (2.10)$$

as shown in Figure 2.9. For example, the average final particle formation time for the case corresponding to Figure 2.5 is found to be $(8.83 \pm 2.0)\text{x}10^{-7}$ s from the LMC simulations and $1.073\text{x}10^{-6}$ s from Eq. 2.16. Equation 2.16 is obtained by non-linear fitting of an allometric functional form on the data sets.

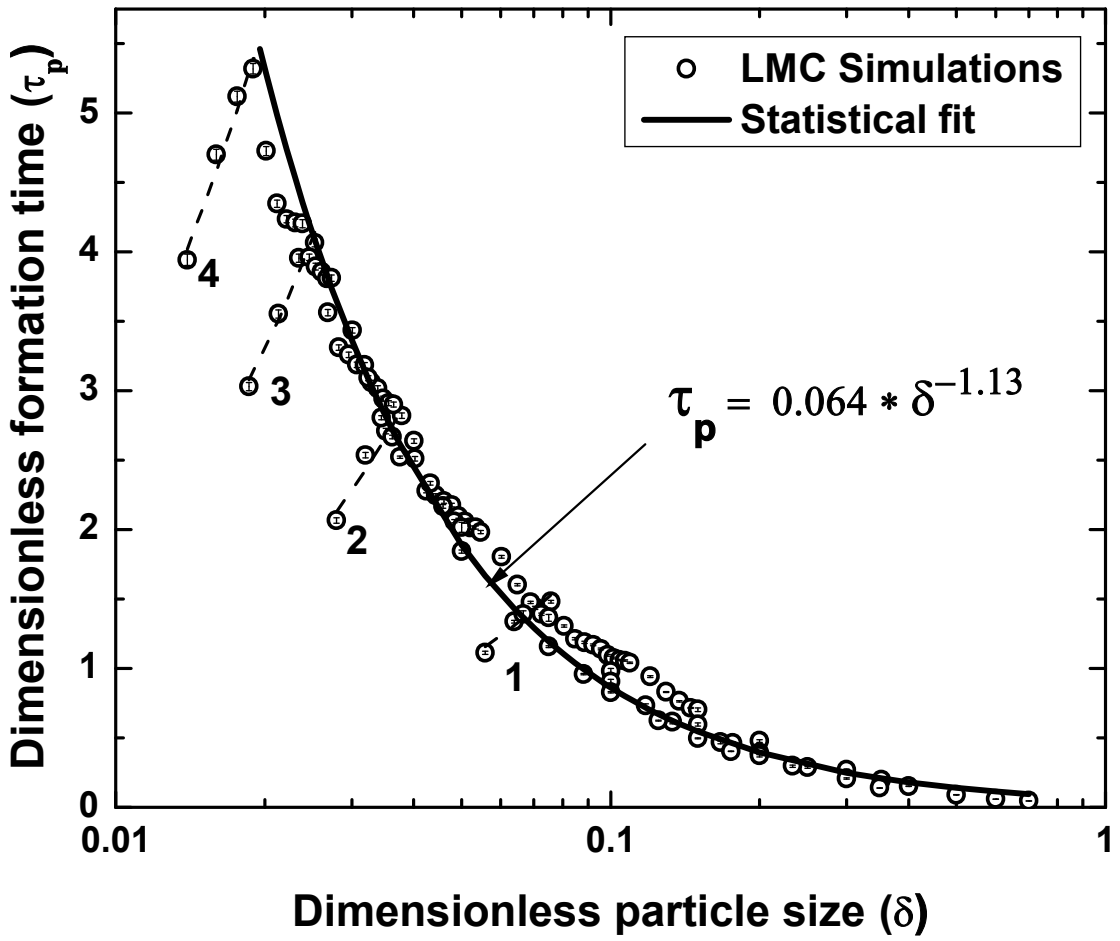

Figure 2.9. Fitting of LMC data to obtain a generalized equation for the dimensionless formation time as function of dimensionless final particle size for particles bigger than $(Zn\text{-}Se)_5$. Same final particle sizes as Figure 2.4. The LMC simulations correspond to droplet diameters (d_D) of (1) 10 nm, (2) 20 nm, (3) 30 nm, and (4) 40 nm.

The effects of changing the diffusivity of the precursor and clusters were also investigated to simulate the effects of changing the dispersing medium and to validate the proposed scaling. The first had diffusivity values multiplied by 0.1 and the second multiplied by 10. Three droplet diameters were used: 20nm, 30nm, and 40nm. The final particle diameter was varied from 1.5nm to 7nm, which is the practical range of sizes for growth of ZnSe QDots. The results on scaled final particle formation time vs. scaled final particle size obtained by averaging the data of 10,000 LMC runs for each final particle

size are plotted in Figure 2.10 together with the prediction from Eq. 2.16. It is evident that Eq. 2.16 approximates the LMC data reasonably well.

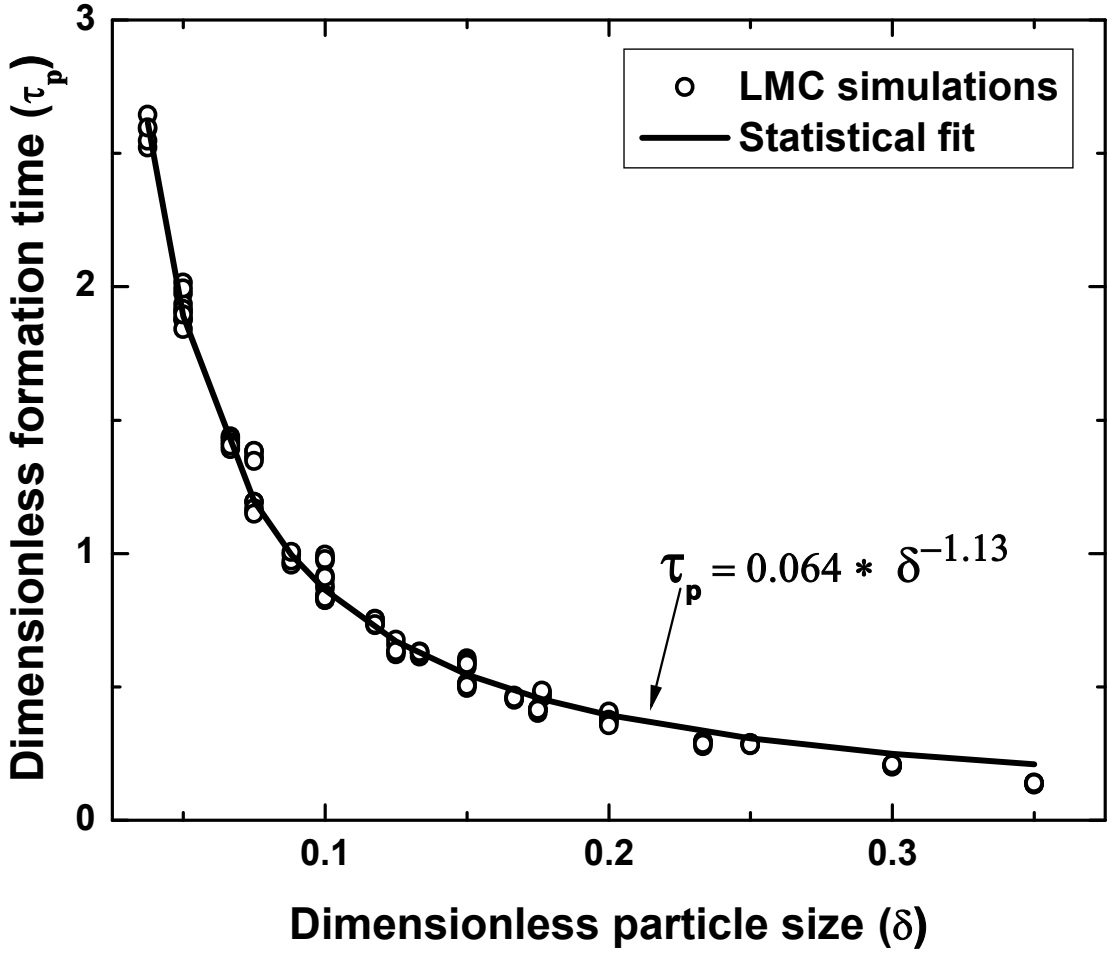

Figure 2.10. Dimensionless final particle formation time vs. dimensionless final particle size for three different droplet diameters: 20, 30 and 40 nm, and three different precursor diffusivities equal to 0.1, 1, and 10 times the base case value. Final ZnSe particle diameters: 1.5nm to 7nm.

The effects of changing the probability of reaction of precursor A with precursor B at the droplet interface, that produces $(ZnSe)_1$ nuclei, were investigated next. The LMC simulation results are plotted in Figure 2.11. The final particle formation time is relatively insensitive to the rate of the nucleation reaction. This is because the cluster-cluster coalescence takes much longer to yield a single particle compared to the time

required for complete consumption of precursor A by the nucleation reaction, as discussed in Figure 2.5. For reaction probabilities between 1 and 10^{-2}, the LMC simulations predict no significant changes in the final particle formation time (curve 1 in Figure 2.11). Only when the probability of the nucleation reaction was reduced to 10^{-3}, i.e. only when 1 in 1000 collisions of Zn precursor molecules and Se precursor molecules at the droplet interface resulted in the formation of a $(ZnSe)_1$ nucleus, did the formation time significantly increase, as shown in Figure 2.11 (curve 2). This analysis is also equivalent to reducing the interfacial flux of reactant B, which is a process parameter that can be controlled in an experimental system.

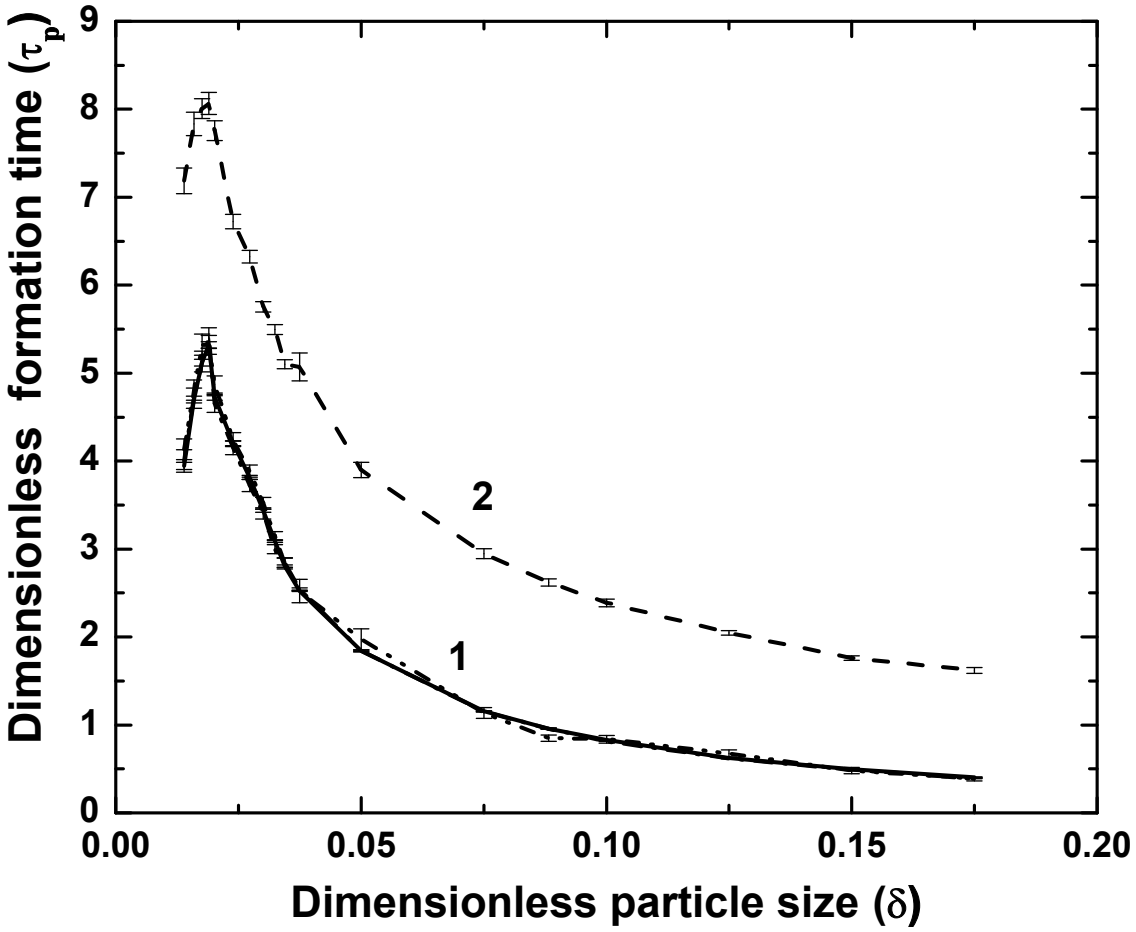

Figure 2.11. Dimensionless final particle formation time vs. dimensionless final particle size for various probabilities of the nucleation reaction: (1) 1.0, 0.1, and 0.01 (change

indistinguishable); (2) 0.001. Same final particle sizes as Figure 2.4. Domain diameter: 40nm.

The effects of the probability of cluster-cluster coalescence were also studied, and the results are plotted in Figure 2.12. In addition to the base case that corresponds to coalescence probability equal to 1, two additional cases corresponding to coalescence probability equal to 0.5 and 0.1 are also plotted. It is evident that as the probability of coalescence is decreased, the final particle formation time increases, and this effect is more pronounced for smaller final particle sizes. As the final particle size increases, the sensitivity of the formation time to the probability of coalescence decreases. For large final particles, the concentration of intermediate clusters in the droplet is high. This increases the collision frequency between a large sweeper cluster and other clusters, thus attenuating the adverse effects of smaller coalescence probability on final particle formation time.

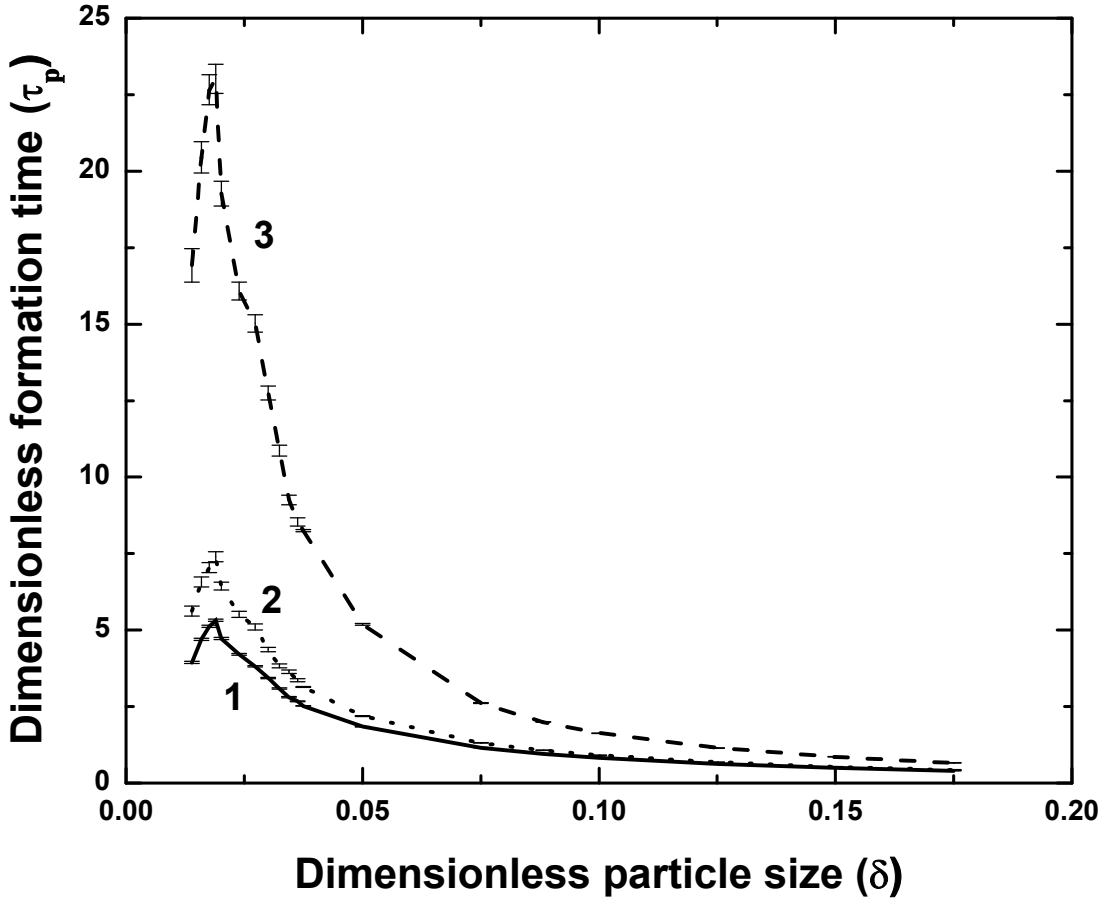

Figure 2.12. Dimensionless final particle formation time vs. dimensionless final particle size for various probabilities of cluster-cluster coalescence: (1) 1.0, (2) 0.5, and (3) 0.1. Same final particle sizes as Figure 2.4. Domain diameter: 40nm.

2.6 Summary and Conclusions

A lattice Monte-Carlo model has been developed to describe the synthesis of semiconductor nanocrystals (quantum dots) in microemulsion templates exhibiting slow droplet-droplet coalescence kinetics. The final particle formation time initially increases with final particle size, but quickly passes through a maximum and subsequently decreases due to the formation of large intermediate clusters that become effective collision partners for the smaller ones. The evolution of precursor population and clusters

of smallest two sizes and total cluster number indicated the relatively fast nucleation process and the process time controlled by the late stage coalescence of few clusters. As the final particle size is increased, the difference in diameters of the two clusters just before the final collision increases indicating the formation of a relatively large "sweeper" cluster during the synthesis of larger particles. Artificial scenarios where the diffusivities and size of the intermediate clusters were varied elucidated the effect of the sweeper clusters in accelerating the particle formation process. The evolution of cluster size distributions was studied and the underlying mechanism leading to the final particle formation through cluster-cluster coalescence was investigated. A generalized dimensionless equation was formulated that correlates the dimensionless final particle formation time with the dimensionless final particle size for a range of droplet sizes and diffusivities of the dissolved precursor and clusters. The particle formation time was scaled with the characteristic time for diffusion of the final particle, and the final particle size with the droplet diameter. A parametric study was performed and the results indicate that the final particle formation time is sensitive to the cluster-cluster coalescence probability, but quite insensitive to the rate of the nucleation reaction at the droplet interface.

In conclusion, a lattice Monte-Carlo modeling technique was developed to describe the formation of a single particle of semiconductor nanocrystal inside microemulsion droplets. The LMC model reveals that the particle formation time for bigger particle sizes is reduced due to the formation of intermediate "sweeper" clusters. The predictions from the model were used to obtain a generalized correlation relating the particle formation time with size and operating conditions such as medium diffusivity.

The mechanism of nanocrystal formation was elucidated and the model could be used to study similar templated process by using appropriate governing rules.

CHAPTER 3

CLUSTER COALESCENCE KINETICS

3.1 Introduction

Diffusion and coalescence of particles is important in many systems, including aerosols, colloids, thin film epitaxial growth, and droplets or bubbles dispersed in liquids. Coarsening of island sizes during deposition on thin films has been extensively studied due to their application in material science and engineering. The diffusion and coalescence of atoms and clusters play an important role in controlling the island sizes which in turn affects the property of the film (Zhang and Lagally, 1997; Jensen, 1999; Jensen and Combe, 2002). In colloids, the diffusion and coalescence of dispersed phase leads to aggregation and determines the stability of the colloidal solution (Robinson and Earnshaw, 1992; Quellet et al., 1991).

The classical Smoluchowski equation provides a theoretical description of the evolution of concentration of various particle sizes during coalescence (Smoluchowski, 1916). It was initially used to describe diffusion and coalescence of colloids in liquids and subsequently extended to describe coagulation of particles in aerosols (Fuchs, 1989). A broad review of the literature on stochastic (Marcus-Lushnikov) models of coalescence and their deterministic approximation given by the Smoluchowski equation has been presented (Aldous, 1999). Gelbard and Seinfeld, 1979 developed a discrete-continuous method for describing aerosol coagulation, derived conservation equations for clusters, and simulated the evolution of particle sizes in an infinite domain. Studies of Brownian coagulation of aerosol particles in an infinite domain have shown that the aerosol attains

a self-preserving particle size distribution (Friedlander and Wang, 1966; Vemury and Pratsinis, 1995).

In this chapter the LMC model described in Chapter 2 (Kuriyedath et al., 2010a) is used to simulate the formation of a single zinc selenide (ZnSe) QDot inside a droplet of a microemulsion consisting of heptane as dispersed phase, formamide as continuous phase and a poly(ethylene oxide)-poly(propylene oxide)-poly(ethylene oxide) amphiphilic block copolymer as surfactant (Karanikolos et al., 2004). In this template, ZnSe QDots are formed by an irreversible reaction between diethyl zinc dissolved in heptane and hydrogen selenide that is bubbled through the microemulsion. In the LMC model it was assumed that the irreversible nucleation reaction between diethyl zinc and hydrogen selenide takes place at the droplet interface and $(ZnSe)_1$ nuclei subsequently diffuse back into the droplet and coalesce to form clusters and eventually a single particle. A hard sphere potential was used to model particle-particle interactions.

The focus is to understand the coalescence kinetics of hard spheres in finite spherical domains using LMC simulations. The practical objective is to study the formation of a single ZnSe Qdot in a spherical heptane droplet and design more efficient experimental techniques. We compare the kinetics of the formation of ZnSe QDots in a microemulsion droplet for two scenarios. The first scenario involves very rapid (spontaneous) conversion of a precursor dispersed in the droplet to nuclei that diffuse and coalesce into a single particle. The second scenario involves diffusion of a precursor to the droplet interface where an irreversible reaction with a second precursor forms nuclei that subsequently diffuse into the droplet and coalesce.

The chapter is arranged as follows. In Section 3.2, the modeling methodology for the LMC simulation is described briefly including the modeling of coalescence starting with uniformly distributed nuclei. Also, the classical equations describing Brownian coalescence of monodispersed aersols in infinite medium is discussed. In Section 3.3, the results of using the LMC model was used to simulate the evolution of cluster populations and the final particle formation times for each of the two scenarios are presented. To explain differences in the predicted final particle formation times we studied the evolution of cluster size distributions for each of the two scenarios. In Section 3.4, the classical analysis of diffusion-limited coalescence of a monodisperse population of particles, which is valid for an infinite domain, was modified to describe coalescence of an initially monodisperse particle population that evolves into a polydisperse population and ultimately a single final particle inside a spherical droplet of finite size. An appropriate characteristic time was identified for scaling the process time that takes into account the size of the droplet and the final particle size. The classical generalized equation that describes diffusion-limited coalescence of monodisperse aerosols in an infinite domain (Friedlander, 1977) was modified by using the new characteristic time to predict the LMC simulation results for coalescence of an initially monodisperse particle population in a finite spherical domain.

3.2 Modeling Methodology

The LMC model used in this section is described in detail in Section 2.3 of Chapter 2 (Kuriyedath et al., 2010a). A brief summary is provided here. A spherical domain representing a microemulsion droplet was inscribed inside a cube, and discretized.

The optimal lattice spacing for the type of LMC simulations discussed is equal to the diameter of the $(ZnSe)_1$ nucleus and this lattice spacing was used throughout. Two particle formation processes were simulated: (1) A pure coalescence run that starts with an initially monodisperse population of $(ZnSe)_1$ nuclei that are uniformly dispersed in the heptane droplet. (2) A synthesis run that starts with diethyl zinc precursor molecules uniformly dispersed in the heptane droplet. The two cases differ in the way they represent nucleation. In the pure coalescence case it is assumed that nucleation of ZnSe is spontaneous throughout the droplet. The simulation starts with $(ZnSe)_1$ nuclei randomly distributed inside the droplet that diffuse and coalesce to ultimately form a single nanoparticle. In the synthesis case, the simulation starts with diethyl zinc molecules randomly distributed inside the heptane droplet. The diethyl zinc molecules undergo Brownian diffusion and are converted to $(ZnSe)_1$ nuclei via an irreversible chemical reaction with hydrogen selenide that takes place at the droplet interface. The results of the final formation time, intermediate cluster size distribution and parametric studies for the synthesis run have been discussed in detail in Chapter 2.

The particle-particle interactions are modeled in the LMC simulations using a hard sphere potential. For interactions involving precursor molecules (precursor-precursor or precursor-cluster) we assume repulsion upon particle overlap. For interactions involving only nuclei or clusters we assume coalescence with a certain probability upon particle overlap. The $(ZnSe)_k$ (k = 1,2 …) clusters are treated as spheres having volume equivalent to the volume occupied by the same number of Zn and Se atoms in a zinc blende (cubic) structure. The ZnSe clusters will tend to form structures that minimize their surface area and hence this assumption is more accurate for larger

clusters. The diffusivity of a cluster is calculated using the Stokes-Einstein equation and is inversely related to its effective diameter.

In the LMC simulations, the coordinates of spheres representing ZnSe clusters or precursor molecules correspond to certain lattice points. Each lattice point is considered to be the center of a unit cell whose sides are equal to the lattice spacing. Multiple precursor molecules can occupy the same unit cell up to the solid fraction limit of randomly packed equal-sized sphere in a cube, i.e. 0.64 (Jaeger and Nagel, 1992; Torquato et al., 2000). ZnSe clusters that are bigger than nuclei have volumes that exceed the volume of a single unit cell and are allowed to partially or fully occupy neighboring unit cells.

At each computational step, each particle present in the simulation is allowed to move to one of six neighboring lattice points with equal probability. This probability depends on the size of each cluster which determines its diffusivity. The particles with the smallest size are assigned a probability to diffuse that is equal to unity. A LMC step is converted to an actual time interval by estimating the time required for the smallest cluster to diffuse a distance equal to the lattice spacing.

To analyze the LMC simulation predictions of QDot synthesis when the nucleation occurs at the droplet interface, the final particle formation time, $t_{p,}$ was scaled using the characteristic time of diffusion of the final ZnSe particle over the radius of the droplet,

$$\tau_p = \frac{t_p}{\left(\frac{R^2}{D_p}\right)} \tag{3.1}$$

where τ_p is the scaled final particle formation time, R is the radius of the droplet, and D_p is the diffusivity of the final particle. The final particle formation time is the time required for the coalescence of ZnSe clusters to lead to the formation of a single ZnSe particle inside the droplet. The proposed scaling was used to obtain a generalized correlation between the final particle formation time and final particle size for a variety of droplet sizes and process conditions that include variations in solvent viscosity, particle diffusivity, and operating temperature discussed in Chapter 2.

For the case of Brownian coagulation of aerosols, a dimensionless time, τ, is defined as (Friedlander, 1977)

$$\tau = \frac{Kn_{p0}t}{2} \tag{3.2}$$

where n_{p0} is the initial number of particles per unit volume, K is the collision frequency function for Brownian coagulation of monodisperse aerosols with particle sizes much greater than the mean free path and t is the time.

The rate of collisions of two particles having volumes v_i and v_j per unit volume of solution, ω_{ij}, is given by

$$\omega_{ij} = \beta(v_i, v_j) C_i C_j \tag{3.3}$$

where C_i and C_j, are the number concentrations of particles with volumes v_i and v_j, respectively, and $\beta(v_i, v_j)$ a collision frequency function with units of volume per time. The collision frequency function for Brownian coagulation is given by (Friedlander, 1977)

$$\beta(v_i, v_j) = \frac{2k_b T}{3\mu}\left(\frac{1}{v_i^{1/3}} + \frac{1}{v_j^{1/3}}\right)\left(v_i^{1/3} + v_j^{1/3}\right) \tag{3.4}$$

For the special case of a monodisperse particle population ($v_i = v_j$), the collision frequency function, used in Equation (3.2), K, becomes

$$K = \beta(v_i , v_i) = \beta_0 = \frac{8k_bT}{3\mu} \tag{3.5}$$

In the cases studied here, an initially monodisperse particle population becomes polydisperse as it coalesces to form a single final particle. To account for polydispersity, an effective collision frequency function, β_e, was defined by averaging the two extreme values of $\beta(v_i , v_j)$, i.e. the minimum value that corresponds to a monodisperse population, $\beta(v_i , v_i)$ or β_0, and the maximum value that corresponds to the collision frequency function of the two extreme particle sizes, $\beta(v_1 , v_{N-1})$:

$$\beta_e = \frac{\beta(v_i, v_i) + \beta(v_1, v_{N-1})}{2} = \alpha\beta_0 \tag{3.6}$$

Here v_{N-1} corresponds to the volume of a particle with (N-1) Zn and Se atoms, which can form the final particle with volume v_N upon coalescence with a particle with volume v_1. By setting $\beta_e = \alpha\beta_0$, a correction factor α was obtained for polydisperse particle populations:

$$\alpha = \frac{1}{2} + \frac{1}{8}\left(\frac{1}{v_1^{1/3}} + \frac{1}{v_{N-1}^{1/3}}\right)\left(v_1^{1/3} + v_{N-1}^{1/3}\right) \tag{3.7}$$

The values of the correction factor α for particle sizes ranging from 1 to 7 nm are listed in Table 3.1.

The scaled final particle diameter, δ, is obtained by dividing the final particle diameter (d_p) with the droplet diameter (d_D=2R)

$$\delta = \frac{d_p}{(2R)} \tag{3.8}$$

Table 3.1. Values of parameter α for ZnSe QDots obtained from Equation (3.7).

d_p (nm)	k	α
1	12	1.09
2	92	1.35
3	310	1.62
4	735	1.90
5	1436	2.18
6	2482	2.47
7	3941	2.75

The numerical values of the parameters of the LMC model used in the simulations are the same as in Chapter 2: Droplet diameter (d_D) =20-40 nm, lattice spacing (l) = 0.44 nm. The physical property values used are given in Table A.1

The LMC Model was validated by simulating the diffusion of diethyl zinc in a droplet with a mass sink at the interface and comparing the simulation results with the solution of a deterministic model describing the diffusion of a solute out of a spherical domain. The results of the validation are discussed in Section 2.3.

3.3 Simulation of Nanoparticle Formation

The LMC simulations were performed for the two nucleation cases discussed in Section 3.2. The effect of the interfacial nucleation on the intermediate cluster coalescence dynamics and the final formation time was studied by comparing the two cases.

In Figure 3.1, the average final particle formation time, τ_p, is plotted as function of the final particle size, δ, the each of the two particle formation scenarios. For each

particle size, the data was obtained from 1000 LMC runs in a 40nm droplet. The final particle size was varied from 0.56 nm, corresponding to a $(ZnSe)_2$ cluster, to 7 nm. The predicted dimensionless final particle formation time is almost indistinguishable up to a final particle size of about 3.5 nm. For both growth scenarios, the predicted average formation time initially increases with final particle size, passes through a maximum at a final size equal to $(ZnSe)_5$, and subsequently decreases. This behavior is due to the formation of a relatively large and slow-moving particle ('sweeper'), which is an effective collision partner for smaller clusters because of its large size and despite the fact that it diffuses more slowly (Kuriyedath et al., 2010a).

An unexpected result predicted by the LMC simulations is that for final particle size larger than about 3.5 nm the final particle formation time is longer when the particle is formed by coalescence of randomly dispersed nuclei compared to a synthesis run. One would expect that, for the same final particle size, a pure coalescence run would be completed first because the nucleation step in this case is assumed to be instantaneous. A synthesis run that involves diffusion of the precursor molecules to the droplet interface, formation of $(ZnSe)_1$ nuclei by an irreversible reaction, and subsequent diffusion of the nuclei back into the droplet and coalescence into a single final particle, would be expected to take longer to complete.

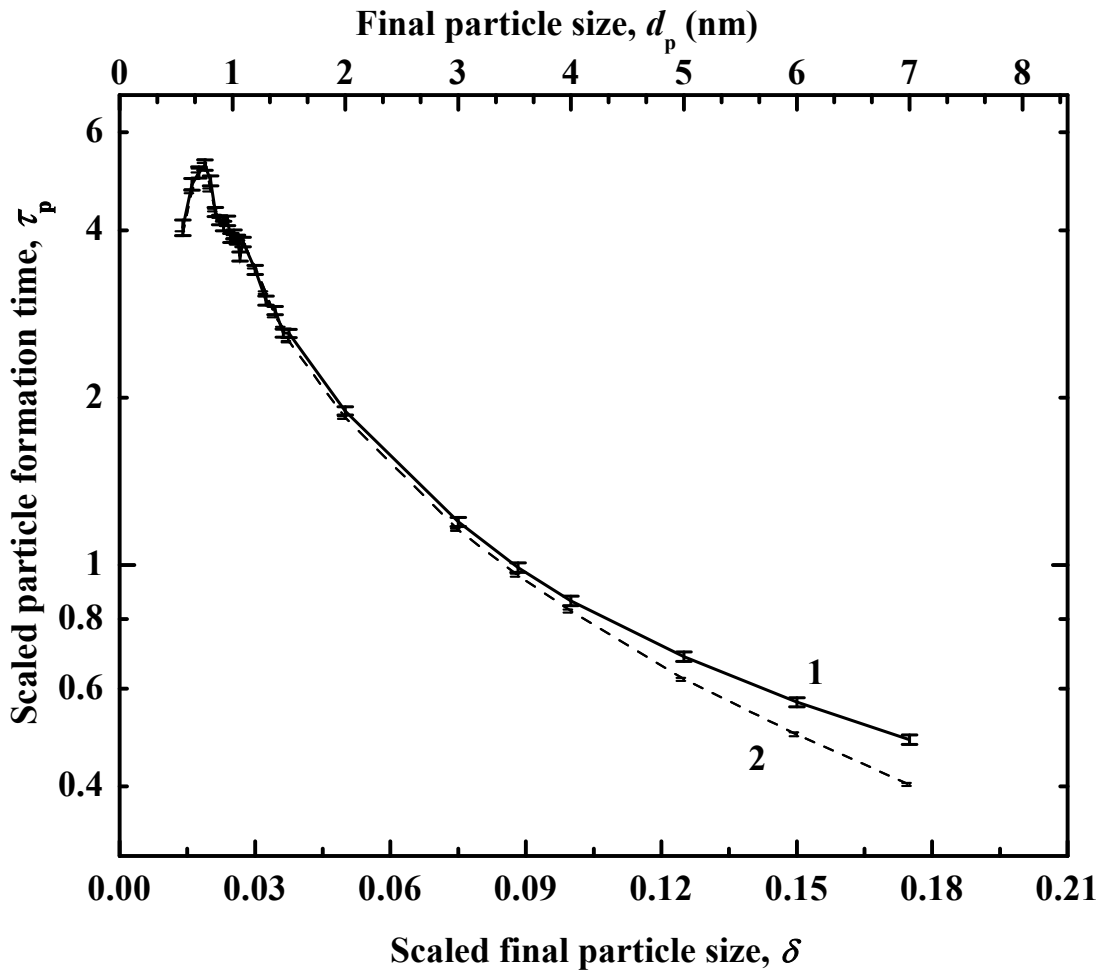

Figure 3.1. Predicted dimensionless final particle formation time as function of the dimensionless final particle size for (1) pure coalescence and (2) synthesis runs. Droplet diameter d_D = 40 nm; the particle diameter d_p ranges from 0.56 nm to 7 nm.

To explain this observation we studied the evolution of the particle population in the droplet for each of the two cases. In Figure 3.2, the evolution of the total cluster number for forming a final particle with diameter 7nm is shown for a representative pure coalescence run and a representative synthesis run. As expected, the total cluster number in the pure coalescence run decreases monotonically with process time. In the synthesis run, the total cluster number initially increases due to the formation of $(ZnSe)_1$ nuclei at the droplet interface, passes through a maximum, and then decreases when cluster depletion by coalescence becomes faster than the formation of $(ZnSe)_1$ nuclei. Initially

the total cluster number in the synthesis run is smaller than that in the pure coalescence run. It soon becomes larger than the corresponding total cluster number in the pure coalescence run due to the continuous formation of $(ZnSe)_1$ nuclei. However, when the total cluster number reaches a value of about ten, the coalescence of the remaining clusters during a typical synthesis run is completed faster compared to a typical pure coalescence run. This indicates that the intermediate cluster populations arising in each case determine the completion time of the process and merit some further investigation.

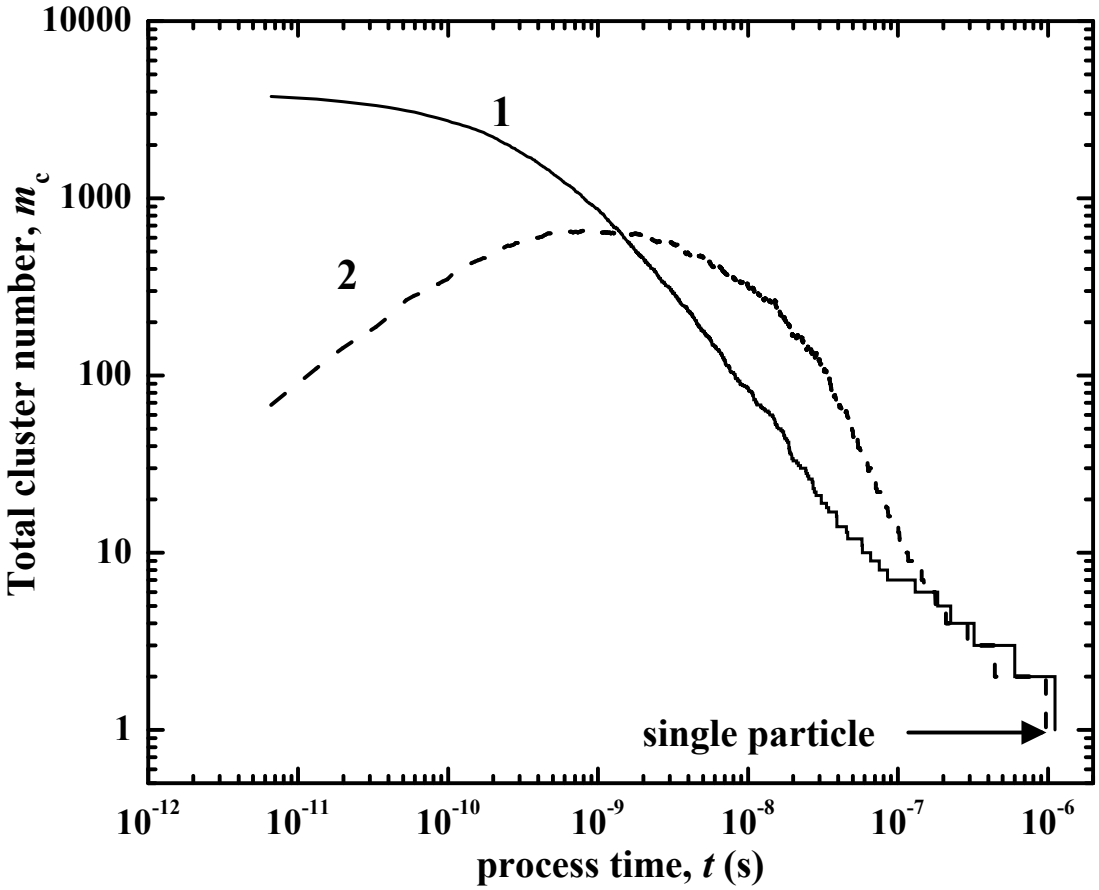

Figure 3.2. Evolution of normalized total cluster number (m_c) for an average run corresponding to: (1) pure coalescence and (2) synthesis scenario. Droplet diameter d_D = 40 nm; final particle diameter d_p= 7 nm.

The major difference between the two processes as they near the formation of a single particle is the size distribution of the clusters remaining in the system. In Figures

3.3 and 3.4, cluster size distributions are plotted corresponding to a total cluster number, m_c, of 400, 300, 200, and 100, for a 7 nm final particle formed in a droplet with a diameter of 40 nm. Figure 3.3 corresponds to pure coalescence runs and Figure 3.4 to synthesis runs. The corresponding process time for each plot is noted in the figure captions. The cluster size distribution for a typical pure coalescence run is relatively flat. As the system coarsens, it contains clusters of different sizes with approximately equal number density. In contrast, during a typical synthesis run the smaller cluster sizes, especially $(ZnSe)_1$ and $(ZnSe)_2$, are present at higher numbers compared to larger ones.

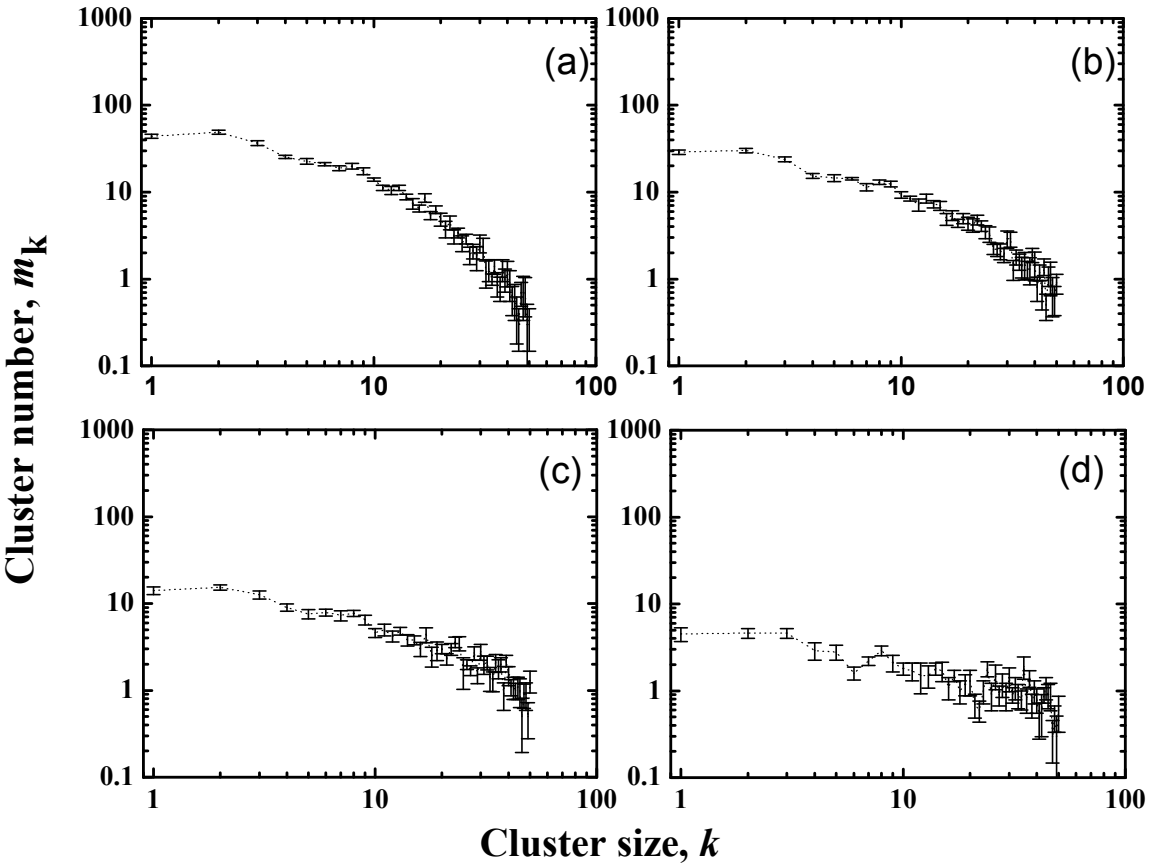

Figure 3.3. Cluster size distribution snapshots during pure coalescence runs corresponding to various total cluster numbers and process times. (a) m_c = 400 and t = 2.30x10^{-9} s; (b) m_c = 300 and t = 3.02x10^{-9} s; (c) m_c = 200 and t = 4.45x10^{-9} s; and (d) m_c = 100 and t = 8.13x10^{-9} s. The final particle formation time is 9.74 x10^{-7} s. Droplet diameter d_D = 40 nm; final particle diameter d_p= 7 nm.

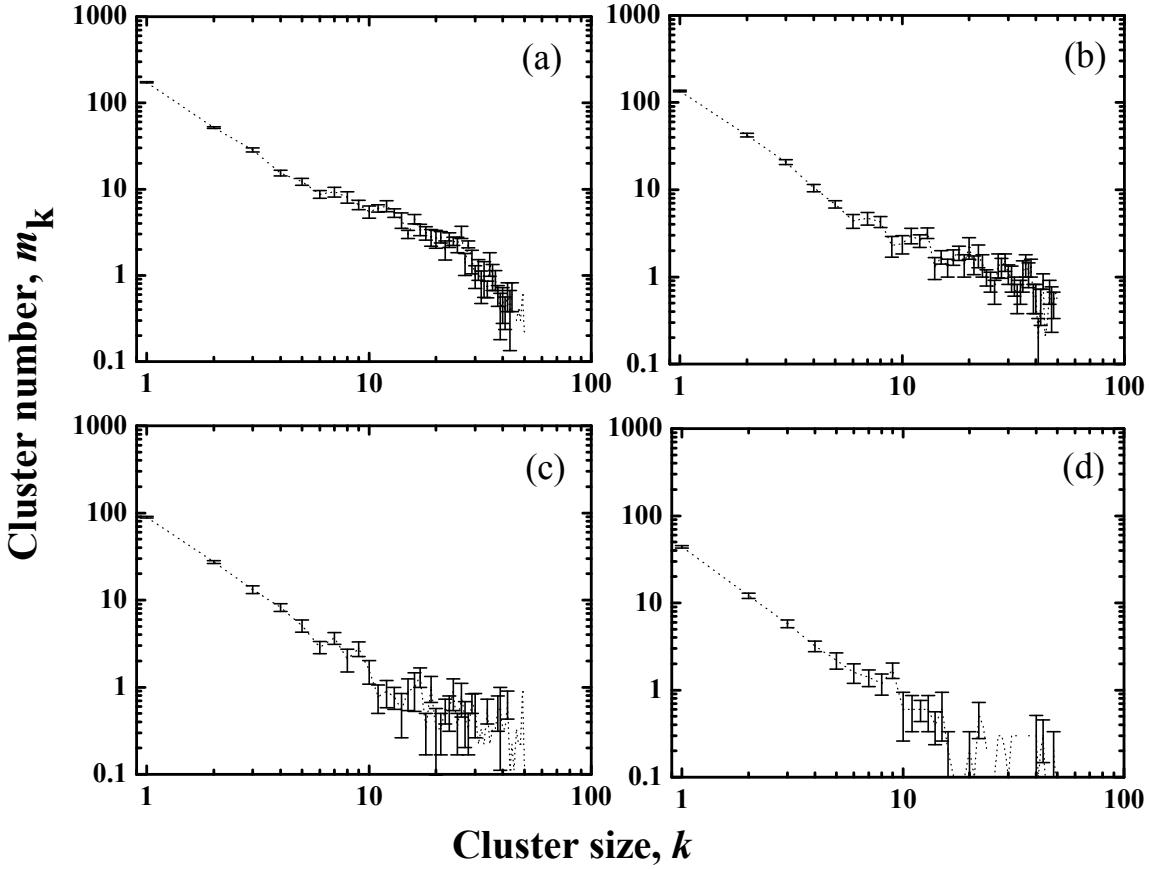

Figure 3.4. Cluster size distribution snapshots during synthesis runs corresponding to various total cluster numbers and process times. (a) m = 400 and t = 6.30x10^{-9}; (b) m = 300 and t = 1.06x10^{-8}; (c) m = 200 and t = 1.73x10^{-8} s; and (d) m = 100 and t = 3.14x10^{-8} s. The final particle formation time is 8.67x10^{-7} s. Droplet diameter d_D = 40 nm; final particle diameter d_p= 7 nm.

A larger number of $(ZnSe)_1$ and $(ZnSe)_2$ clusters are also present at later times during a synthesis run due to the continuing formation of new $(ZnSe)_1$ nuclei at the droplet interface until all Zn precursor molecules are depleted from the droplet. A comparison between two particle populations corresponding to approximately the same process time for each of the two scenarios is shown in Figure 3.5. The particle size distributions plotted in Figure 3.5 correspond to m=300 for the synthesis run and m=100 for the pure coalescence run. The synthesis run will be completed first although the

droplet contains three times as many particles at this stage of the process when compared to the pure coalescence run. This occurs because the additional clusters contained in the droplet during a synthesis run are fast-diffusing smaller clusters, whereas the system undergoing pure coalescence has an almost uniform distribution of all cluster sizes.

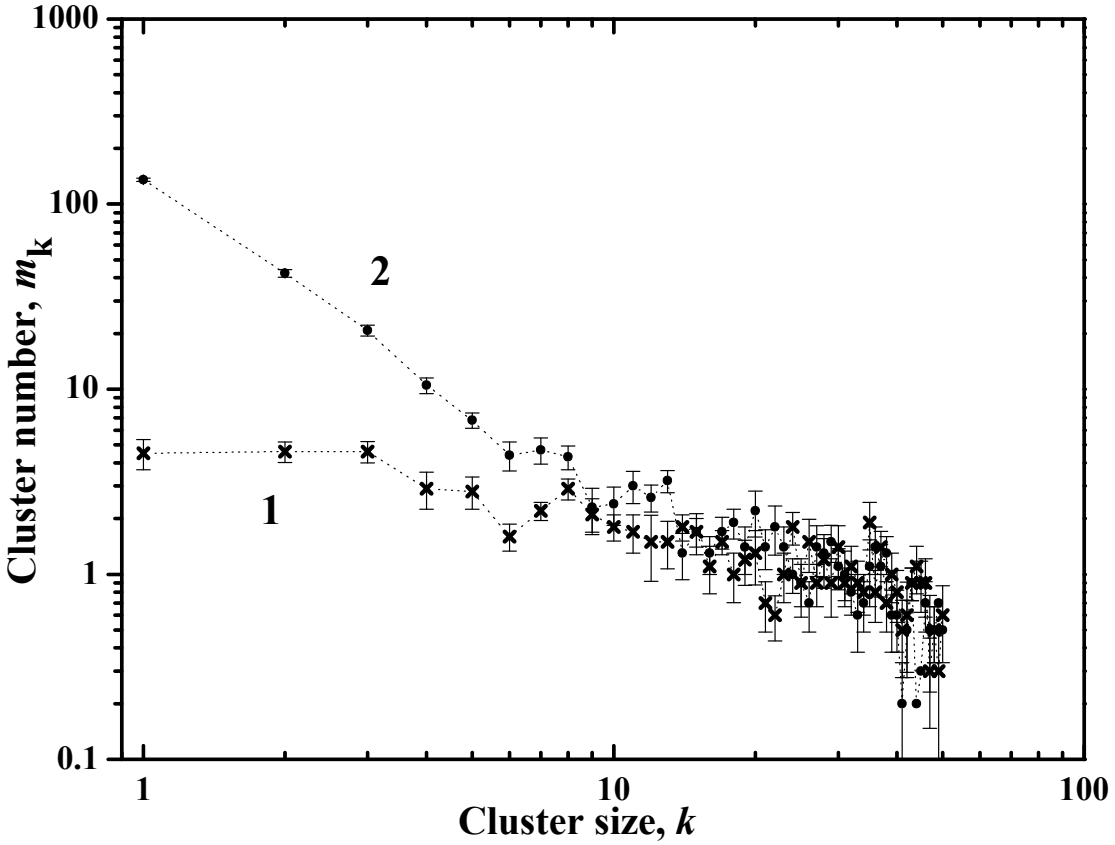

Figure 3.5. Comparison of cluster size distributions during pure coalescence and synthesis runs corresponding to an approximately equal process time. (1) Pure coalescence: m_c = 100 and t = 8.13x10^{-9} s. (2) Synthesis: m_c = 300 and t = 1.06x10^{-8} s. Droplet diameter d_D = 40 nm; final particle diameter d_p= 7 nm.

In Figure 3.6 the radial distribution of the scaled particle concentration of $(ZnSe)_1$ nuclei and all clusters is plotted for the two scenarios at an "early" and an "intermediate" process time. The LMC simulations were performed for a 40nm droplet in which a 7nm particle is formed. The radial distribution of the particle concentration was computed by

dividing the droplet volume into spherical shells (bins) with radial thickness equal to the LMC lattice spacing, except for the inner most spherical bin, whose size was selected so that its volume is equal to the volume of the adjacent spherical shell that has a thickness equal to the LMC lattice spacing. This was done to avoid having an inner bin with very small volume, which will introduce an error in the estimation of the local particle concentration near the center of the droplet. The number of particles in each bin was divided with its volume to obtain the local particle concentration (number density). This value was scaled with the initial average particle concentration obtained by dividing the number of initial nuclei or precursor molecules by the volume of the droplet. For the case of pure coalescence, the distribution of all particles in the droplet remains rather uniform and simply decreases with process time, as expected. For the synthesis run, nuclei are formed at the droplet interface and diffuse inward while coalescing. There is a higher concentration of particles closer to the interface and particle penetration towards the initially particle-free inner core of the droplet increases with process time. The fact that the particles in this case are concentrated in a smaller region of the droplet, compared to the pure coalescence case where the particles are uniformly distributed over the entire volume of the droplet, helps accelerate the formation of a single particle during a synthesis run.

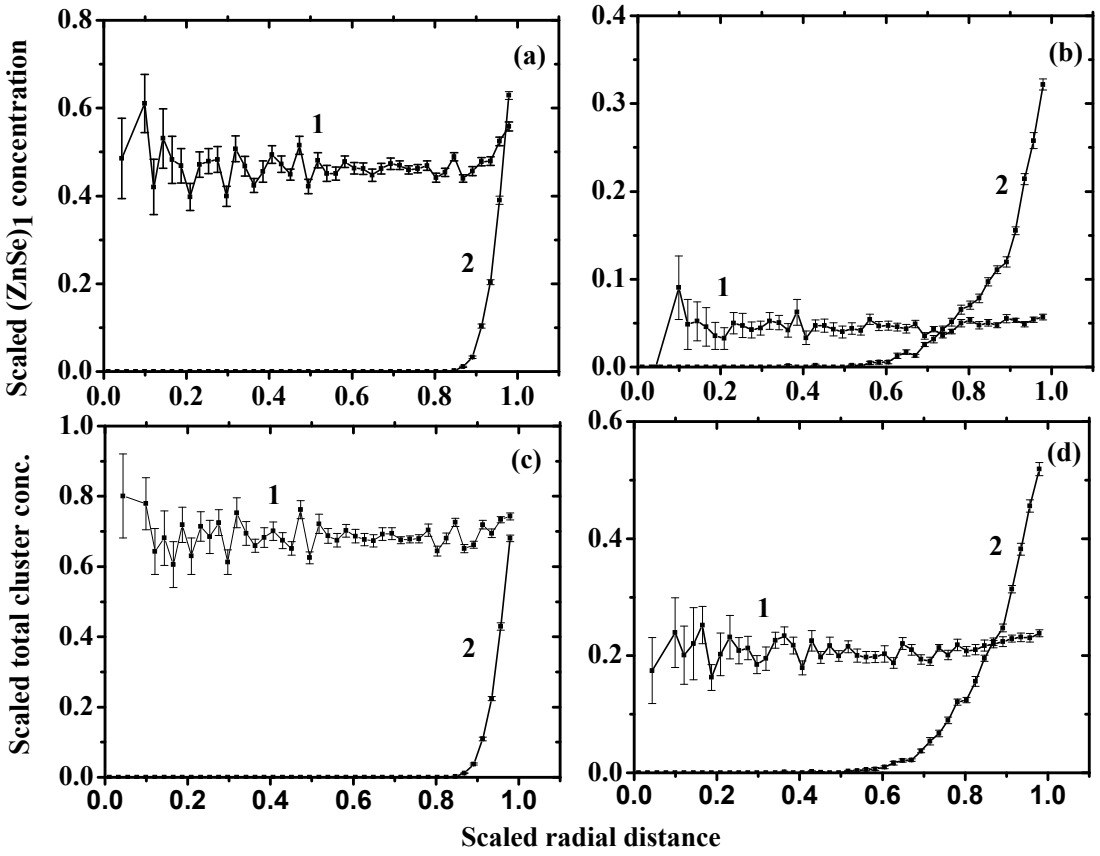

Figure 3.6. Predicted radial distribution of scaled cluster concentration of $(ZnSe)_1$ nuclei (plots a and b) and all clusters (plots c and d) for pure coalescence (1) and synthesis scenario (2) at two process times: $t = 1x10^{-10}$ s (plots a and c); $t = 1x10^{-9}$ s (plots b and d). Droplet diameter $d_D = 40$ nm; final particle diameter $d_p = 7$ nm.

To further investigate the reasons behind the accelerated coarsening of the cluster populations arising during a synthesis run, we studied the average size of the last two remaining particles before the final collision. A normalized diameter difference, Δd, was defined as

$$\Delta d = \frac{(d_1 - d_2)}{d_p} \quad , \qquad (3.9)$$

where d_1 is the diameter of the biggest cluster, and d_2 the diameter of the second biggest cluster. In Figure 3.7, the average value of normalized diameter difference, Δd, of 100

LMC runs is plotted for various final particle sizes ranging from 0.64 nm to 7 nm, formed by either pure coalescence or synthesis runs. The results indicate that for large final particle sizes the 'sweeper' particle is bigger for synthesis runs when compared to pure coalescence runs. The formation of a larger 'sweeper' particle during a synthesis run is probably the key reason behind the faster completion of that process when compared to a pure coalescence run. A 'sweeper' particle becomes a very efficient collision partner for smaller clusters in the population because of its size. This further increases the size of the sweeper particle and enables the accelerated coarsening of the populations arising from synthesis runs. In contrast, the coarsening of a population arising from a pure coalescence run is more 'symmetric' and takes longer to complete because the size difference between the final few particles remaining in the population is smaller and they take longer to coalesce into a single particle.

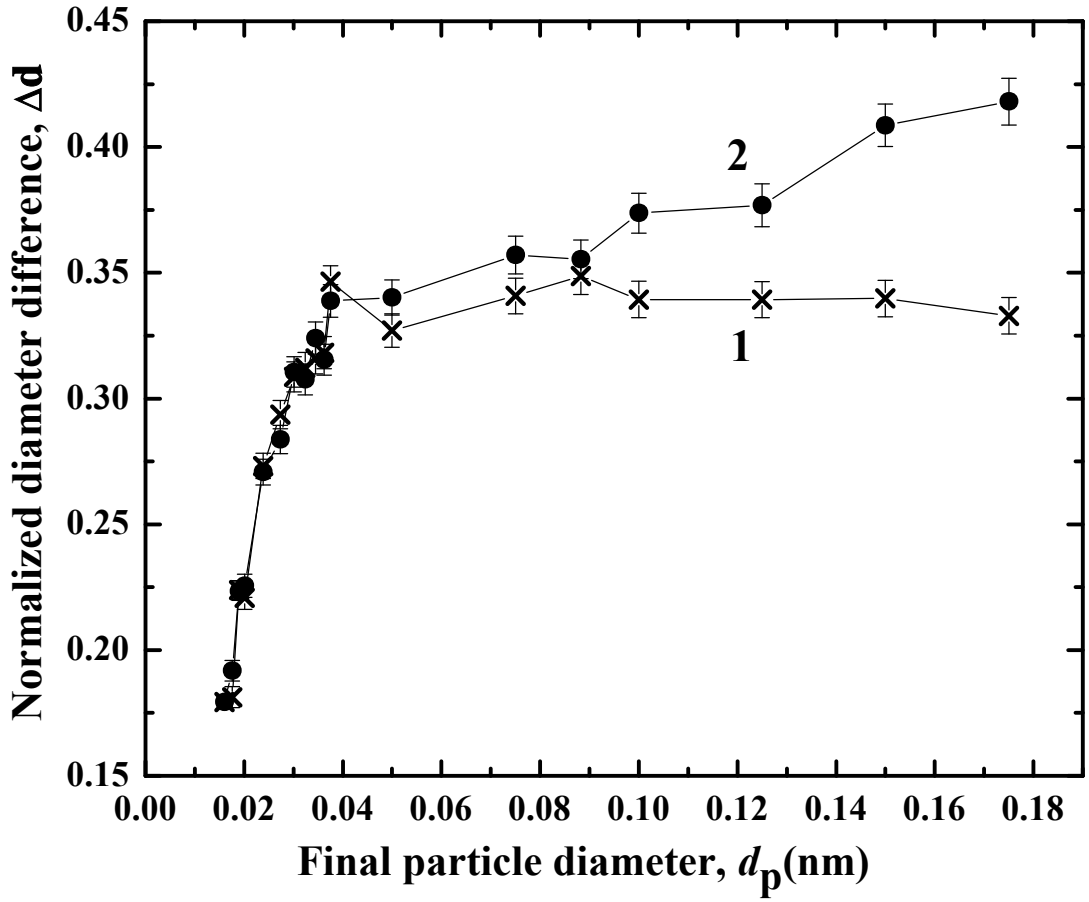

Figure 3.7. Normalized diameter difference between the two biggest clusters, before the last collision that yields a single final particle, as a function of dimensionless final particle size for (1) pure coalescence and (2) synthesis scenario. Each point is the average of 100 LMC runs. Droplet diameter d_D = 40nm; final particle diameter d_p= 0.56nm to 7nm.

3.4 Evolution of Cluster Population in Pure Coalescence

The LMC Model was also used to study coalescence kinetics of an initially monodisperse particle population in a finite spherical domain corresponding to the pure coalescence case discussed before. We performed a series of LMC simulations for various droplet sizes and initial particle (nuclei) numbers aiming to extend the classical theory of diffusion-limited coalescence of monodisperse particle populations in an infinite domain (Friedlander, 1977). We developed a generalized deterministic model of

the dynamics of discrete size distribution that can be used to describe the evolution of the total cluster concentration and the concentrations of individual cluster sizes during coalescence of initially monodisperse particle populations in spherical domains of finite size.

LMC simulations were performed to study the evolution of the total cluster number (m_c), $(ZnSe)_1$ nuclei (m_1) and $(ZnSe)_2$ clusters (m_2) for final particle sizes ranging from 5 nm to 7 nm and droplet diameters ranging from 20 nm to 40 nm during pure coalescence runs. A dimensionless time, τ, was defined using the effective collision frequency function defined in Equation (3.6),

$$\tau = \frac{\beta_e m_{c0} t}{2(\pi d_D^3 / 6)} \tag{3.10}$$

where m_{c0} is the initial number of $(ZnSe)_1$ clusters.

In Figure 3.8, the normalized total cluster number is plotted as function of the dimensionless process time, τ. In Figure 3.9, the normalized concentration of cluster sizes 1 and 2 is plotted as function of the dimensionless process time. The total cluster number, m_c, and the number of clusters of size k, m_k, can be correlated reasonably well by using the expression for diffusion-limited coalescence of monodisperse aerosols (Friedlander, 1977) with the modified dimensionless time defined by Equation (10):

$$\frac{m_c}{m_{c0}} = \frac{1}{(1+\tau)} \tag{3.11}$$

$$\frac{m_k}{m_{c0}} = \frac{(\tau)^{k-1}}{(1+\tau)^{k+1}} \tag{3.12}$$

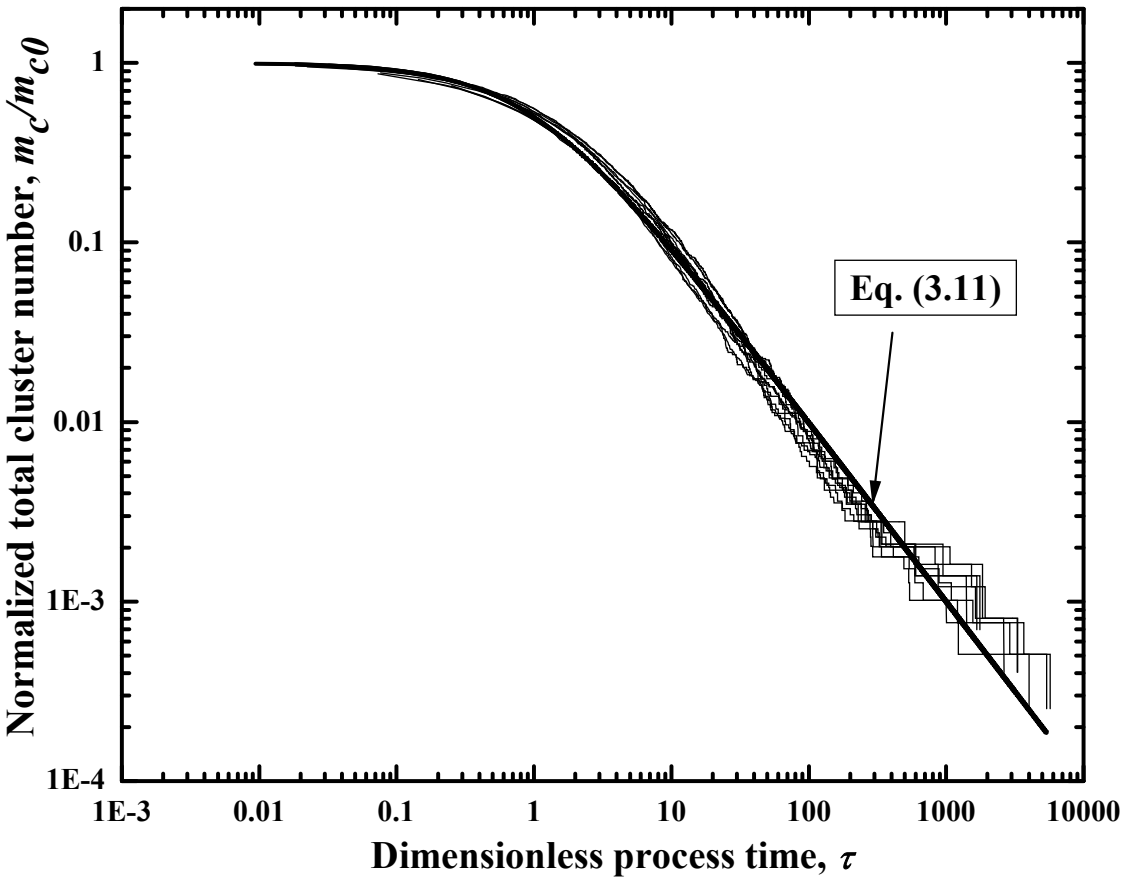

Figure 3.8. Normalized total cluster number during coalescence of hard spheres in a spherical domain as function of dimensionless process time obtained from LMC simulations for d_D= 20-40 nm and d_p=5-7 nm. The prediction of Equation (3.11) is also plotted for comparison.

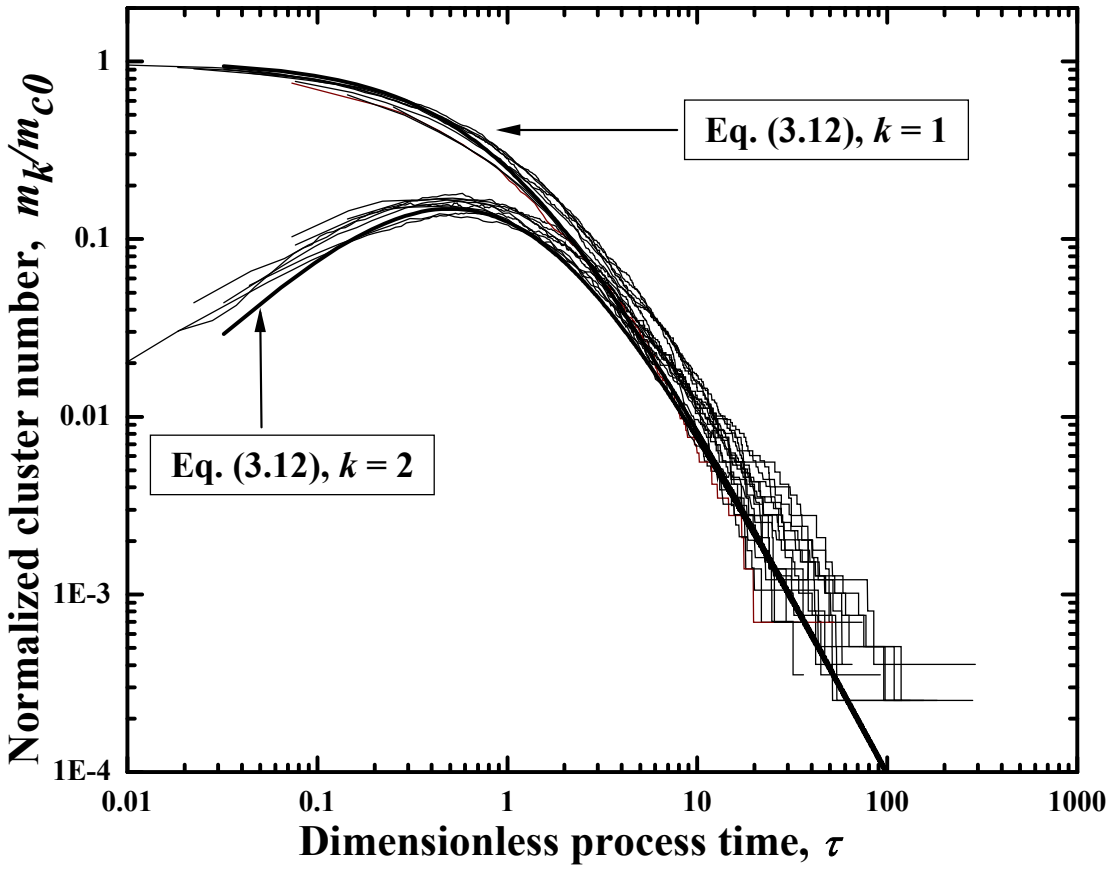

Figure 3.9. Normalized $(ZnSe)_1$ and $(ZnSe)_2$ cluster numbers during coalescence of hard spheres in a spherical domain as function of dimensionless process time obtained from LMC simulations for d_D= 20-40 nm and d_p=5-7 nm. The predictions of Equation (3.12) for k=1 and 2 are also plotted for comparison.

These equations can be used to estimate the evolution of various cluster sizes during coalescence of an initially monodisperse population of particles (hard spheres) in a spherical domain with a reflective (impermeable) boundary.

3.5 Summary and Conclusions

A previously developed Lattice Monte-Carlo model that describes nucleation and coalescence of clusters into a single nanoparticle inside a microemulsion droplet was used to compare two particle formation scenarios: (1) A pure coalescence case in which an initially monodisperse population of nuclei that are randomly distributed in a droplet coalesces into a single particle; and (2) A synthesis case in which molecules of a precursor that are initially dissolved in a droplet diffuse to the interface and react to form nuclei that subsequently diffuse back into the droplet and coalesce into a single particle. The formation of ZnSe QDots in the droplets of a microemulsion was used as an example.

The simulations predict that the final particle formation time for both cases initially increases with final particle size, passes through a maximum, and subsequently decreases due to the formation of large sweeper clusters that accelerate the coalescence of clusters in the late stage of the process. The predicted formation times for a particle of given size being formed in a certain droplet are initially similar for each of the two growth scenarios, but deviate for larger particle sizes with the synthesis runs being completed earlier than the pure coalescence runs. This seemingly counter-intuitive prediction was explained by studying the intermediate particle populations in both the cases. The synthesis runs produce a larger "sweeper" particle that is a more efficient collision partner for smaller clusters because of its size and despite its slow mobility as shown in Chapter 2. In the case of the pure coalescence, the cluster size distribution was more uniform even towards the end of the process indicating that the process does not get accelerated as much due to the "sweeper" particle production. The intermediate radial distribution of clusters and nuclei were compared during the process which indicates the

concentration of clusters close to the interface in the synthesis case which enables a faster coalescence compared to the pure coalescence case.

An investigation of the kinetics of coalescence of initially monodisperse hard spheres confined in a spherical domain having an impermeable boundary, which corresponds to the pure coalescence runs discussed above, was used to identify generalized equations that can be used to predict the evolution of the number of all clusters and of individual cluster sizes. The equations were obtained by modifying the classical equation governing Brownian coagulation of particles taking into account the concentration of the nuclei and the droplet volume and using an average collision frequency function to account for the time-dependent polydispersity of the population.

In conclusion, the LMC model developed to describe the synthesis of quantum dot was extended to study the influence of the nucleation reaction on the process. The synthesis process was compared to a case where the droplet is randomly seeded with nuclei. The simulation results indicate the role of the nucleation process in determining the intermediate size distribution and radial distribution of clusters. This difference in the distributions leads to a more efficient formation of "sweeper" particles which accelerates the synthesis case over the pure coalescence case. A modified Brownian coagulation equation was developed to explain the kinetics of confined coalescence of polydisperse population in the pure coalescence case.

CHAPTER 4

THERMAL ANALYSIS OF NANOPARTICLE COALESCENCE

4.1 Introduction

The formation of quantum dots (QDots) in microemulsion droplets involves diffusion of precursor molecules to the droplet interface, an irreversible reaction at the interface to form the smallest cluster, and subsequent diffusion and coalescence of the clusters to ultimately form a single particle. The driving force for coalescence is the reduction in surface area of the coalescing particles, which is accompanied by the formation of additional chemical bonds as surface atoms become part of the interior of the particles. The energy released due to bond formation can lead to an increase in temperature of the final particle. Such an increase in particle temperature during coalescence can play an important role in determining the structure of the final nanocrystal (Barnard, 2010).

There have been several studies on coalescence of nanoparticles driven by the need to predict their size and structure, which affect their physical, thermal, and optical properties. Zachariah and Carrier (Zachariah and Carrier, 1999) used classical Molecular Dynamics (MD) to study the temperature rise and morphology change during the collision of small Si nanoparticles, containing between 30 and 240 Si atoms, in vacuum and compared the MD predictions with a phenomenological model. Assuming an adiabatic process with no heat transfer to the surroundings, they found a significant increase in the temperature of the coalescing particles (~ 400 K for the smallest particle) that was attributed to the reduction in surface area and the consequent elimination of

dangling bonds. The kinetic energy of the nanoparticles was a small fraction of the total energy released.

Hendy et al. (Hendy et al., 2003) used constant energy MD simulations to study the coalescence of metal nanoclusters in an inert gas. They studied the temperature rise and evolution of size of the clusters for different initial temperatures and found evidence of melting of the coalescing clusters due to significant temperature rise upon coalescence of smaller clusters. McCarthy and Brown (McCarthy and Brown, 2009) studied the coalescence of faceted nanoparticles using kinetic Monte Carlo simulations. The coalescence involved neck formation at the intersection of (001) and (111) facets. A time-dependent exponent for the power-law behavior of the evolution of the neck radius was obtained. The effect of a monolayer of hydrogen atoms that passivate the surface of the Si nanoparticles undergoing coalescence was studied by Hawa and Zachariah (Hawa and Zachariah, 2004). Nanoparticles whose surface was apssivated by hudrogen required a higher kinetic energy in order for a collision to lead to coalescence. Lewis et al. (Lewis et al., 1997) used constant-temperature MD simulations to study the coalescence of clusters of gold nanoparticles which are initially liquid-liquid, liquid-solid, and solid-solid. They found that the macroscopic sintering theory based on surface diffusion underestimates the coalescence time between a liquid and solid or two solid nanoparticles.

Molecular simulations have been helpful in elucidating the underlying mechanism of nanocluster coalescence. These simulations are strongly influenced by the initial conditions of coalescence, such as the orientation of facets. It is not computationally feasible to simulate all possible orientations existing before coalescence and their effect on the final particle.

In this chapter, a generalized continuum model that describes the energy release during coalescence of nanoparticles is developed and the change in the temperature of the coalescing nanoparticles is predicted as function of time for a variety of process conditions. The coalescence of two ZnSe nanoparticles in n-heptane during synthesis by the the microemulsion gas contact process (Karanikolos et al, 2004) and in hydrogen during vapor-phase synthesis in a counterflow jet reactor (Sarigiannidis et al., 2002, 2006; Cho et al., 2011) are used as case studied. The chapter is organized as follows: In Section 4.2, the mass and energy balance equations governing the evolution of the temperature of the coalescing nanoprticles are discussed. In Section 4.3 the effects of particle size on the melting point of ZnSe nanoparticles and the mass fraction of the resulting nanoparticle that melts during adiabatic coalescence are discussed. In Section 4.4, the temperature of two coalescing ZnSe nanoparticles under adiabatic conditions is calculated for various nanoparticle sizes. In Section 4.5 a generalized model is presented that can be used to estimate the temperature rise during coalescence of nanoparticles with heat transfer to the surroundings. A surface diffusion mechanism for coalescence is assumed because it is more energetically favorable than the bulk diffusion mechanism. Typical values of the model parameters are computed for coalescence of ZnSe nanoparticles and their limits are established. The governing equations are solved numerically for various values of the parameters to investigate their effects on the temperature rise of the coalescing nanoparticles and the time required for complete coalescence. The results are summarized in Section 4.6.

4.2 Modeling of Nanoparticle Coalescence

During coalescence of two nanoparticles, the total surface area decreases and results in a release of energy because the excess surface atoms of the two initial particles that had dangling bonds move to the interior of the coalesced particle and form chemical bonds with the neighboring atoms. This energy released by the saturation of the excess dangling bonds can elevate the temperature of the nanoparticle. Heat transfer to the surroundings eventually lowers the temperature of the coalescing system back to the temperature of the surrounding medium.

The rate of change of the surface area, a, of two coalescing spherical nanoparticles with initial surface areas a_1 and a_2, respectively, can be represented approximately by a simple function of a that depends on the characteristic time for coalescence, τ_c (Koch and Friedlander, 1990; Friedlander and Wu, 1994):

$$\frac{da}{dt} = -\frac{(a - a_f)}{\tau_c} \tag{4.1}$$

with initial condition at $t = 0$: $a = a_0 = a_1 + a_2$. Here t is the time and a_f is the surface area of the final coalesced particle, assumed to be spherical. The characteristic time for coalescence, τ_c, depends on the mechanism that leads to fusion of the two nanoparticles. Possible mechanisms include solid-state (bulk) diffusion, surface diffusion, evaporation-condensation, and viscous flow (Kingery and Berg, 1955; Friedlander and Wu, 1994; Lewis et al., 1997).

Equation (4.1) was initially developed to describe the final stages of coalescence of aerosol particles, but it has been shown to be approximately valid for the entire range of times of coalescence (Koch and Friedlander, 1990). The rate of change of the surface

area predicted by this equation is a linear function of a, when τ_c is independent of time, such as in the case of coalescence under isothermal conditions. The equation has been used to predict the evolution of particle size during coalescence of aerosols. It was found that it tends to underestimate the primary particle sizes for very small particles (Lehtinen and Zachariah, 2001, 2002).

The coalescence of molten nanoparticles invloves viscous flow and the characteristic time for this process is given by

$$\tau_c = \frac{\mu d_p}{\sigma} \tag{4.2}$$

where μ is the viscosity of the molten particles, σ the surface tension (or surface energy per unit surface area), and d_p the diameter of the final particle (Kingery and Berg, 1955).

A possible mechanism that can lead to coalescence of nanoparticles at elevated temperatures, but below their melting point, involves solid-state or bulk diffusion of the atoms of the two nanoparticles (Friedlander and Wu, 1994). The characteristic coalescence time in this case can be obtained from

$$\tau_c = \frac{3k_B TN}{64\pi\sigma D} \tag{4.3}$$

where k_B is the Boltzmann constant, T the absolute temperature of the coalescing nanoparticles, N is the number of atoms in the nanoparticle resulting from the coalescence of two smaller ones, and D is the bulk diffusion coefficient.

At lower temperatures, well below the melting point of the nanoparticles, coalescence proceeds by surface diffusion of one particle (typically the smaller) onto the surface of the other (Nichols and Mullins, 1965; Nichols 1966; Lewis et al., 1997;

McCarthy and Brown, 2009). The characteristic coalescence time in such a case is given by

$$\tau_c = \frac{k_B T R^4}{25 D_s \sigma d_s^{\,4}} \tag{4.4}$$

where R is the initial radius of the two coalescing particles (assumed to be equal in size), D_s is the surface diffusion coefficient, and d_s is the diameter of the diffusing species. For a $(ZnSe)_1$ species, equation (2.3) yields $d_s = 0.44$ nm. The surface diffusion mechanism is the most probable one for coalescence of a small nanoparticle with a bigger one. In such a case, the mass of the smaller particle diffuses over the surface of the bigger one and the two particles fuse into one. Pan et al. (Pan et al., 1998) developed a simulation scheme for the coalescence of spherical particles of different sizes based on the surface diffusion mechanism.

For coalescence of ZnSe nanoparticles at temperatures well below their melting point, the surface diffusion mechanism is assumed to be dominant. For the case of ZnSe nanoparticle synthesis in microemulsion droplets, Lattice Monte Carlo (LMC) simulations reveal that the intermediate particle populations consist of a few large particles and many smaller ones. The larger "sweeper" particles are effective collision partners for smaller particles and clusters and coalescence to a final nanoparticle in this system proceeds by fusion of smaller particles with a larger one (Kuriyedath et al., 2010a, b).

In this work we assume for simplicity that the surface tension of the nanoparticles is isotropic and independent of the nanoparticle size. There is experimental evidence indicating that the surface tension of a particle depends on its size (Nanda et al., 2003), but such variations are neglected in our analysis. Also, nanoparticles are not perfect

spheres, but polyhedra consisting of facets of various orientations. As a result, their surface tension is not isotropic and depends on the crystallographic orientation of each facet. Furthermore, the relative area of various facets on the equilibrium surface of a nanoparticle depends on the surface energy of that facet. Facets corresponding to lower surface energies are the ones that are energetically more favorable to form the surface of the nanoparticle (Erwin et al, 2005; Singh et al., 2008). Hamad et al. (Hamad et al., 2002) performed a computational investigation of surface energies for various zinc blende structures and found that the (110) surface is the most stable one. The surface energy of ZnSe (110) has been estimated computationally and experimentally (Cai et al., 2006; Zangwill, 1996). In our study, the (110) surface was assumed to represent the surface of the ZnSe nanoparticles. The surface energy of the (110) surface of ZnSe was assumed to be 1.92 J/m^2. It was also assumed to be independent of temperature. The value used in our simulation is the upper limit of values reported in the literature for the surface energy of the (110) surface of ZnSe. The value of liquid ZnSe surface tension was calculated using the method of Goldstein et al. (Goldstein et al., 1992), who used the experimental values of size-dependent melting point of CdS nanoparticles to fit the difference between the surface tension of solid and liquid.

The surface diffusion coefficient for ZnSe was estimated using an Arrhenius expression that is similar to the one used to fit experimentally-obtained surface diffusion data for Si (Mo et al., 1991). The frequency factor was kept the same at $1x10^{-7}$ m^2/s and the activation energy was adjusted by a factor equal to the ratio of the bond energy in ZnSe divided by the bond energy in Si. The resulting expression for surface diffusion of ZnSe is:

$$D_s = 1\times10^{-7}\exp(-\frac{0.38eV}{k_BT}) \quad \text{m}^2/\text{s} \tag{4.5}$$

The bond energy of ZnSe was assumed to be 1.3 eV (Rohrer, 2001) and that of Si 2.3 eV (Walsh, 1981).

The energy conservation equation for two coalescing nanoparticles can be expressed as:

$$mC_p\frac{dT}{dt} = -\frac{d(\sigma a)}{dt} - ha(T - T_0) \tag{4.6}$$

with initial condition at $t = 0$: $T = T_o$. Here m is the total mass of the coalescing system, i.e. the sum of the masses of the two coalescing particles, T is the temperature of the particles, T_o is the temperature of the surrounding medium, C_p is the specific heat of the material that is in general a function of T, σ is the surface energy per unit area, and h is the overall heat transfer coefficient for heat transfer from the coalescing nanoparticles to the surrounding medium by convection and conduction. The effects of radiative heat transfer are neglected. In the analysis presented here, the temperature of the coalescing system, T, is assumed to be uniform due to the small size of the nanoparticles. The temperature dependence of the specific heat of the nanoparticles was taken into account. For the case of solid ZnSe, the specific heat is a weak function of temperature (Zhvavyi and Zykov, 2008) whose value was assumed to be the average of the values corresponding to the initial and maximum temperature that the system attains.

In equation (4.6), the first term describes the accumulation of thermal energy in the coalescing system, the second term the energy generation due to loss of surface area and formation of additional bonds, and the third term represents the heat transfer to/from

the surroundings. This equation governs the evolution of the temperature of the coalescing system.

4.3 Effects of Size on the Melting Point of Nanoparticles

The melting point of nanoparticles depends on their size and is depressed as the size of nanoparticles becomes smaller (Buffat et al., 1976; Goldstein et al., 1992). An equation that can be used to predict the melting point of nanoparticles was developed by Buffat et al. (Buffat et al., 1976), who studied the effects of size on the melting point of gold nanoparticles:

$$T_{mp} = T_{mb}\left[1 - \frac{4}{\rho_s L d}\left(\sigma_s - \sigma_l\left(\frac{\rho_s}{\rho_l}\right)^{2/3}\right)\right] \tag{4.7}$$

Here T_{mp} and T_{mb} are the melting point of the nanoparticle and melting point of the bulk material, respectively, ρ_{s} and ρ_{l} are the solid and liquid density, respectively, L is the latent heat of melting, σ_{l} and σ_{s} and are the liquid surface tension and solid surface energy per unit surface area, respectively, and d is the diameter of the nanoparticle.

4.4 Coalescence of Two Nanoparticles under Adiabatic Conditions

If the coalescence takes place without any heat loss to the surroundings, then the overall energy conservation equation under adiabatic conditions can be written as:

$$mC_p(T_f - T_0) + \sigma(a_f - a_0) = 0 \tag{4.8}$$

where T_0 and T_{f} are the initial and the final temperature of the nanoparticle, respectively, a_{f} is the total surface area of the final coalesced particle (assumed to be a perfect sphere),

and a_0 is the sum of the initial surface areas of the two coalescing spherical nanoparticles. From equation (4.8) the final temperature can be computed from

$$T_f = T_0 + \frac{\sigma \Delta a_0}{mC_p} \tag{4.9}$$

where $\Delta a_0 = a_0 - a_f$.

For spherical nanoparticles, equation (4.8) can be rewritten as

$$\sigma_s \pi (d_1^{\,2} + d_2^{\,2} - d_p^{\,2}) = mC_p (T_f - T_0) \tag{4.10}$$

where d_1 and d_2 are the initial diameters of the two coalescing nanoparticles, and d_p is the diameter of the nanoparticle formed after complete coalescence. This equation is valid if $T_f < T_{\mathrm{mp}}$, where T_{mp} is the melting point of the resulting spherical nanoparticle.

If the value of T_{f} obtained from Equation (4.10) is equal to the melting point of the nanoparticle of diameter d_p, the energy conservation equation must be rewritten to take into account the latent heat of the fraction of the nanoparticle that melts:

$$\sigma_s \pi (d_1^{\,2} + d_2^{\,2} - \frac{\sigma_l}{\sigma_s} d_p^{\,2}) = mC_p (T_{mp} - T_0) + xmL \tag{4.11}$$

Here x ($0 \le x \le 1$) is the mass fraction of the final nanoparticle which has melted, and L the latent heat of fusion of the material per unit mass.

If the value of T_{f} obtained from Equation (4.10) is larger than the melting point of the nanoparticle of diameter d_p and the energy released during coalescence is sufficient to completely melt the final nanoparticle, the energy balance becomes

$$\sigma_s \pi (d_1^{\,2} + d_2^{\,2} - \frac{\sigma_l}{\sigma_s} d_p^{\,2}) = mC_p (T_{mp} - T_0) + mL + mC_{pl} (T_f - T_{mp}) \tag{4.12}$$

where C_{pl} is the average heat capacity of the molten material.

Equations (4.10), (4.11), and (4.12) can be used to estimate the final temperature of the nanoparticle during adiabatic coalescence between nanoparticles of various sizes.

In Table 4.1, the results for coalescence of ZnSe nanoparticles of various sizes are listed. The physical properties of ZnSe used in these calculations can be found in Appendix Table A1.1. The value of x is calculated assuming that the final temperature, T_f, is equal to the melting point of the final particle with diameter d_p. The melting point of the nanoparticles becomes size dependent for small sizes (Buffat et al., 1976; Goldstein et al., 1992).

Table 4.1. Adiabatic temperature rise and mass fraction of the final nanoparticle that melts for coalescence of two ZnSe nanoparticles with different sizes under adiabatic conditions (T_0 = 300 K).

d_1 (nm)	d_2 (nm)	d_p (nm)	T_f (K)	T_{mp} (K)	x
1	1	1.26	1678.3	980.0	1.0
1	1.2	1.40	1397.7	1060.5	1.0
1	1.4	1.55	1134.5	1134.5	0.96
1	1.6	1.72	1048.7	1199.4	0.0
1	1.8	1.90	896.5	1255.2	0.0
1	2	2.08	776.7	1302.9	0.0
1	3	3.04	477.3	1459.2	0.0
1	4	4.02	381.7	1542.4	0.0
1	5	5.01	343.8	1593.2	0.0
2	2	2.52	957.4	1389.5	0.0
2	3	3.27	718.8	1483.5	0.0
2	4	4.16	538.4	1551.0	0.0
2	5	5.10	441.1	1596.8	0.0
3	3	3.78	738.3	1526.0	0.0
3	4	4.50	634.0	1569.6	0.0
3	5	5.34	531.4	1605.6	0.0
4	4	5.04	628.7	1594.2	0.0
4	5	5.74	572.0	1619.2	0.0
5	5	6.30	563.0	1635.2	0.0

As shown in Table 4.1, the final temperature of the nanoparticle decreases as the size of the coalescing particles increases and quickly becomes less than the melting point

of the final coalescing particle. The model predicts that coalescence of ZnSe nanoparticles with initial temperature equal to 300 K will raise the temperature of the final nanoparticle to its melting point or above only for small nanoparticles with initial diameters about 1nm. The results indicate that melting is not likely to occur during coalescence of two ZnSe nanoparticles that are initially at room temperature if at least one of them is larger than 1.5 nm.

The evolution of the nanoparticle temperature under adiabatic conditions can be , modeled using equation (4.6) without the term corresponding to heat transfer to the surroundings . The resulting energy balance is

$$mC_p \frac{dT_p}{dt} = -\sigma \frac{da}{dt} \tag{4.13}$$

with initial condition at $t = 0$: $T = T_o$.

This equation is valid if the coalescence does not result in melting of the nanoparticles, i.e. if $T < T_{mp}$. When the temperature becomes equal to T_{mp}, then the temperature will experience an arrest, Additional energy released will melt the final nanoparticle. If there is excess energy available, the temperature of the molten particle will increase beyond T_{mp}.

Equation (4.13) can be solved simultaneously with equation (4.1) to obtain the evolution of temperature and surface area of the coalescing system as function of time. Equation (4.4) is used for computing the characteristic time for coalescence, τ_c, and equation (4.5) for computing the surface diffusivity.

In Figure 4.1, the results from computations corresponding to coalescence of ZnSe nanoparticles under adiabatic conditions are shown. The time has been scaled using

the value of the characteristic coalescence time at T_0. The temperature is plotted in the form of a dimensionless temperature rise, θ, defined as

$$\theta = \frac{\left(T - T_0\right)}{\left(\frac{\sigma \Delta a_0}{m C_p}\right)} \tag{4.14}$$

where $\sigma\Delta a_0/(mC_p)$ corresponds to the maximum possible temperature rise under adiabatic conditions without melting, $\Delta T_{adiabatic}$.

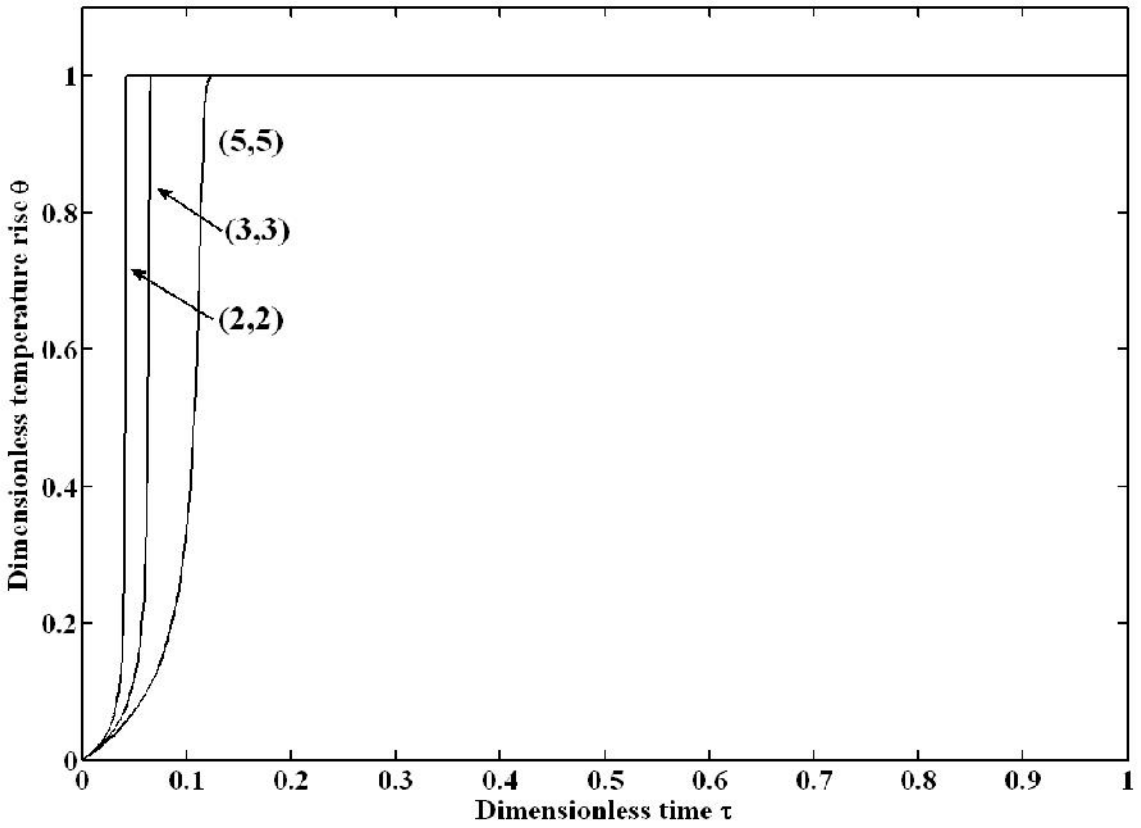

Figure 4.1. The evolution of dimensionless temperature during coalescence of two nanoparticles under adiabatic conditions with particles sizes (2,2), (3,3), and (5,5)nm.

Figure 4.1 shows the evolution of the dimensionless temperature rise θ of different pairs of ZnSe nanoparticles under adiabatic conditions. For pairs that experience no melting the dimensionless temperature rise reaches a maximum value of 1. For pairs that experience partial melting, the maximum temperature attained is the melting point of the final coalesced system. In such cases, the maximum dimensionless temperature rise is smaller than 1. If complete melting occurs, the final temperature of the particle might be higher than the melting point and the material will be in the liquid state. In such cases, the coalescence mechanism will be based on the viscous flow model.

The equations of the model can be simplified by using a constant value for the characteristic time for coalescence, τ_c. In such a case, equation (4.1) can be solved analytically and give the surface area, a, as function of time:

$$a = a_0 + \Delta a_0 \exp(-\frac{t}{\tau_c}) \tag{4.15}$$

Then, the rate of change of the surface area of the coalescing system can be written as:

$$\frac{da}{dt} = -\frac{\Delta a_0 \exp(-t/\tau_c)}{\tau_c} \tag{4.16}$$

By substituting Equation (4.16) into Equation (4.13), we obtain:

$$mC_p \frac{d(T-T_0)}{dt} = \sigma \frac{\Delta a_0 \exp(-t/\tau_c)}{\tau_c} \tag{4.17}$$

with initial condition at $t = 0$: $T = T_o$

This equation can be written in dimensionless form as:

$$\frac{d\theta}{d\tau} = e^{-\tau} \tag{4.18}$$

with initial condition at $\tau = 0$: $\theta = 0$

Integration of this equation from dimensionless time 0 to τ yields the dimensionless temperature evolution of the coalescing system under adiabatic conditions with the assumption of constant characteristic coalescence time and other physical properties:

$$\theta = 1 - e^{-\tau} \tag{4.19}$$

Figure 4.2 shows a comparison of the predicted dimensionless temperature rise θ vs. τ for coalescence of two 5nm ZnSe particles under adiabatic conditions obtained from the numerical solution of the (1) full model and from the (2) approximate solution described by Equation (4.19). In the second case, the average value of the characteristic coalescence time was computed at the average temperature $(T_o+T_f)/2$.

The temperature of the coalescing system reaches the maximum value faster when using temperature-dependent physical properties (case 1).

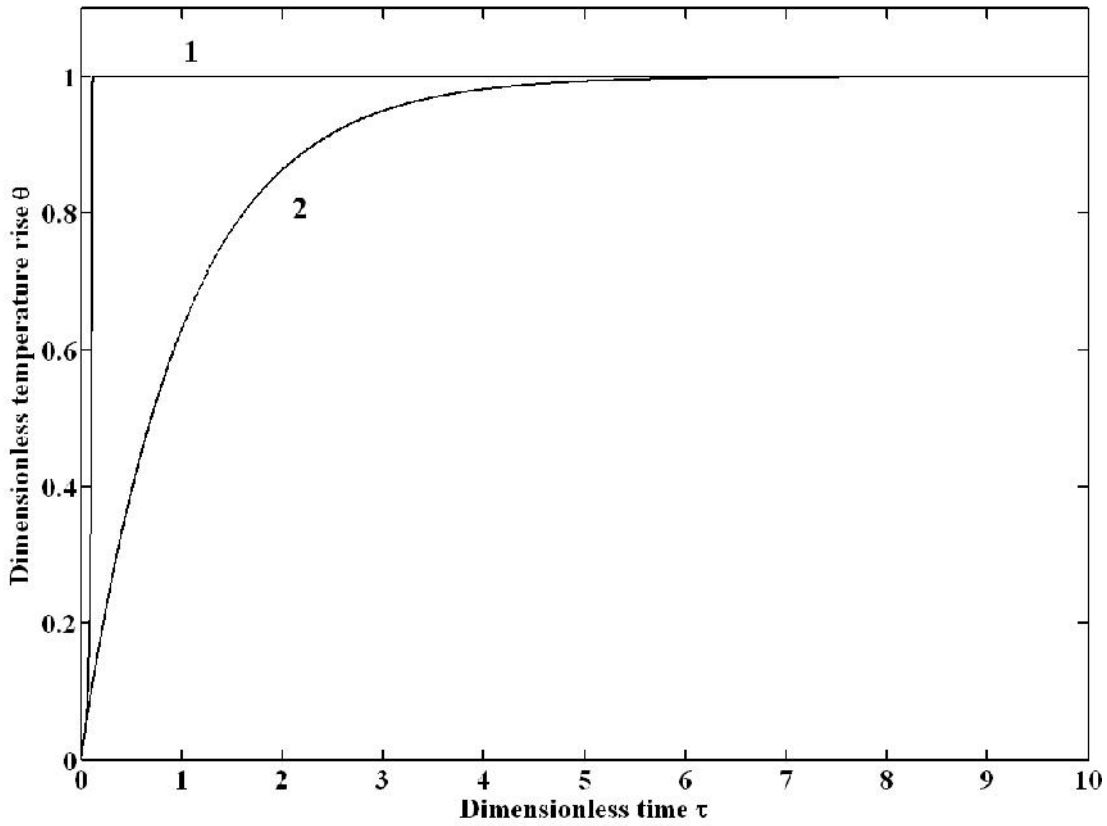

Figure 4.2. Temperature rise during coalescence of two 5 nm ZnSe nanoparicles in n-heptane. (1) full model solved numerically, and (2) approximate model based on equation (4.19).

4.5 Coalescence of Two Nanoparticles with Heat Transfer to the Surrounding Medium

The two physical parameters controlling the temperature rise of the nanoparticles during coalescence with heat transfer to the surrounding medium are the characteristic coalescence time, τ_c, and the overall heat transfer coefficient, h.

The resistance to heat transfer from a nanoparticle to a surrounding fluid, kept at a lower temperature, is the sum of an overall heat transfer resistance due to conduction and

convection in the surrounding medium and an interfacial resistance to heat transfer from the solid nanoparticle to the surrounding medium, called the Kapitza resistance (Pollack, 1969; Swartz and Pohl, 1989). The effects of radiation are neglected in this study because the temperatures under consideration are not high enough for radiation to have a significant contribution as a heat transfer mechanism.

The Kapitza resistance was initially observed in heat transfer experiments involving a metal-liquid helium interface at temperatures close to absolute zero (Kapitza, 1941). It was subsequently found that this resistance is significant during interfacial heat transfer in nanoscale materials (Swartz and Pohl, 1989). For this reason, there is extensive ongoing research focusing on the Kapitza resistance during heat transfer in microelectronic devices. The mechanism of the Kapitza resistance is still not fully understood, but it is generally attributed to the lattice discontinuity at the solid-liquid interface and the nanoscale size of the material, which adversely affects the transfer of energy by vibrational motion from the solid to the liquid by causing phonon confinement and phonon-boundary scattering (Swartz and Pohl, 1987; Zou and Balandin, 2001). Due to the Kapitza resistance, the temperature at the solid side of the interface will be higher than the temperature of the liquid side of the interface.

The heat flux across the particle-liquid interface can be expressed as

$$J = h(T - T_0) = \frac{(T - T_{l,\text{int}})}{R_k} = h_{liq}(T_{l,\text{int}} - T_0) \qquad (4.20)$$

Here h is the overall heat transfer coefficient, $T_{\text{l,int}}$ is the temperature of the liquid side of the interface, R_{k} is the Kapitza resistance and h_{liq} is the heat transfer coefficient for conductive and convective heat transfer from the interface to the surrounding liquid.

From Equation (4.20) we obtain

$$h = \frac{1}{(1/h_{liq} + R_k)} \tag{4.21}$$

The heat transfer coefficient for a sphere immersed in a fluid is given by (Bird et al., 2002):

$$h_{liq} = \frac{(Nu)k}{d_p} \tag{4.22}$$

where

$$Nu = 2 + 0.6\,\mathrm{Re}^{1/2}\,\mathrm{Pr}^{1/3} \tag{4.23}$$

Here *Nu* is the Nusselt number, *Re* is the Reynolds number ($Re = d_p \rho_l v / \mu_f$), *Pr* is the Prandtl number ($Pr = C_{pl}\mu_f / k$), μ_f is the viscosity of fluid undergoing forced convection, *v* is the bulk liquid velocity, C_{pl} is the specific heat of the liquid, and *k* is the thermal conductivity of the fluid.

If the nanoparticles are assumed to be spheres undergoing Brownian motion in the surrounding fluid, then in that case Re <<1 and *Nu* ~ 2. Coalescence of two ZnSe nanoparticles with initial diameters equal to 3nm in n-heptane (k=0.124 W/m/K at 300K (Perry and Green, 2008), T_{bp}=371.4K (Perry and Green, 2008)) yields a final spherical particle with d_p = 3.78nm and value of h_{liq} equal to 6x10^7 W/m^2/K. For comparison, the interfacial conductance (which is the same as the heat transfer coefficient in our case) for Au-Pd alloy nanoparticles of size ranging from 3 to 20nm in water or alcohol was found experimentally to be of the order of 10^8 W/m^2/K (Ge et al., 2004).

If the Kapitza resistance is neglected to simulate conditions at which the heat transfer rate from the solid to the liquid is maximized, then the overall heat transfer

coefficient $h = h_{liq}$. For such a case, the full model predicts a very small temperature rise during coalescence of ZnSe nanoparticles in heptane at room temperature of less than 1 K, even for the smallest pair of two 1 nm particles.

By using constant values of the physical properties, the energy balance equation can be written in dimensionless form as:

$$\frac{d\theta}{d\tau} = e^{-\tau} - B(1 + \frac{\Delta a_0}{a_f} e^{-\tau})\theta \tag{4.24}$$

with initial condition at $\tau = 0$: $\theta = 0$.

The dimensionless parameter

$$B = \frac{h\tau_c a_f}{mC_p} \tag{4.25}$$

represents a measure of the energy transferred to the surrounding medium in comparison to the energy accumulated in the coalescing particle system

The analytical solution of Equation (4.24) is:

$$\theta = e^{-B(\tau - \frac{\Delta a_0}{a_f} e^{-\tau})} \left[\int_0^{\tau} e^{B(\xi - \frac{\Delta a_0}{a_f} e^{-\xi}) - \xi} d\xi \right] \tag{4.26}$$

Using equation (4.24), the value of θ can be computed numerically as function of τ for different sizes of coalescing nanoparticles corresponding to different values of the two parameters $\Delta a_0/a_f$ and B. This analysis is valid for particles that do not melt during coalescence.

The value of the dimensionless parameter B is maximized when the heat transfer coefficient, h, is maximum. By assuming that Nu=2 and neglecting the Kapitza resistance, the maximum possible value of B for ZnSe nanoparticles was computed for coalescence

in heptane. The values of ($\Delta a_0/a_f$) for the nanoparticle sizes used in Table 4.1 and values of B_{max} for ZnSe nanoparticle coalescing in n-heptane (k=0.124 W/m/K at 300K (Perry and Green, 2008)) and hydrogen (k=0.183 W/m/K at 300K and 1Mpa ((Perry and Green, 2008))) respectively are listed in Table 4.2.

Table 4.2. Values of ($\Delta a_0/a_f$) and B_{max} for coalescence of ZnSe nanoparticles in n-heptane and hydrogen at 300 K under maximum heat transfer conditions (Nu = 2 and no Kapitza resistance).

d_1 (nm)	d_2 (nm)	d_p (nm)	$\Delta a_0/a_f$	B_{max} (in heptane)	B_{max} (in hydrogen)
1	1	1.26	0.26	1740	2800
1	2	2.08	0.16	640	1030
1	3	3.04	0.08	300	480
1	4	4.02	0.05	170	270
1	5	5.01	0.03	110	180
2	2	2.52	0.26	6950	11200
2	3	3.27	0.21	4130	6650
2	4	4.16	0.16	2550	4110
2	5	5.10	0.11	1700	2730
3	3	3.78	0.26	15650	25200
3	4	4.50	0.24	11050	17800
3	5	5.34	0.19	7850	12640
4	4	5.04	0.26	27810	44800
4	5	5.74	0.24	21450	33450
5	5	6.30	0.26	43460	70010

The equations (4.6) and (4.1) can also be solved numerically by taking the temperature dependence of characteristic coalescence time into account and scaling the temperature rise (as in equation (4.14)) and time with the characteristic coalescence time at T_0.

The rate of change of surface area can be expressed as

$$\frac{d\Delta\tilde{a}}{d\tau} = \frac{-\Delta\tilde{a}}{1+\frac{\theta\Delta T_{adiabatic}}{T_0}} \exp\left(-\frac{Ea}{K_B T_0}\left(\frac{1}{1+\frac{\theta\Delta T_{adiabatic}}{T_0}}-1\right)\right) \qquad (4.27)$$

where $\Delta\tilde{a} = \dfrac{(a - a_f)}{(a_0 - a_f)} = 1$ at $\tau = 0$

And the governing energy balance becomes

$$\frac{d\theta}{d\tau} = \frac{\Delta\tilde{a}}{1 + \dfrac{\theta\Delta T_{adiabatic}}{T_0}} \exp\left(-\frac{Ea}{K_B T_0}\left(\frac{1}{1 + \dfrac{\theta\Delta T_{adiabatic}}{T_0}} - 1 \right) \right) - B(1 + \frac{\Delta a_0}{a_f}\Delta\tilde{a})\theta \qquad (4.28)$$

with $\theta = 0$ at $\tau = 0$

In Figures 4.3 and 4.4 the dimensionless temperature rise is plotted as function of dimensionless time for different values of B and ($\Delta a_0/a_f$).

The temperature of the coalescing system initially increases for τ less than 1, due to the energy generation, and then decays as the energy generation decreases and heat transfer to the surroundings results in cooling of the coalesced nanoparticles. The maximum temperature rise is larger for smaller values of *B* for coalescence between particles of any size ratio. For $\Delta a_0/a_f$ values 0.1 and below (Figures 4.3 (a) and (b)), the temperature of the coalescing nanoparticle takes longer time to decay as the value of B decreases. For $\Delta a_0/a_f$ values of 0.2 and above (Figures 4.4 (a) and (b)), the temperature decay rate for B=10 is slower than that for smaller values of B and a crossover of the temperature decay curve is observed. This is due to the effect of the higher temperature on the diffusivity of the surface atoms which accelerates the coalescence at higher temperatures. For larger values of B, the temperature increase of the coalescing system is small and the rate of coalescence is slow. This effect is most prominent for larger values of $\Delta a_0/a_f$. For such systems the change in the surface area during coalescence is higher.

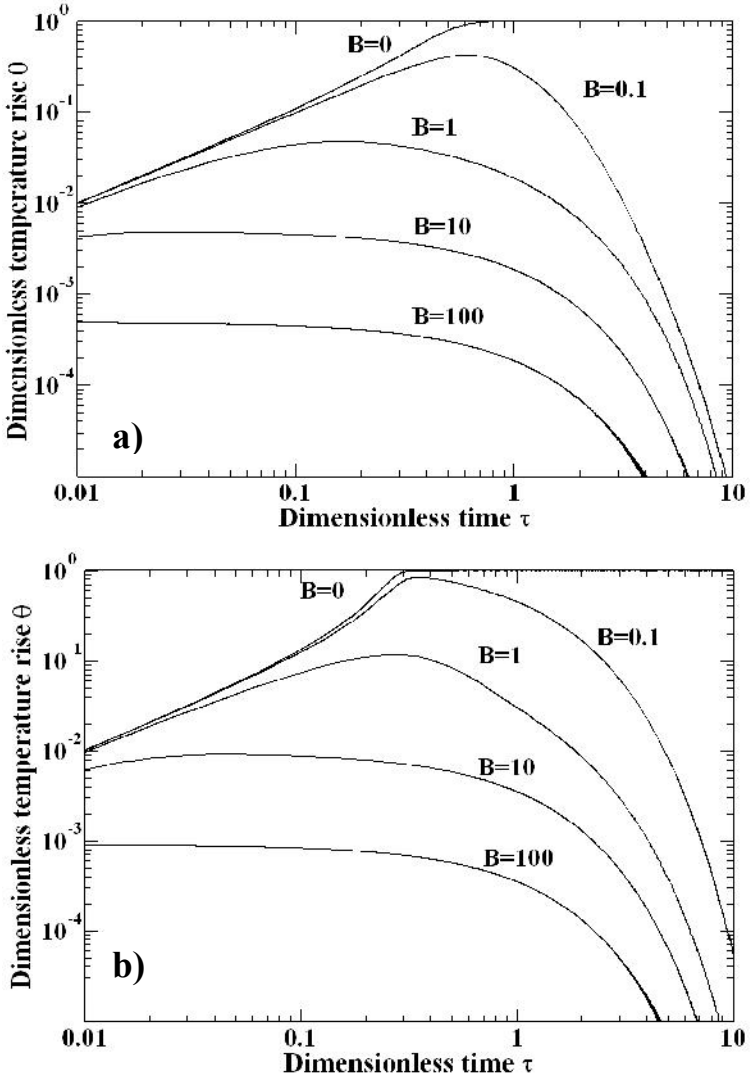

Figure 4.3. Dimensionless temperature rise evolution during coalescence of two nanoparicles for different values of B at a constant value of ($\Delta a_0/a_f$) of (a) 0.05 and (b) 0.1

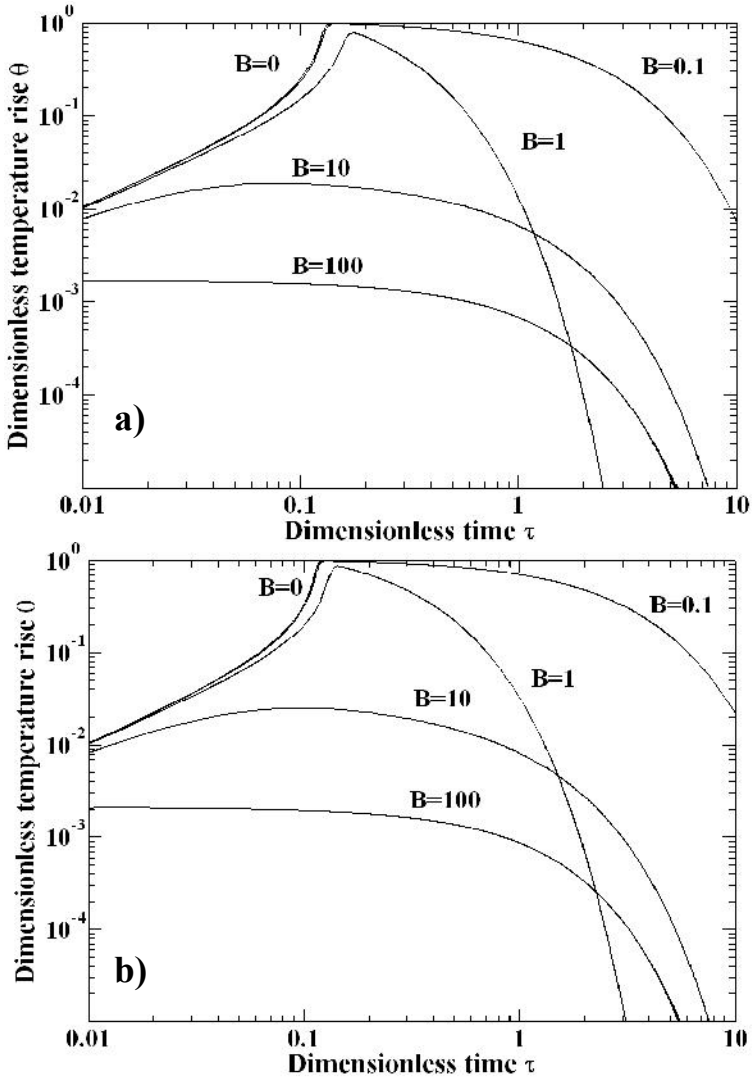

Figure 4.4. Dimensionless temperature rise evolution during coalescence of two nanoparicles for different values of B at a constant value of ($\Delta a_0/a_f$) of (a) 0.2 and (b) 0.26

The time required for complete coalescence, t_c, was defined as the time at which the dimensionless temperature rise has decreased to 0.1% of the maximum temperature rise obtained under adiabatic conditions (B=0). In Figure 4.5, the dependence of the coalescence time on the value of the dimensionless parameter B ranging from 0.1 to 10 is shown for values of $\Delta a_0/a_f$ between 0.05 and 0.26. A higher value of $\Delta a_0/a_f$ indicates coalescence of particles with similar size. The maximum value of this parameter is 0.26 and corresponds to two equal-sized particles.

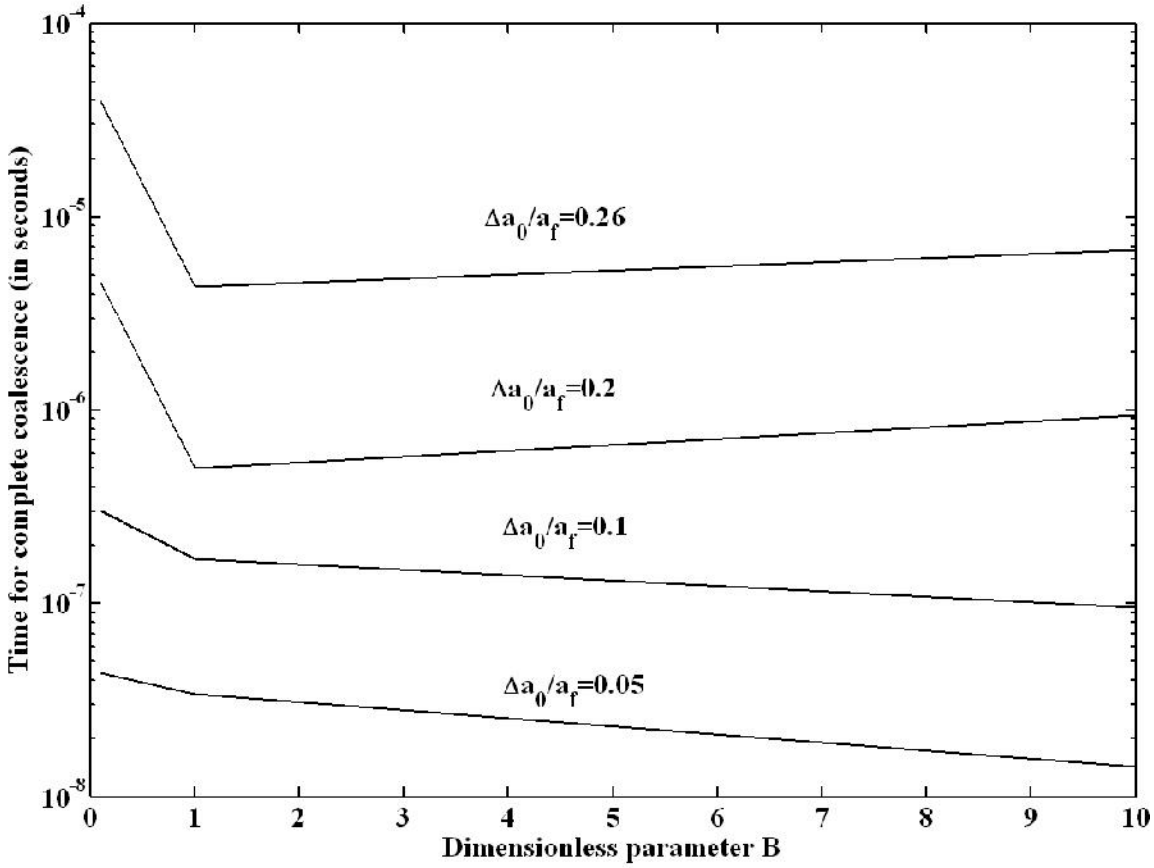

Figure 4.5. The time for complete coalescence of two ZnSe nanoparticles in n-heptane vs. dimensionless parameter B for $\Delta a_0/a_f$ values between 0.05 and 0.26. In the calculations the size of one of the particles (the larger of the two) was fixed at 5nm and the size of the second particle was calculated from the value of the specific value of $\Delta a_0/a_f$.

In Table 4.3, the maximum temperature rise and coalescence time at different values of B and $\Delta a_0/a_f$ are shown. The maximum temperature attained by the nanoparticle increases as the value of $\Delta a_0/a_f$ increases and decreases as the value of the dimensionless parameter B increases. As the value of $\Delta a_0/a_f$ increases, there is a higher percentage change in surface area which leads to a higher energy released per mass of coalescing nanoparticles. This leads to a higher final temperature for such cases.

The increase in value of B is associated with a decrease in the heat transfer resistance to the surrounding consequently leading to a higher value of the heat dissipation term. Hence, the maximum temperature achieved by the coalescing nanoparticle decreases with increase in the value of B.

Table 4.3. Values of maximum temperature, T_{max}, and time for complete coalescence, t_c, of two ZnSe nanoparticles in n-heptane for different values of ($\Delta a_0/a_f$) and B. In the calculations the size of one of the particles (the larger of the two) was fixed at 5nm and the size of the second particle was calculated from the value of $\Delta a_0/a_f$.

$\Delta a_0/a_f$	B	T_{max} (K)	t_c (s)
0.05	**0.1**	**328.4**	**4.38×10^{-8}**
0.05	**1**	**303.2**	**3.40×10^{-8}**
0.05	**10**	**300.3**	**1.43×10^{-8}**
0.05	**100**	**300**	#
0.1	**0.1**	**408.3**	**3.02×10^{-7}**
0.1	**1**	**314.9**	**1.70×10^{-7}**
0.1	**10**	**301.2**	**9.51×10^{-8}**
0.1	**100**	**300**	#
0.2	**0.1**	**538.1**	**4.65×10^{-6}**
0.2	**1**	**490. 3**	**5×10^{-6}**
0.2	**10**	**304.6**	**9.34×10^{-7}**
0.2	**100**	**300.4**	**1.96×10^{-7}**
0.26	**0.1**	**565.0**	**4.04×10^{-5}**
0.26	**1**	**533.7**	**4.36×10^{-6}**
0.26	**10**	**306.8**	**6.75×10^{-6}**
0.26	**100**	**300. 6**	**1.91×10^{-6}**

for these cases, the temperature rise was less than $0.001*\Delta T_{adiabatic}$

4.6 Summary and Conclusions

In this chapter, a model that describes the energy generation and dissipation during coalescence of two nanoparticles has been developed. The model predicts the evolution of the temperature of the coalescing nanoparticles. A linear rate law with a characteristic coalescence time was assumed to be valid for the decay of the total surface area of the coalescing system, as it asymptotically approaches a spherical final shape. The maximum possible temperature rise is obtained for the case of adiabatic coalescence. This value was used to scale the temperature rise for coalescence with heat transfer to the surrounding medium, while the characteristic coalescence time was used to scale time. The characteristic coalescence time decreases exponentially with temperature, which means that a faster energy generation rate will be obtained if the nanoparticle synthesis occurs at a high temperature. The temperature dependence of the characteristic coalescence time was taken into account in the model for adiabatic coalescence and its predictions were compared to those obtained from an approximate model based on a constant characteristic coalescence time evaluated at an average temperature.

The energy released during coalescence of ZnSe nanoparticles was found to be insufficient to melt the final nanoparticle, except for pairs of very small nanoparticles. The mechanism for coalescence was assumed to be surface diffusion of atoms to form a spherical shape. This mechanism is more likely to occur during coalescence between two particles of unequal sizes.

The model for energy release during coalescence of two ZnSe nanoparticles with heat transfer was developed. An approximate model where the characteristic coalescence time was temperature-independent is discussed. A dimensionless parameter B was

defined which gives an estimate of the ratio of the rate of energy dissipation to energy accumulation in the coalescing system and a geometric ratio $\Delta a_0/a_f$ which depends on the relative change in surface area for different sized particles was also defined. The full model includes the temperature dependence of the characteristic coalescence time and the value of B ranges from 0 (corresponding to an adiabatic system with no heat loss to the surrounding) to a maximum value when both the heat transfer resistance and the characteristic coalescence time are at their maximum value. The value of $\Delta a_0/a_f$ is close to 0 for coalescence between unequal particles and has a maximum value of 0.26 for coalescence of two equal sized particles.

Generalized plots showing the evolution of dimensionless temperature rise with dimensionless time were constructed for a range of values of the parameter B and the geometric ratio $\Delta a_0/a_f$ which is a measure of the fractional change in surface area. The maximum temperature rise during coalescence was found to decrease as the value of B increases due to heat dissipation to the medium. For coalescence with particle pairs whose $\Delta a_0/a_f$ values were 0.1 or less, a crossover in the temperature decay curve at longer time was observed.

A parametric study was performed to investigate the effects of B and $\Delta a_0/a_f$ on the temperature rise and the time required for the system to return to the initial temperature.. The time for complete coalescence increases as the value of $\Delta a_0/a_f$ increases for a fixed value of B. For a given value of B, the maximum temperature rise was also found to be higher for higher values of $\Delta a_0/a_f$. For coalescence between relatively equal sized particles, the higher relative change in surface area leads to increased energy release, a

higher temperature rise and a longer time for the temperature to return to that of the surrounding medium.

Models that predict the temperature rise and the time required for complete coalescence of nanoparticles can be very useful for predicting the structure of coalescing particles.

CHAPTER 5

SUMMARY, CONCLUSION AND FUTURE DIRECTIONS

5.1 Summary and Conclusions

This thesis focused on understanding the formation of semiconductor nanocrystals or Quantum Dots (QDs) inside microemulsions. The application was to model the mechanism in a process synthesizing zinc selenide (ZnSe) QDs using microemulsion droplets as templates. The size of the QD is an important factor affecting its optical and electronic properties and its proper control is an important requirement for the process. In this process the size of the QD is controlled by the initial concentration of one of the precursors. The nucleation takes place at the interface where the second precursor is present, followed by the diffusion of the nuclei, its coalescence to form bigger clusters and ultimately a single QD.

In Chapter 2, a lattice Monte-Carlo simulation technique was developed and used to understand the kinetics of formation of a single QD in the droplet. The model describes the Brownian diffusion of a Zn-containing precursor (reactant) inside a droplet, formation of ZnSe nuclei via an irreversible reaction with a Se-containing precursor at the droplet interface, Brownian diffusion and coalescence of nuclei into clusters ultimately leading to the formation of a single nanoparticle inside the droplet.

The simulation results indicate that as the final particle size was increased the time required for formation of a nanoparticle initially increases, but after quickly reaching a maximum, it decreases. The kinetics of the cluster coalescence was studied by studying the intermediate population size and distribution. During the formation of larger nanoparticles, a relatively large intermediate cluster appeared which was a more effective

collision partner for the other clusters and hence accelerates the synthesis. The cluster size distribution during smaller QD synthesis was relatively more uniform and hence took comparatively longer to complete.

From the results of the LMC simulations, a generalized dimensionless equation was obtained that relates the formation time of the final particle to its size for the range of QD sizes and droplet sizes experimentally used. The equation was also found to be valid for a range of diffusivity of the precursor and clusters inside the droplet. The final particle formation time was found to be more sensitive to changes in the cluster coalescence probability than in the probability of nucleation. This supports the picture obtained from the intermediate population evolution that nucleation is relatively fast and most of the process time is spent in the coalescence of the final few clusters.

The LMC model was used to simulate a case of instantaneous and uniform nucleation which was compared with the interfacial nucleation during actual synthesis and the results are discussed in Chapter 3. In the first scenario, the simulation started with the droplet populated with ZnSe nuclei which diffuse inside the droplet to form a single nanoparticle. The objective was to compare the kinetics of this process with the actual synthesis scenario to understand the relative importance of nucleation and coalescence in the process.

It was found the particle formation time in the two cases were approximately same for particle sizes smaller than 3.5 nm. However, the formation of larger nanoparticle sizes reveal that the scenario involving the diffusion of precursor to the interface for nucleation took less time than the coalescence of already existing nuclei inside the droplet. During the formation of these larger nanoparticles, the intermediate

cluster population reveals that the “sweeper” cluster was larger in the scenario requiring interfacial nucleation compared to the spontaneous nucleation which leads to a faster coalescence. Further, the scenario starting with nuclei uniformly dispersed in the droplet was analyzed to compare with the classical theory of coalescence of monodisperse aerosols in infinite domain. We obtained corrections to the scaling of formation time to account for the polydispersity of cluster sizes and confinement of the spherical domain to extend the classical theory to this specific case.

Finally in Chapter 4, we discuss a thermal analysis for the coalescence of two nanoparticles during the ZnSe QD synthesis. A phenomenological model describing the energy conservation during the coalescence is described. The source of the thermal energy release was the reduction in the surface area due to the formation of chemical bonds by the coalescing particles. The adiabatic coalescence predicted the maximum possible temperature rise during the coalescence of two nanoparticles. Generalized equation was developed by scaling the temperature rise with the maximum value under adiabatic conditions and the time with a characteristic coalescence time. The characteristic time corresponding to a surface diffusion mechanism for coalescence was used. The effect of energy dissipation to the surrounding medium was then included by taking into account the conductive and convective heat transfer to the surrounding medium and the effect of the Kapitza resistance. An approximate model where the characteristic coalescence time was evaluated at an average temperature in adiabatic conditions was developed and compared with the full model where the explicit temperature dependence was taken into account.

A dimensionless parameter was obtained from the model which was a ratio of the heat dissipation to heat generation. The effect of varying this parameter and the geometric ratio during coalescence on the temperature rise was studied. The temperature evolution was found to be controlled by the heat generation and heat dissipation with the latter dominating the temperature evolution for the nanoparticle coalescence considered here. The time for complete coalescence of nanoparticle for different values of the geometric ratios was obtained for coalescence of ZnSe nanoparticles in n-heptane droplets.

5.2 Future directions

The LMC modeling technique discussed in this thesis for the study of nanoparticle formation in nanoscale droplets can be extended to study of other situations involving diffusion and reaction at nanoscale. The formation of nanoparticle in the conventional hot injection colloidal synthesis method (described in Section 1.3) involves the nucleation of precursors and diffusion of clusters and their coalescence in common with the process studied here. In such a system, two fundamental differences with the nanoparticle formation in droplet exist. Firstly, the diffusion of precursor molecules and clusters is due to convection and not just Brownian diffusion. Also, the final particle size is not constrained by the precursor concentration and would require introducing a size dependent probability of cluster coalescence. The rules for the simulation used here a fixed value for the coalescence of clusters which is appropriate for the coalescence inside nanoscale droplet. The coalescence probability of large clusters would rapidly diminish in colloidal system because they would be passivated by surfactant or solvent molecules.

Additional physical phenomena such as dissolution of bigger clusters back into the solution may be modeled by introducing a probability of cluster dissociation.

The study of nanoparticle nucleation and coalescence in microemulsions presented in this thesis revealed new phenomena. The formation of quantum wires and quantum wells using the ternary mixture of PEO-PPO-PEO surfactant, polar and non-polar solvent has been demonstrated (Karanikolos, 2005, 2006). The extension of the model from QD formation in microemulsion droplet to complex nanostructure formation in other templating geometries can help elucidate the mechanisms of template-assisted synthesis of complex nanostructures.

The generalized model for thermal analysis of nanoparticle coalescence presented in this work is valid for binary coalescence of two nanoparticles. During nanoparticle formation, additional collisions before complete coalescence are expected or even rare ternary collisions. A further extension to this model accounting for such phenomena would provide a more detailed picture of the temperature of the coalescing nanoparticle. The role of the elevated temperature in assisting the crystallization of the nanoparticle at room temperature is expected to be more explicit with such an analysis.

APPENDIX A

PHYSICAL AND CHEMICAL PROPERTIES OF ZNSE

Table A1.1 Physical and chemical properties of ZnSe (Madelung et al., 1999):

Melting point, T_{mp}	1799 K
Solid density, ρ_s	5270 Kgm^{-3}
Liquid density, ρ_l	4580 Kgm^{-3}
Latent heat of melting, L	361 J g^{-1}
Surface energy of solid, σ_s	1.92 Jm^{-2}
Surface tension of liquid, σ_s	1.5 Jm^{-2}
Heat of formation, ΔH^0_f	-160.0 KJ mol^{-1}
Heat Capacity, C_p	343 $JKg^{-1}K^{-1}$
Lattice constant, λ	0.5667 nm (Zinc Blende)

APPENDIX B

EFFECT OF LATTICE SPACING ON

LATTICE MONTE CARLO SIMULATION RESULTS

Table A2.1. Behavior of Root Mean Square (RMS) difference of total formation time with the value for coarsest mesh (lattice spacing =4nm).

Number of lattice points	*Number of cells in the cubic lattice*	*Lattice Spacing (nm)*	*RMS Difference with coarsest mesh (N=10)*	*Normalized RMS Difference*
10	1000	4.0	0	0
15	3375	2.67	2.26E-6	0.76
20	8000	2.0	2.666E-6	0.89
40	64000	1.0	2.85E-6	0.96
91	753571	0.44	2.97E-6	1.0

Diameter of a Zn precursor = 0.25nm

Equivalent diameter of a $(ZnSe)_1$ nucleus = 0.44nm

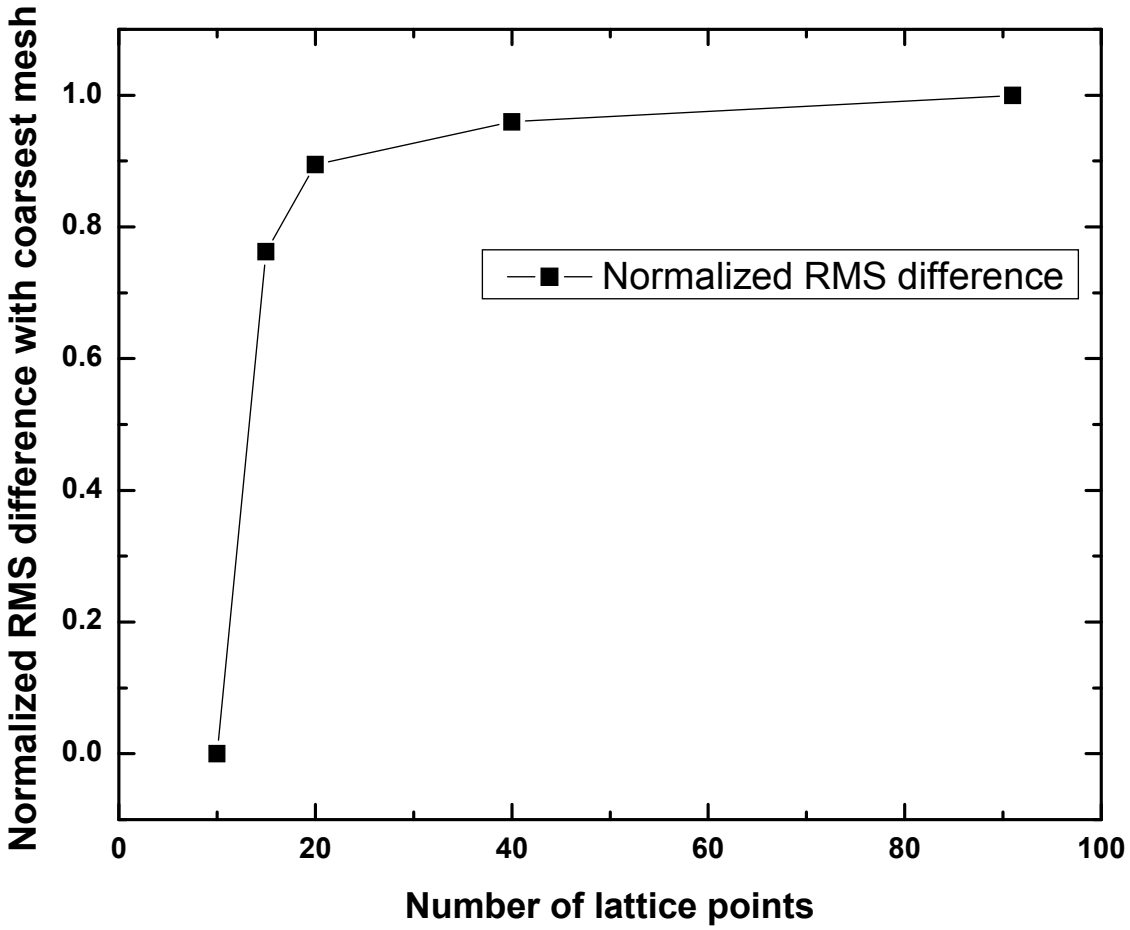

Figure A2.1. Normalized root mean square difference between the predicted final particle formation time for finer lattice spacing minus the ones obtained from the initial LMC simulation that employed a lattice spacing of 4nm. The RMS difference saturates as finer lattice is used.

BIBLIOGRAPHY

Aldous, D. J., Deterministic and stochastic models for coalescence (aggregation and coagulation): a review of the mean-field theory for probabilists. *Bernoulli* **1999,** 5, (1), 3-48.

Alexandridis, P.; Olsson, U.; Lindman, B., A record nine different phases (four cubic, two hexagonal, and one lamellar lyotropic liquid crystalline and two micellar solutions) in a ternary isothermal system of an amphiphilic block copolymer and selective solvents (water and oil). *Langmuir* **1998,** 14, (10), 2627-2638.

Alivisatos, A. P., Semiconductor clusters, nanocrystals, and quantum dots. *Science* **1996,** 271, (5251), 933-937.

Allen, M. P.; Tildesley, D. J., *Computer simulation of liquids*. Clarendon Press;Oxford University Press: Oxford [England] New York, 1987.

Assael, M. J.; Charitidou, E.; Decastro, C. A. N.; Wakeham, W. A., The thermal conductivity of n-hexane, n-heptane, and n-decane by the transient hot-wire method. *Int. J. Thermophys.* **1987,** 8, (6), 663-670.

Bandyopadhyaya, R.; Kumar, R.; Gandhi, K. S., Simulation of precipitation reactions in reverse micelles. *Langmuir* **2000,** 16, (18), 7139-7149.

Barnard, A. S., Modelling of nanoparticles: approaches to morphology and evolution. *Rep. Prog. Phys.* **2010,** 73, (8), 52.

Beichl, I.; Sullivan, F., The metropolis algorithm. *Comput. Sci. Eng.* **2000,** 2, (1), 65-69.

Bird, R. B.; Stewart, W. E.; Lightfoot, E. N., *Transport phenomena*. 2nd, Wiley international ed.; J. Wiley: New York, 2002.

Brus, L. E., Electron-electron and Electron-hole interaction in small semiconductor crystallites – the size dependence of the lowest excited electronic state. *J. Chem. Phys.* **1984,** 80, (9), 4403-4409.

Buffat, P.; Borel, J. P., Size effect on melting temperature of gold particles. *Phys. Rev. A* **1976,** 13, (6), 2287-2298.

Cai, Y.; Chan, S. K.; Soar, I. K.; Chan, Y. T.; Su, D. S.; Wang, N., The size-dependent growth direction of ZnSe nanowires. *Adv. Mater.* **2006,** 18, (1), 109-114.

Caruge, J. M.; Halpert, J. E.; Wood, V.; Bulovic, V.; Bawendi, M. G., Colloidal quantum-dot light-emitting diodes with metal-oxide charge transport layers. *Nat. Photonics* **2008,** 2, (4), 247-250.

Chatterjee, A.; Vlachos, D. G., An overview of spatial microscopic and accelerated kinetic Monte Carlo methods. *J. Comput-Aided Mater. Des.* **2007,** 14, (2), 253-308.

Cho, J; Koutsona M; Sarigiannidis C; Mountziaris T. J., Modeling and simulation of vapor-phase synthesis of compound semiconductor nanoparticles in a counterflow jet reactor. *Ind. Eng. Chem. Res.* **2010,** 50, (6), 3227-3238.

Crank, J., *The mathematics of diffusion*. Clarendon Press: Oxford,, 1956

Dai, Q. Q.; Duty, C. E.; Hu, M. Z., Semiconductor-Nanocrystals-Based White Light-Emitting Diodes. *Small* **2010,** 6, (15), 1577-1588.

de Dios, M.; Barroso, F.; Tojo, C.; Lopez-Quintela, M. A., Simulation of the kinetics of nanoparticle formation in microemulsions. *J. Colloid Interface Sci.* **2009,** 333, (2), 741-748.

Efros, A. L., Interband absorption of light in a semiconductor sphere. *Soviet Physics Semiconductors-Ussr* **1982,** 16, (7), 772-775.

Ekimov, A. I.; Onushchenko, A. A., Quantum size effect in the optical spectra of semiconductor microcrystals, *Soviet Physics Semiconductors-Ussr* **1982,** 16, (7), 775-778.

Erwin, S. C.; Zu, L. J.; Haftel, M. I.; Efros, A. L.; Kennedy, T. A.; Norris, D. J., Doping semiconductor nanocrystals. *Nature* **2005,** 436, (7047), 91-94.

Ethayaraja, M.; Bandyopadhyaya, R., Population balance models and Monte Carlo simulation for nanoparticle formation in water-in-oil microemulsions: Implications for CdS synthesis. *J. Am. Chem. Soc.* **2006,** 128, (51), 17102-17113.

Fichthorn, K. A.; Weinberg, W. H., Theoretical foundations of dynamic monte-carlo simulations. *J. Chem. Phys.* **1991,** 95, (2), 1090-1096.

Friedlander, S. K., *Smoke, dust, and haze:fundamentals of aerosol behavior*. Wiley: New York, 1977

Friedlander, S. K.; Wang, C. S., Self-preserving particle size distribution for coagulation by Brownian motion. *J. Colloid Interface Sci.* **1966,** 22, (2), 126-132.

Friedlander, S. K.; Wu, M. K., Linear rate law for the decay of the excess surface area of a coalescing solid particle. *Phys. Rev. B* **1994,** 49, (5), 3622-3624.

Fuks, N. A.; Davies, C. N., *The mechanics of aerosols*. Dover Publications: New York, 1989

Ge, Z. B.; Cahill, D. G.; Braun, P. V., Au-Pd metal nanoparticles as probes of nanoscale thermal transport in aqueous solution. *J. Phys. Chem. B* **2004,** 108, (49), 18870-18875.

Gelbard, F.; Seinfeld, J. H., General dynamic equation for aerosols – Theory and application to aersol formation and growth. *J. Colloid Interface Sci.* **1979,** 68, (2), 363-382.

Goldstein, A. N.; Echer, C. M.; Alivisatos, A. P., Melting in semiconductor nanocrystals. *Science* **1992,** 256, (5062), 1425-1427.

Gratzel, M., Solar energy conversion by dye-sensitized photovoltaic cells. *Inorg. Chem.* **2005,** 44, (20), 6841-6851.

Gudiksen, M. S.; Lieber, C. M., Diameter-selective synthesis of semiconductor nanowires. *J. Am. Chem. Soc.* **2000,** 122, (36), 8801-8802.

Gupta, V.; Safvi, S. A.; Mountziaris, T. J., Gas-phase decomposition kinetics in a wall-less environment using a counterflow jet reactor: Design and feasibility studies. *Ind. Eng. Chem. Res.* **1996,** 35, (9), 3248-3255.

Hamad, S.; Cristol, S.; Callow, C. R. A., Surface structures and crystal morphology of ZnS: Computational study. *J. Phys. Chem. B* **2002,** 106, (42), 11002-11008.

Hastings, W. K., Monte-Carlo sampling methods using Markov chains and their applications. *Biometrika* **1970,** 57, (1), 97-109.

Hawa, T.; Zachariah, M. R., Internal pressure and surface tension of bare and hydrogen coated silicon nanoparticles. *J. Chem. Phys.* **2004,** 121, (18), 9043-9049.

Heine, M. C.; Pratsinis, S. E., Brownian coagulation at high concentration. *Langmuir* **2007,** 23, (19), 9882-9890.

Hendy, S.; Brown, S. A.; Hyslop, M., Coalescence of nanoscale metal clusters: Molecular-dynamics study. *Phys. Rev. B* **2003,** 68, (24), 4.

Hines, M. A.; Guyot-Sionnest, P., Bright UV-blue luminescent colloidal ZnSe nanocrystals. *J. Phys. Chem. B* **1998,** 102, (19), 3655-3657.

Holmes, J. D.; Bhargava, P. A.; Korgel, B. A.; Johnston, K. P., Synthesis of cadmium sulfide Q particles in water-in-CO2 microemulsions. *Langmuir* **1999,** 15, (20), 6613-6615.

Jaeger, H. M.; Nagel, S. R., Physics of the granular state. *Science* **1992,** 255, (5051), 1523-1531.

Jain, R.; Mehra, A., Monte Carlo models for nanoparticle formation in two microemulsion systems. *Langmuir* **2004,** 20, (15), 6507-6513.

Jain, R.; Shukla, D.; Mehra, A., Coagulation of nanoparticles in reverse micellar systems: A Monte Carlo model. *Langmuir* **2005,** 21, (24), 11528-11533.

Jensen, P., Growth of nanostructures by cluster deposition: Experiments and simple models. *Rev. Mod. Phys.* **1999,** 71, (5), 1695-1735.

Jensen, P.; Combe, N., Understanding the growth of nanocluster films. *Comput. Mater. Sci.* **2002,** 24, (1-2), 78-87.

Kamat, P. V., Quantum Dot Solar Cells. Semiconductor Nanocrystals as Light Harvesters. *J. Phys. Chem. C* **2008,** 112, (48), 18737-18753.

Kapitza, P. L., The study of heat transfer in helium II. *J. Phys.-USSR* **1941,** 4, (1-6), 181-210.

Karanikolos, G. N. Templating the synthesis of compound semiconductor nanostructures using microemulsions and lytropic liquid crystals. PhD, State University of New York, 2005.

Karanikolos, G. N.; Alexandridis, P.; Itskos, G.; Petrou, A.; Mountziaris, T. J., Synthesis and size control of luminescent ZnSe nanocrystals by a microemulsion-gas contacting technique. *Langmuir* **2004,** 20, (3), 550-553.

Karanikolos, G. N.; Alexandridis, P.; Mallory, R.; Petrou, A.; Mountziaris, T. J., Templated synthesis of ZnSe nanostructures using lyotropic liquid crystals. *Nanotechnology* **2005,** 16, (10), 2372-2380.

Karanikolos, G. N.; Law, N. L.; Mallory, R.; Petrou, A.; Alexandridis, P.; Mountziaris, T. J., Water-based synthesis of ZnSe nanostructures using amphiphilic block copolymer stabilized lyotropic liquid crystals as templates. *Nanotechnology* **2006,** 17, (13), 3121-3128.

Kasuya, A.; Sivamohan, R.; Barnakov, Y. A.; Dmitruk, I. M.; Nirasawa, T.; Romanyuk, V. R.; Kumar, V.; Mamykin, S. V.; Tohji, K.; Jeyadevan, B.; Shinoda, K.; Kudo, T.; Terasaki, O.; Liu, Z.; Belosludov, R. V.; Sundararajan, V.; Kawazoe, Y., Ultra-stable nanoparticles of CdSe revealed from mass spectrometry. *Nat. Mater.* **2004,** 3, (2), 99-102.

Kingery, W. D.; Berg, M., Study of the initial stages of sintering solids by viscous flow, evaporation-condensation, and self-diffusion. *J. Appl. Phys.* **1955,** 26, (10), 1205-1212.

Koch, W.; Friedlander, S. K., The effect of particle coalescence on the surface area of coagulating aerosol. *J. Colloid Interface Sci.* **1990,** 140, (2), 419-427.

Kongkanand, A.; Tvrdy, K.; Takechi, K.; Kuno, M.; Kamat, P. V., Quantum dot solar cells. Tuning photoresponse through size and shape control of CdSe-TiO2 architecture. *J. Am. Chem. Soc.* **2008,** 130, (12), 4007-4015.

Kuriyedath, S. R.; Kostova, B.; Kevrekidis, I. G.; Mountziaris, T. J., Lattice Monte Carlo Simulation of Semiconductor Nanocrystal Synthesis in Microemulsion Droplets. *Langmuir* **2010a,** 26, (13), 11355-11362.

Kuriyedath, S. R.; Kostova, B.; Kevrekidis, I. G.; Mountziaris, T. J., Lattice Monte Carlo Simulation of Cluster Coalescence Kinetics with Application to Template-Assisted Synthesis of Quantum Dots. *Ind. Eng. Chem. Res.* **2010b,** 49, (21), 10442-10449.

Ledentsov, N. N.; Ustinov, V. M.; Shchukin, V. A.; Kop'ev, P. S.; Alferov, Z. I.; Bimberg, D., Quantum dot heterostructures: fabrication, properties, lasers (Review). *Semiconductors* **1998,** 32, (4), 343-365.

Lehtinen, K. E. J.; Zachariah, M. R., Effect of coalescence energy release on the temporal shape evolution of nanoparticles. *Phys. Rev. B* **2001,** 63, (20), 7.

Lehtinen, K. E. J.; Zachariah, M. R., Energy accumulation in nanoparticle collision and coalescence processes. *J. Aerosol. Sci.* **2002,** 33, (2), 357-368.

Lewis, L. J.; Jensen, P.; Barrat, J. L., Melting, freezing, and coalescence of gold nanoclusters. *Phys. Rev. B* **1997,** 56, (4), 2248-2257.

Li, Y. C.; Park, C. W., Particle size distribution in the synthesis of nanoparticles using microemulsions. *Langmuir* **1999,** 15, (4), 952-956.

Li, Y. C.; Park, C. W., Particle size distribution in the synthesis of nanoparticles using microemulsions. *Langmuir* **1999,** 15, (4), 952-956.

Lianos, P.; Thomas, J. K., Cadmium-Sulfide of small dimensions produced in inverted micelles. *Chem. Phys. Lett.* **1986,** 125, (3), 299-302.

Lianos, P.; Thomas, J. K., Small CdS particles in inverted micelles. *J. Colloid Interface Sci.* **1987,** 117, (2), 505-512.

Lopez-Quintela, M. A.; Tojo, C.; Blanco, M. C.; Rio, L. G.; Leis, J. R., Microemulsion dynamics and reactions in microemulsions. *Curr. Opin. Colloid Interface Sci.* **2004,** 9, (3-4), 264-278.

McCarthy, D. N.; Brown, S. A., Evolution of neck radius and relaxation of coalescing nanoparticles. *Phys. Rev. B* **2009,** 80, (6), 8.

Medintz, I. L.; Uyeda, H. T.; Goldman, E. R.; Mattoussi, H., Quantum dot bioconjugates for imaging, labelling and sensing. *Nat. Mater.* **2005,** 4, (6), 435-446.

Metropolis, N.; Rosenbluth, A. W.; Rosenbluth, M. N.; Teller, A. H.; Teller, E., Equation of state calculations by fast computing machines. *J. Chem. Phys.* **1953,** 21, (6), 1087-1092.

Michalet, X.; Pinaud, F. F.; Bentolila, L. A.; Tsay, J. M.; Doose, S.; Li, J. J.; Sundaresan, G.; Wu, A. M.; Gambhir, S. S.; Weiss, S., Quantum dots for live cells, in vivo imaging, and diagnostics. *Science* **2005,** 307, (5709), 538-544.

Mo, Y. W.; Kleiner, J.; Webb, M. B.; Lagally, M. G., Activation energy for surface diffusion of Si on Si(001) – A scanning tunneling microscopy study. *Phys. Rev. Lett.* **1991,** 66, (15), 1998-2001.

Murray, C. B.; Kagan, C. R.; Bawendi, M. G., Synthesis and characterization of monodisperse nanocrystals and close-packed nanocrystal assemblies. *Annu. Rev. Mater. Sci.* **2000,** 30, 545-610.

Murray, C. B.; Norris, D. J.; Bawendi, M. G., Synthesis and characterization of nearly monodisperse CdE (E = S, Se, Te) semiconductor nanocrystallites. *J. Am. Chem. Soc.* **1993,** 115, (19), 8706-8715.

Nagasaka, Y.; Nagashima, A., Precise measurements of the thermal conductivity of toluene and n-heptane by the absolute transient hot-wire method. *Industrial & Engineering Chemistry Fundamentals* **1981,** 20, (3), 216-220.

Nanda, K. K.; Maisels, A.; Kruis, F. E.; Fissan, H.; Stappert, S., Higher surface energy of free nanoparticles. *Phys. Rev. Lett.* **2003,** 91, (10), 4.

Nichols, F. A., Coalescence of 2 spheres by surface diffusion. *J. Appl. Phys.* **1966,** 37, (7), 2805-2808.

Nichols, F. A.; Mullins, W. W., Morphological changes of a surface of revolution due to capillarity induced surface diffusion. *J. Appl. Phys.* **1965,** 36, (6), 1826-1835.

Nozik, A. J., Quantum dot solar cells. *Physica E* **2002,** 14, (1-2), 115-120.

Ozasa, K.; Aoyagi, Y.; Park, Y. J.; Samuelson, L., Reversible transition between InGaAs dot structure and InGaAsP flat surface. *Appl. Phys. Lett.* **1997,** 71, (6), 797-799.

Pan, J.; Le, H.; Kucherenko, S.; Yeomans, J. A., A model for the sintering of spherical particles of different sizes by solid state diffusion. *Acta Mater.* **1998,** 46, (13), 4671-4690.

Parak, W. J.; Pellegrino, T.; Plank, C., Labelling of cells with quantum dots. *Nanotechnology* **2005,** 16, (2), R9-R25.

Perry, R. H.; Green, D. W., *Perry's chemical engineers' handbook*. 8th ed.; McGraw-Hill: New York, 2008.

Petit, C.; Lixon, P.; Pileni, M. P., In-situ synthesis of silver nanocluster in AOT reverse micelles. *J. Phys. Chem.* **1993,** 97, (49), 12974-12983.

Pileni, M. P., Nanosized particles made in colloidal assemblies. *Langmuir* **1997,** 13, (13), 3266-3276.

Pillai, V.; Kumar, P.; Hou, M. J.; Ayyub, P.; Shah, D. O., Preparation of nanoparticles of silver halides superconductors and magnetic materials using water-in-oil microemulsions as nanoreactors. *Adv. Colloid Interface Sci.* **1995,** 55, 241-269.

Pollack, G. L., Kapitza resistance. *Rev. Mod. Phys.* **1969,** 41, (1), 48-81.

Madelung, O.; Rossler U.; Schulz M. (Series editors), *The Landolt-Börnstein Database*. SpringerMaterials: 1999; Vol. 41B.

Quellet, C.; Eicke, H. F.; Sager, W., Formation of microemulsion-based gelatin gels. *J. Phys. Chem.* **1991,** 95, (14), 5642-5655.

Quinlan, F. T.; Kuther, J.; Tremel, W.; Knoll, W.; Risbud, S.; Stroeve, P., Reverse micelle synthesis and characterization of ZnSe nanoparticles. *Langmuir* **2000,** 16, (8), 4049-4051.

Reid, R. C.; Prausnitz, J. M.; Sherwood, T. K., *The properties of gases and liquids*. 3d ed.; McGraw-Hill: New York, 1977.

Robinson, D. J.; Earnshaw, J. C., Experimental study of colloidal aggregation in 2 dimensions. 1. Structural aspects. *Phys. Rev. A* **1992,** 46, (4), 2045-2054.

Rohrer, G. S., *Structure and bonding in crystalline materials*. Cambridge University Press: Cambridge ; New York, 2001.

Rossetti, R.; Hull, R.; Gibson, J. M.; Brus, L. E., Excited electronic states and optical spectra of ZnS and CdS crystallites in the 15 to 50 A size range: Evolution from molecular to bulk semiconducting properties. *J. Chem. Phys.* **1985,** 82, (1), 552-559.

Sarigiannidis C; Koutsona M; Petrou A; Mountziaris T. J., Vapor-phase synthesis and surface passivation of ZnSe nanocrystals. *J. Nanopart. Res.* **2006,** 8, (3-4), 533-542.

Sarigiannidis C; Peck J.D.; Kioseoglou G; Petrou A; Mountziaris T. J., Characterization of vapor-phase-grown ZnSe nanoparticles. *Appl. Phys. Lett.* **2002,** 80, (21), 4024-4026.

Sharma, R. C.; Chang, Y. A., Thermodynamic analysis and phase equilibria calculations for the ZnTe, ZnSe, and ZnS systems. *J. Cryst. Growth* **1988,** 88, (2), 193-204.

Shields, A. J., Semiconductor quantum light sources. *Nat. Photonics* **2007,** 1, (4), 215-223.

Shih, C. C.; Yariv, A., A theoretical model of the linear electrooptic effect. *Journal of Physics C-Solid State Physics* **1982,** 15, (4), 825-846.

Singh, T.; Mountziaris, T. J.; Maroudas, D., First-principles theoretical analysis of dopant adsorption and diffusion on surfaces of ZnSe nanocrystals. *Chem. Phys. Lett.* **2008,** 462, (4-6), 265-268.

Smoluchowski, M. V., Drei Vortrage uber Diffusion, Brownsche Bewegung und Koagulation von Kolloidteilchen. *Physik. Z.* **1916,** 17, 557-585.

Swartz, E. T.; Pohl, R. O., Thermal resistance at interfaces. *Appl. Phys. Lett.* **1987,** 51, (26), 2200-2202.

Swartz, E. T.; Pohl, R. O., Thermal boundary resistance. *Rev. Mod. Phys.* **1989,** 61, (3), 605-668.

Tojo, C.; Blanco, M. C.; LopezQuintela, M. A., Preparation of nanoparticles in microemulsions: A Monte Carlo study of the influence of the synthesis variables. *Langmuir* **1997a,** 13, (17), 4527-4534.

Tojo, C.; Blanco, M. C.; Rivadulla, F.; LopezQuintela, M. A., Kinetics of the formation of particles in microemulsions. *Langmuir* **1997b,** 13, (7), 1970-1977.

Torquato, S.; Truskett, T. M.; Debenedetti, P. G., Is random close packing of spheres well defined? *Phys. Rev. Lett.* **2000,** 84, (10), 2064-2067.

Trindade, T.; O'Brien, P.; Pickett, N. L., Nanocrystalline semiconductors: Synthesis, properties, and perspectives. *Chem. Mat.* **2001,** 13, (11), 3843-3858.

Vemury, S.; Pratsinis, S. E., Self-preserving size distributions of agglomerates. *J. Aerosol. Sci.* **1995,** 26, (2), 175-185.

Walsh, R., Bond-dissociation energy values in silicon-containing compounds and some of their implications. *Accounts Chem. Res.* **1981,** 14, (8), 246-252.

Wang, J. Synthesis, Functionalization, and Biological Tagging Applications of II-VI Semiconductor Nanocrystals. PhD, State University of New York, Buffalo, 2006.

Yoffe, A. D., Semiconductor quantum dots and related systems: electronic, optical, luminescence and related properties of low dimensional systems. *Adv. Phys.* **2001,** 50, (1), 1-208.

Zachariah, M. R.; Carrier, M. J., Molecular dynamics computation of gas-phase nanoparticle sintering: A comparison with phenomenological models. *J. Aerosol. Sci.* **1999,** 30, (9), 1139-1151.

Zangwill, A., *Physics at surfaces*. Cambridge University Press: 1996.

Zhang, Z. Y.; Lagally, M. G., Atomistic processes in the early stages of thin-film growth. *Science* **1997,** 276, (5311), 377-383.

Zou, J.; Balandin, A., Phonon heat conduction in a semiconductor nanowire. *J. Appl. Phys.* **2001,** 89, (5), 2932-2938.